Investigation of Environmental Effects on Intrinsic and Galvanic Corrosion of Mild Steel Weldment

A thesis presented to

the faculty of

the Russ College of Engineering and Technology of Ohio University

In partial fulfillment

of the requirement for the degree

Master of Science

Lei Huang

June 2012

This thesis entitled

Investigation of Environmental Effects on Intrinsic and Galvanic Corrosion of Mild Steel Weldment

by

LEI HUANG

has been approved for

the Department of Chemical and Biomolecular Engineering

and the Russ College of Engineering and Technology by

Srdjan Nesic

Professor of Chemical and Biomolecular Engineering

Dennis Irwin

Dean, Russ College of Engineering and Technology

ABSTRACT

HUANG, LEI, M.S., June 2012, Chemical and Biomolecular Engineering

Investigation of Environmental Effects on Intrinsic and Galvanic Corrosion of Mild Steel Weldment

Director of Thesis: Srdjan Nesic

Welding is one of the most important fabrication processes that joins metallic structures. Weldment structures are commonly seen in the oil and gas industry such as production tubing, co-rod, gathering pipeline, *etc*. Corrosion of weldments may lead to a severe production failure. In this study, the environmental effects on intrinsic and galvanic corrosion of weldments in CO_2 and CO_2/H_2S environments have been investigated using different types of electrochemical techniques. A non-alloyed standard carbon steel weldment was selected as the test material in this study. During this study, intrinsic corrosion rates of each weldment segment (*i.e.* parent metal, heat effected zone and weld material), as well as galvanic currents between each weldment segment were measured under different test conditions.

Various environmental effects including salt concentration, temperature, acetic acid, H_2S and addition of inhibitor (24% active Tall oil fatty acid/ diethylenetriamine Imidazoline) on weldment corrosion were studied. Experimental results show that the intrinsic corrosion rates of the different segments of the non-alloyed standard weldment are not significantly different under the same test conditions. It was also found that the galvanic current measured on the weld metal always appeared to be positive, the galvanic current on the heat affected zone (HAZ) was always neutral and the galvanic current on

parent metal was always negative. This suggests that for the non-alloyed standard weldment, the corrosion of weld metal becomes worse and the parent metal is protected due to the galvanic effects between the segments.

The experimental results also show that an increase of salt concentration significantly affected the intrinsic CO_2 corrosion rate in a nonlinear fashion. High salt concentration leads to a decrease of the corrosion rate at 25°C, but an increase of the corrosion rate at 60°C. The weight loss method confirmed the corrosion rate magnitude. The galvanic currents were unaffected by the different salt concentrations (1~10 wt% NaCl). However, in comparison with the galvanic current at 25°C, the galvanic currents significantly increased at 60°C.

It was also found the addition of 50 ppm H_2S and/or 20 ppm inhibitor reduced the intrinsic corrosion rate of weld segments (weld metal, metal, and HAZ) and led to lower galvanic corrosion rates between different weld segments, compared with that observed in CO_2 environment. The addition of acetic acid under the same conditions increased the intrinsic corrosion rate of all weld segments and lead to a higher magnitude of galvanic corrosion rate.

Surface analysis techniques including scanning electron microscopy (SEM), energy dispersive spectroscopy (EDS) and infinite focus microscopy (IFM) were applied to this study to characterize the surface morphology, identify the chemical composition of corrosion products and quantify the possible localized corrosion.

Approved: ____

Srdjan Nesic

Professor of Chemical Engineering and Biomolecular Engineering

DEDICATION

To

Mingdi Huang and Daoyong Yin (my parents)

Haitao Fang (my husband)

Ella Fang (my daughter)

Chuntao Huang and Chunyu Huang (my sister and brother)

ACKNOWLEDGEMENTS

I would like to express my great gratitude to Dr. Srdjan Nesic for his generous guidance and support of my research.

I would like to acknowledge my indebtedness to Mr. Bruce Brown, Dr. David Young and Dr. Yoon-Seok Choi for their invaluable advice.

I would also like to thank the technical staff at the Institute for Corrosion and Multiphase Technology, including Mr. Al Schubert Mr. Cody Shafer and Mr. Danny Cain for their assistance in technical matters, and my fellow students: Gheorghe Bota, Jin Huang and Yang Yang for providing a wonderful research environment.

In addition I would like to acknowledge the contribution of the consortium of companies whose continuous financial support and technical guidance made this research possible.

TABLE OF CONTENTS

Page

LIST OF TABLES

LIST OF FIGURES

CHAPTER 1 INTRODUCTION

In the oil and gas industry, welding is a fundamental process in the construction of transportation pipelines, production tubing, and other related operational facilities. The welding process connects metallic structures by melting a filler material in between the two structures at high temperature. Carbon steel is by far the most frequently welded metallic material in all heavy industrial applications including the petroleum and petrochemical industry[1]. Carbon steel weldment may experience all classical forms of corrosion depending upon the environment to which it is exposed[1]. Weldments naturally possess compositional and microstructural heterogeneities, therefore, the corrosion of weldment appears to be more erratic and is difficult to predict.

According to its special structure, a weldment can be divided into three sections[1]: weld metal, heat affected zone (HAZ), and parent metal. A schematic representation of a weldment cut directly from a pipeline is shown in **Error! Reference source not found.**. The weldment was specially treated with 3% Nital (3% Nitric acid in ethanol) solution to expose the region of the weld and HAZ. It is clearly seen that the parent metal is on the side, the weld metal is in the middle and the heat affected zone is in between.

Figure 1. The weldment specimen etched with 3% Nital (3% Nitric acid in ethanol) solution.

The *weld metal* is the result of melting, which fuses the base metal and filler metal to produce a zone with a composition that is typically different from that of the base metal[1]. It is located in the middle of the weldment. The compositional difference could lead to a galvanic couple that may significantly affect the corrosion process of the metal in close proximity to the weld metal.

The *heat affected zone* (HAZ) is the area of the base metal which has experienced extremely intense heat during the weld process[1]. The heat from the welding process and subsequent re-cooling produce solid-state micro-structural changes in the heat affected zone, which may also alter the corrosion resistance of the affected metal.

The *parent metal* is the base metal which is a certain distance from the weld area and is not affected by the heat brought on by the welding process[1]. The metallurgical structure as well as the corrosion resistivity of the parent metal remains unchanged during the welding process.

A weldment can experience different types of corrosion due to this dissimilarity of the metallurgical structures within it. As mentioned before, the compositional difference of the weld and base metal may cause a potential difference and hence lead to a galvanic couple. The galvanic corrosion may significantly accelerate or retard the overall corrosion process. When only the corrosion without galvanic effects is considered, then it is herein called intrinsic corrosion. To study the weldment corrosion, intrinsic and galvanic corrosion behaviors have to be considered simultaneously. The combined effects of intrinsic and galvanic corrosion may cause a focus of corrosion attack in a specific location on the weldment, thus lead to severe localized attack. This type of corrosion is also called preferential corrosion of weldment[1].

Preferential weld corrosion of carbon steel has been investigated since the 1950s[2]. Studies have shown that preferential weld corrosion is significantly affected by environmental factors[3-6]. The morphology and location of preferential weld corrosion in CO_2-containing media are influenced by complex interactions of several parameters, including environmental (temperature, flow conditions, water composition, pH value, organic acid and partial pressure of CO_2), scaling effects, weld steel composition relative to the parent pipe and welding procedure[6].

Several issues related to corrosion of carbon steel weldments have been successfully identified in specific cases[7-20]; however, problems still exist today in different applications. It is still difficult to predict whether an attack will occur on the HAZ, weld metal or both, in susceptible situations. Corrosion models have not been established to successfully predict the location of weldment corrosion, corrosion rates, and the effectiveness of inhibitors. More work needs to be done to further the understanding of weldment corrosion problems. The purpose of the present project was to initiate this task in the Institute for Corrosion and Multiphase Technology (ICMT).

CHAPTER 2 LITERATURE REVIEW

2.1 Corrosion of carbon steel in the oil and gas industry

Carbon steel is by far the most common construction material used in oil and gas extraction, transportation and processing because of its advantages related to availability, strength, and price. Corrosion of carbon steel is a major concern for the oil and gas industry. Severe corrosion can lead to an operational failure, which may result in a huge capital loss and a detrimental threat to environmental safety. CO_2 corrosion and H_2S corrosion are the two dominant corrosion modes in the oil and gas industry.

2.1.1 CO_2 corrosion

CO_2 corrosion or ñsweet corrosionò has been investigated for more than three decades. CO_2 itself does not cause corrosion problems if it is dry. It only becomes corrosive when water is present. The CO_2 corrosion mechanism has been well understood and accepted based on the work that has been done in the past[21-37]. The major reactions occurring during the CO_2 corrosion process are illustrated as follows:

CO_2 gas dissolves in the water first and then reacts with water to form carbonic acid:

$$CO_2(g) \Leftrightarrow CO_2(aq)$$

$$CO_2(g) + H_2O(aq) \Leftrightarrow H_2CO_3(aq)$$

Carbonic acid then dissociates to hydrogen ion, bicarbonate ion and carbonate ion in two steps:

$$H_2CO_3(aq) \Leftrightarrow H^+(aq) + HCO_3^-(aq)$$

$$HCO_3^-(aq) \Leftrightarrow H^+(aq) + CO_3^{2-}(aq)$$

The above reactions can occur anywhere in the aqueous system. However, the corrosion reaction (electrochemical reaction) including cathodic reactions and anodic reaction only occur on the steel surface. Hydrogen ion and carbonic acid have been identified to be the corrosive species (cathodic) that are directly involved in the corrosion reactions in CO_2 system.

Two cathodic reactions are direct hydrogen ion reduction and direct carbonic acid reduction:

$$2H^{+}(aq) + 2e^{-} \rightarrow H_2(g)$$

$$2H_2CO_3(aq) + 2e^{-} \rightarrow H_2(g) + 2HCO_3^{-}(aq)$$

The electrons consumed in the cathodic reaction come from the anodic reaction, iron dissolution:

$$Fe(s) \rightarrow Fe^{2+}(aq) + 2e^{-}$$

When the concentration of ferrous ion and carbonic ion exceed the solubility limit, iron carbonate ($FeCO_3$) will be precipitated on the steel surface.

$$Fe^{2+}(aq) + CO_3^{2-}(aq) \Leftrightarrow FeCO_3(s)$$

Depending on the protectiveness of the iron carbonate film, the corrosion rate may be significantly reduced.

The total cathodic current is the summation of the two currents from the cathodic reactions[26]. The CO_2 corrosion rate is usually controlled by the rate of cathodic reactions, which is limited by the concentration of hydrogen ion and carbonic acid ion which can reach the steel surface.

When pH < 4 and CO_2 partial pressure <1 bar, hydrogen ion reduction is the dominant cathodic reaction. At higher pH (>4) and high partial pressure of CO_2 (>1 bar), direct carbonic acid reduction becomes the rate determining reaction.

From the basic reactions mentioned above, it is clearly seen that CO_2 corrosion is affected by a variety of environmental parameters such as temperature, pH, partial pressure of CO_2, flow velocity, formation of corrosion products, *etc*. The effects are discussed separately in the following paragraphs.

2.1.1.1 Temperature

Temperature has a significant effect on CO_2 corrosion. High temperature accelerates the homogeneous chemical reactions occurring in the bulk as well as the heterogeneous electrochemical reaction occurring on the steel surface by increasing the reaction rate. Temperature also facilitates the mass transfer of corrosive species. Therefore, when formation of corrosion products ($FeCO_3$) is not favorable, an increase of temperature will lead to an increase of corrosion rate. However, the statement that higher temperature leads to a higher corrosion rate is not always true in a CO_2 system. At high pH, an increase of temperature also expedites the kinetics of $FeCO_3$ precipitation and leads to a fast formation of $FeCO_3$ on the steel surface, which may significantly reduce the overall corrosion rate.

It has been reported that the CO_2 corrosion rate in a single phase flow reaches the maximum value when temperature reaches 60°C to 90°C[38].

2.1.1.2 CO_2 partial pressure

The concentration of CO_2 in the liquid phase is directly related to the partial pressure of CO_2. According to Henryǿs law, an increase of partial pressure of CO_2 will lead to an increase of the CO_2 concentration in the liquid phase. As a result, the concentration of carbonic acid is increased which will result in an increase of the corrosion rate by accelerating the direct carbonic acid reduction reaction. However, in an environment favorable for $FeCO_3$ formation, an increase of CO_2 partial pressure will also increase the concentration of CO_3^{2-} ion and facilitate the formation of $FeCO_3$, which will cause a decrease of overall corrosion rate[36].

2.1.1.3 pH

pH relates to the concentration of hydrogen ions in the bulk solution, which is one of the major corrosive species in the CO_2 corrosion system. pH has been shown to play an important role in determining the CO_2 corrosion rate. Generally speaking, lower pH leads to a higher corrosion rate. The pH of the solution also can determine the rate controlling step. Direct hydrogen ion reduction reaction dominates the cathodic reactions when pH and partial pressure of CO_2 are both low. When pH is high, the direct carbonic acid reduction reaction becomes the governing reaction.

In addition to the direct effect on cathodic reaction rate, pH also plays an important role in the formation of $FeCO_3$ by affecting the solubility limit[36]. pH affects the solubility limit of $FeCO_3$ in an inversely proportional way, *i.e.*, the higher the pH level the lower the solubility limit. This suggests that $FeCO_3$ is easy to form at high pH conditions.

2.1.1.4 Flow velocity

Flow velocity has a significant effect on the mass transfer involved in the CO_2 corrosion system. A high flow velocity can increase the concentration of corrosive species on the steel surface by accelerating the mass transfer. If the corrosion mechanism is limited by mass transfer, an increase of flow velocity will lead to an increase of corrosion rate. However, if the rate determining step is under charge transfer (activation) control, flow velocity does not have an effect on CO_2 corrosion.

Flow velocity not only affects the corrosion rate, but also affects the formation of $FeCO_3$ by weakening the film on the surface and carrying more corrosive species to the steel surface. These all result in the formation of less protective $FeCO_3$ film[36]. Extremely high flow velocity may even cause the partial removal of the protective film which may lead to a severe localized corrosion.

2.1.1.5 Formation of corrosion product

The dominant corrosion product in a CO_2 system has been determined to be $FeCO_3$. The protective $FeCO_3$ film can significantly reduce the total corrosion rate by generating a diffusion barrier which limits the diffusion path of the corrosive species to the steel surface[39]. However, un-protective (partially covered) $FeCO_3$ layer or partial removal of the $FeCO_3$ film may lead to localized corrosion, which is much more severe than general corrosion.

2.1.2 H_2S corrosion

H_2S corrosion is also called ñsour corrosionò in the oil and gas field. The effect of H_2S on the corrosivity of production fluids has been recognized by oil and gas field engineers since the 1940s[40]. H_2S corrosion has been studied for over 60 years. However, only a small number of detailed studies have focused on the H_2S corrosion of carbon steel. This is mostly due to the fact that much of the research work was concentrated on the H_2S cracking corrosion of different metallic materials[41-46].

The basics of H_2S water chemistry are well accepted. Similar to carbonic acid, H_2S is a weak acid in an aqueous phase. It dissociates into HS^- and S^{2-} in two steps. The following reactions illustrate the behavior of H_2S in the aqueous phase.

$$H_2S(g) \Leftrightarrow H_2S(aq)$$

$$H_2S(aq) \Leftrightarrow HS^-(aq) + H^+(aq)$$

$$HS^-(aq) \Leftrightarrow S^{2-}(aq) + H^+(aq)$$

Hydrogen ion released from the dissociation reaction is one of the corrosive species. H_2S itself in the aqueous phase may be another corrosive substance that is directly involved in corrosion reactions.

Unlike CO_2 corrosion, in the H_2S corrosion of carbon steel a layer of iron sulfide forms in most situations and the corrosion rate is controlled by the presence of this layer on the steel surface. Depending on the corrosion environment, the morphology of iron sulfide may be quite different. Therefore, the way an iron sulfide forms on the steel surface may have a large impact on the H_2S corrosion mechanism.

It is still not clear exactly how an iron sulfide layer forms on the steel surface in the first place. It is well known that the addition of a small amount of H_2S will immediately reduce the general corrosion rate. This is suggested to be due to the fast formation of mackinawite. It is commonly assumed that the corrosion product layer is formed through the precipitation process when the solubility of the corrosion product exceeds the limit. However, even if the iron sulfide is significantly below saturation in the bulk of the solution, it still forms on the steel surface almost instantaneously. Shoesmith, *et al.* studied the formation of FeS at ambient temperature 1 bar H_2S at a wide pH range from 2.0 to 7.0[47,48]. Iron sulfide was hypothesized to be formed by solid state reaction and precipitation. Sun and Nesic proposed a mechanistic model of general H_2S corrosion in 2007[49]. Based on extensive experimental data, the direct reaction between H_2S and iron in the steel is suggested as the mechanism for formation of the first layer of iron sulfide.

Another assumption on the formation of iron sulfide is that precipitation is the sole formation mechanism. Iron sulfide forms on the steel surface only when the concentration of iron sulfide exceeds the solubility limit. However, in some cases, iron sulfide still forms on the steel surface when the concentration of iron sulfide is highly below saturation in the bulk solution. It is argued that the pH on the steel surface is much higher than the bulk due to the depletion of hydrogen ion by corrosion reaction and excessively accumulated ferrous ion. Therefore, the super-saturation of iron sulfide on the steel surface results in the relatively fast formation of iron sulfide. However, more sophisticated study on surface pH measurement needs to be done to verify these assumptions.

2.2 Weldment corrosion

The above sections briefly summarized the basic mechanism of CO_2 and H_2S corrosion. Weldments are broadly used in the oil and gas industry and are exposed to CO_2

and H_2S aqueous environments. All the basic concepts of CO_2 and H_2S corrosion can also be applied to weldment corrosion. However, due to the special structure of weldments, the way to look at the weldment corrosion should be different.

The purpose of applying weldment is to join two metallic structures. As mentioned previously, weldment consists of three parts: weld, HAZ, and parent metal[1]. The welding process involves extremely intense heat, which may change the structure of the metal close to the weld. Therefore, even if there are no compositional differences between the weld material and the parent metal, the heating may still lead to a dissimilarity of the metal around the weld, which may result in a galvanic couple between the segments of the weldment. The preferential corrosion of weldment caused by galvanic effects is the major concern for weldment corrosion. Therefore, to better understand the environmental effects on weldment corrosion, it is necessary to understand the basics of galvanic corrosion.

When a structure is made of more than one material, the occurrence of severe corrosion may be caused by galvanic corrosion[50]. According to Hack[50], three prerequisites have to be satisfied to make the galvanic corrosion occur. First, at least two different materials have to be present in the corrosion system. In this case, it is the same material but the structure of one of them is changed by intense heat. Second, the materials have to be electrically connected. The last prerequisite is that the materials have to be exposed to a corrosive environment. When galvanic corrosion occurs, the corrosion rate of one material may increase due to the galvanic effect while the corrosion rate of the other may decrease or remain mostly unchanged.

Galvanic corrosion is not always undesirable and it also can have beneficial effects[50]. The galvanic corrosion theory is the basis for sacrificial cathodic protection, which is conducted by coupling a less noble cheaper material with a more noble material which is to be protected. The method has been widely applied to protect pipelines, tanks, ships, etc. against corrosion problems.

When two different metals are present in the same corrosive environment, we can identify for each metal its own anodic and cathodic reactions. At equilibrium, the electrochemical potential and individual currents are illustrated in Figure 2 using Fe and Cu as examples[50]. In this case, there is no electric contact between two metals. When an electrical contact between two metals is established, the equilibriums of both metals are disturbed as the potential becomes the same. Consequently, a current will be generated flowing from the more positive metal to the more negative metal to reestablish the equilibrium potential. This current is called the galvanic current. As shown in Figure 3, the anodic reaction of Fe is accelerated by the galvanic effect. The anodic reaction of Cu is retarded for the same reason.

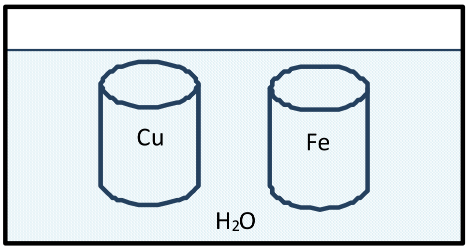

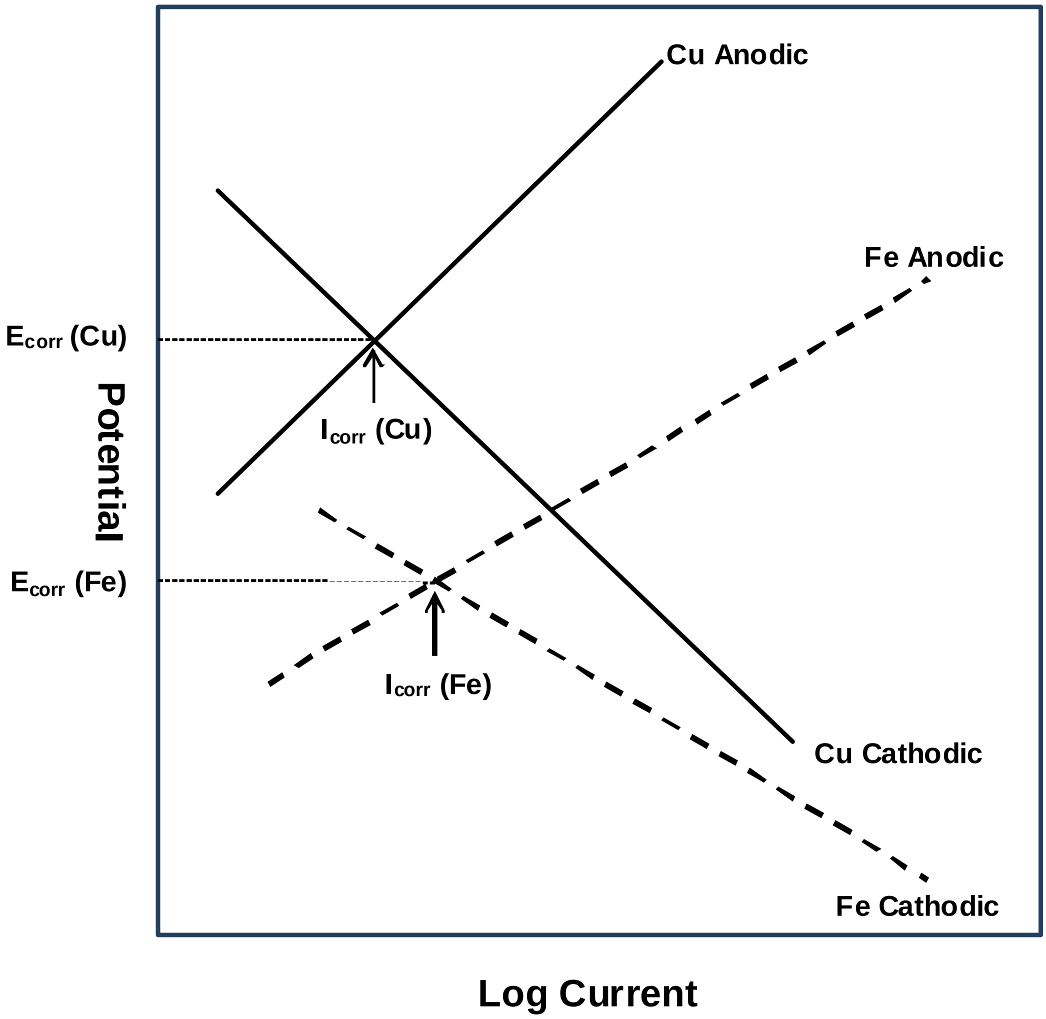

Figure 2. Evans diagram of two uncoupled metals[50].

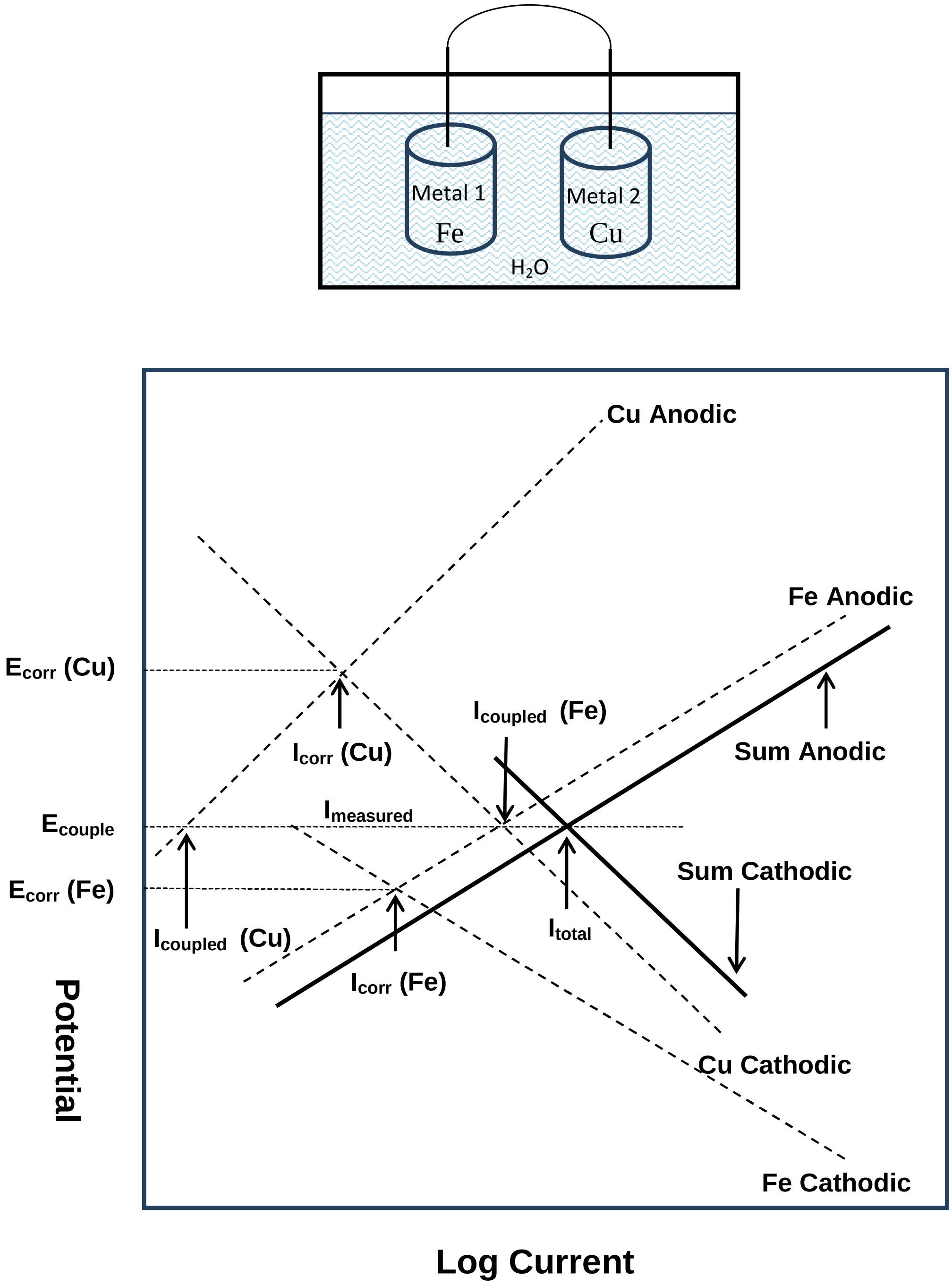

Figure 3. Evans diagram of two coupled metals[50].

For weldment corrosion, the worst case scenario is when weld metal or HAZ becomes the less noble materials (having low corrosion potential) considering their small surface area. The added current by galvanic effects is going to be consumed by a small surface area of weld or HAZ, which may lead to a severe corrosion problem. However, if the parent metal becomes the less noble part, the weld and HAZ are cathodically protected. Even if the anodic reaction of parent metal is accelerated, the corrosion rate of parent metal will not increase significantly due to the humongous surface area of the parent metal.

CHAPTER 3 RESEARCH OBJECTIVES AND TEST METRICES

3.1 Objectives

The overall objective of this study is to investigate the environmental effects on intrinsic and galvanic corrosion of carbon steel weldment. The objective is achieved by applying the following strategy:

Task 1

Investigating the environmental effects on weldment corrosion in pure CO_2 environments with respect to:

- Temperature
- Chloride concentration
- Acetic acid
- Inhibitor
- Combined effect of acetic acid and inhibitor
- Iron carbonate film

Task 2

Investigating the environmental effects on weldment corrosion in CO_2 / H_2S environments with respect to:

- Acetic acid
- Inhibitor

Task 3

Applying new electrochemical measurement methods to investigate the environmental effects on weldment corrosion:

- Electrochemical noise measurement[51,52]
- Micro-electrochemical cell application[53,54]

Task 4

- Corrosion rates calculation by LPR measurement
- Galvanic corrosion rate calculation by using galvanic current
- Electrochemical noise analysis
- Observe the surface morphology of coupons after corrosion by Scanning Electron Microscope and Infinite Focus Microscope.
- Identify elements presence and distribution on the specimen after corrosion by Energy Dispersive Spectroscopy (EDS).

3.2 Test Matrices

The following test matrices were defined to achieve the objective proposed above. The test parameters were defined according to the specific tasks and are shown in Table 1 through Table 5 respectively.

Table 1. Test matrix for experiments investigating temperature and chloride concentration effects in CO_2 environment

Material	Standard Weldment
Solution	1, 5, 10 wt% NaCl purged with CO_2
Total pressure (bar)	1
Temperature (°C)	25, 60
pH	5.0
Test duration	6 days
Measurement methods	Linear Polarization Resistance
	Galvanic Current Measurement
	SEM

Table 2. Test matrix for experiments investigating inhibitor and acetic acid effects in CO_2 environment

Material	Standard Weldment		
Solution	1wt% NaCl purged with CO_2		
	100 ppm Undissociated Acetic acid	20 ppm Inhibitor	100 ppm Undissociated Acetic acid and 20 ppm Inhibitor
Total pressure (bar)	1		
Temperature (°C)	60		
pH	5.0		
Test duration	6 days		
Measurement methods	Linear Polarization Resistance		
	Galvanic Current Measurement		
	SEM		

Table 3. Test matrix for experiments investigating iron carbonate film effects in CO_2 environment

Material	Standard Weldment		
Solution	1 wt% NaCl purged with CO_2		
Total pressure (bar)	1		
Temperature (°C)	80		
	Film formation	Partially film dissolution	Grey zone
pH	6.6	5.6~5.8	
Saturation of $FeCO_3$	200	0.04	0.5~2.0
Test duration	2.3 days	4 hrs	7 days
Measurement methods	Linear Polarization Resistance		
	Galvanic Current Measurement		
	Electrochemical Noise Analysis		
	SEM		

Table 4. Test matrix for experiments investigating inhibitor and acetic acid effects in CO_2/H_2S environment

<table>
<tr><td>Material</td><td colspan="2">Standard Weldment</td></tr>
<tr><td rowspan="2">Solution</td><td colspan="2">1 wt% NaCl purged with CO_2 and 50 ppm H_2S</td></tr>
<tr><td>100 ppm Undissociated Acetic acid</td><td>20 ppm inhibitor</td></tr>
<tr><td>Total pressure (bar)</td><td colspan="2">1</td></tr>
<tr><td>Temperature (ŰC)</td><td colspan="2">60</td></tr>
<tr><td>pH</td><td colspan="2">5.0</td></tr>
<tr><td>Test duration</td><td colspan="2">6 days</td></tr>
<tr><td rowspan="3">Measurement methods</td><td colspan="2">Linear Polarization Resistance</td></tr>
<tr><td colspan="2">Galvanic Current Measurement</td></tr>
<tr><td colspan="2">SEM</td></tr>
</table>

Table 5. Test matrix for experiments investigating application of micro-electrochemical approach to CO_2 corrosion measurements

<table>
<tr><td>Material</td><td>Standard Weldment</td></tr>
<tr><td>Solution</td><td>1 wt% NaCl purged with CO_2</td></tr>
<tr><td>Total pressure (bar)</td><td>1</td></tr>
<tr><td>Temperature (ŰC)</td><td>Room temperature</td></tr>
<tr><td>pH</td><td>3.9</td></tr>
<tr><td>Test duration</td><td>1 days</td></tr>
<tr><td>Test facilities</td><td>Glove box</td></tr>
<tr><td rowspan="3">Measurement methods</td><td>Linear Polarization Resistance</td></tr>
<tr><td>Galvanic Current Measurement</td></tr>
<tr><td>SEM</td></tr>
</table>

CHAPTER 4 EXPERIMENTAL SETUP AND PROCEDURE

All the experiments in this study were conducted in glass cells under atmospheric pressure conditions. The following paragraphs describe the experimental setup and procedures.

4.1 Specimen preparation

A weldment specimen was made from a carbon steel pipe sample that had a weld. All experiments were performed on the standard weldment which has no alloying metals in the weld material. The compositions of parent and weld materials are given in

Table 6. It appears that there is no significant difference between the compositions of parent and weld material.

Table 6. Elemental analysis (wt%) of parent metal and filler material of the weldment.

Element	**Al**	**As**	**C**	**Co**	**Cr**	**Cu**
Parent	0.037%	0.004%	0.21%	0.002%	0.049%	0.021%
Weld	0.013%	0.005%	0.12%	0.002%	0.042%	0.046%
Element	**P**	**S**	**Sb**	**Si**	**Sn**	**Ta**
Parent	0.013%	0.005%	0.007%	0.27%	0.004%	0.030%
Weld	0.012%	0.007%	0.008%	0.39%	0.004%	0.031%
Element	**Fe**	**Mn**	**Mo**	**Nb**	**Ni**	n/a
Parent	98.3%	1.01%	0.010%	0.010%	0.024%	n/a
Weld	98.2%	1.07%	0.013%	0.005%	0.033%	n/a
Element	**Ti**	**V**	**W**	**Zn**	**Zr**	n/a
Parent	0.003%	0.002%	0.016%	0.001	0.002%	n/a
Weld	0.002%	0.003%	0.014%	0.001%	0.003%	n/a

Sample segment A wedge shape weldment segment was cut from a pipeline to make a weldment specimen. The machined specimen, prior to separation of weldment segment components, was 35 mm long, 8mm wide and 13 mm thick. The segment was polished with 150 grit sandpaper on the underside and sides where the weld is exposed. The specimen was then etched with 3% Nital (3% Nitric acid in ethanol) solution to expose the region of the weld and HAZ (as shown in Figure 4). The colored demarcations between weld, HAZ, and parent materials were added after visual observation.

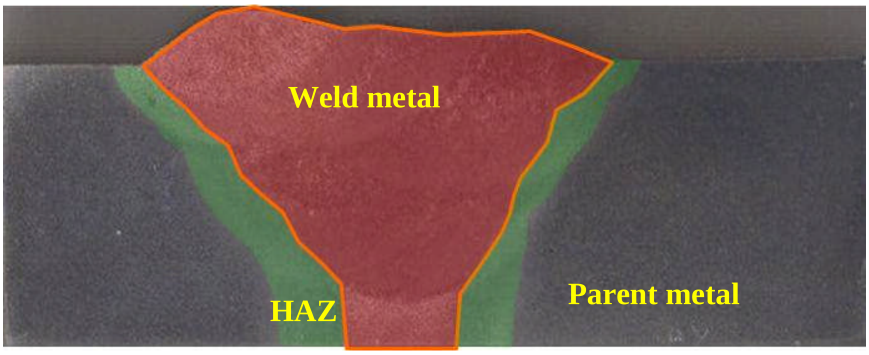

Figure 4. A schematic of the weldment materials used in the experiments

Weldment manufacturing The specimen was cut using a demarcation line on the side of the weld for the portion of the HAZ nearest the weld and on the side of the parent material for the portion of the HAZ away from the weld (shown in Figure 5). In order to use the electrochemical noise method, two weld material segments were needed, so the weld element was cut in half. After that, wires were soldered to each segment, the segments were arranged in a mold, and then the mold was filled with epoxy. The six segments were then separated from each other so that external electrical connections could be made to each segment. The finished specimen is shown in Figure 6. Two groups of segments were included in the finished specimen. The reason why is explained in the following paragraphs.

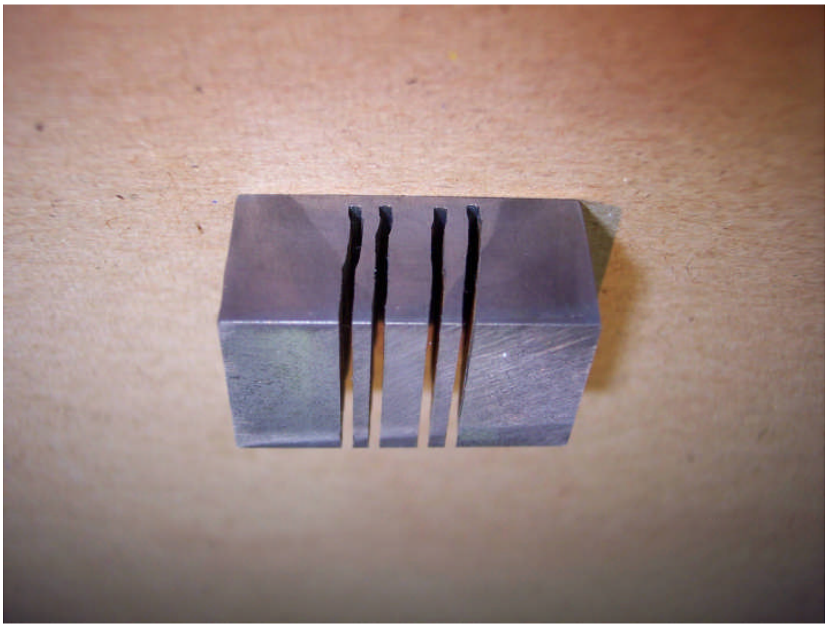

Figure 5. Metal cut including the welded section of the sample.

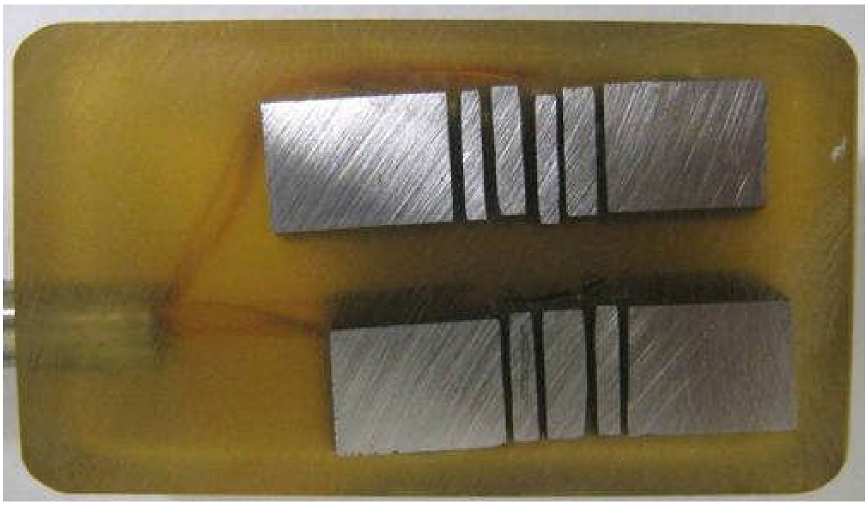

Figure 6. A picture of the weldment sample used in the experiment.

Each weldment surface was polished by silicon carbide sand paper, up to 600 grit, before it was tested. After polishing, the specimen was immersed in an isopropyl alcohol ultrasonic bath for 1 to 2 minutes and then air dried.

4.2 Experimental procedure

The experiment was performed in a glass cell as shown in Figure 7. A Saturated Calomel Electrode was used as the reference electrode. The counter electrode was a platinum wire. The glass cell was filled with 2 liters of de-ionized water and the required amount of NaCl to meet the designated chloride ion concentration. Cell temperature was controlled by a hot plate with a thermocouple feedback. Before the test, the solution was deoxygenated by purging with CO_2 gas for 40 minutes to 1 hour. Purging of the glass cell with CO_2 was maintained during the test period. When the desired temperature was obtained, the pH of the test solution was adjusted from equilibrium pH to the desired pH by adding a deoxygenated sodium bicarbonate solution. A weld segment specimen was then placed into the solution and all electrical connections were made externally for electrochemical monitoring.

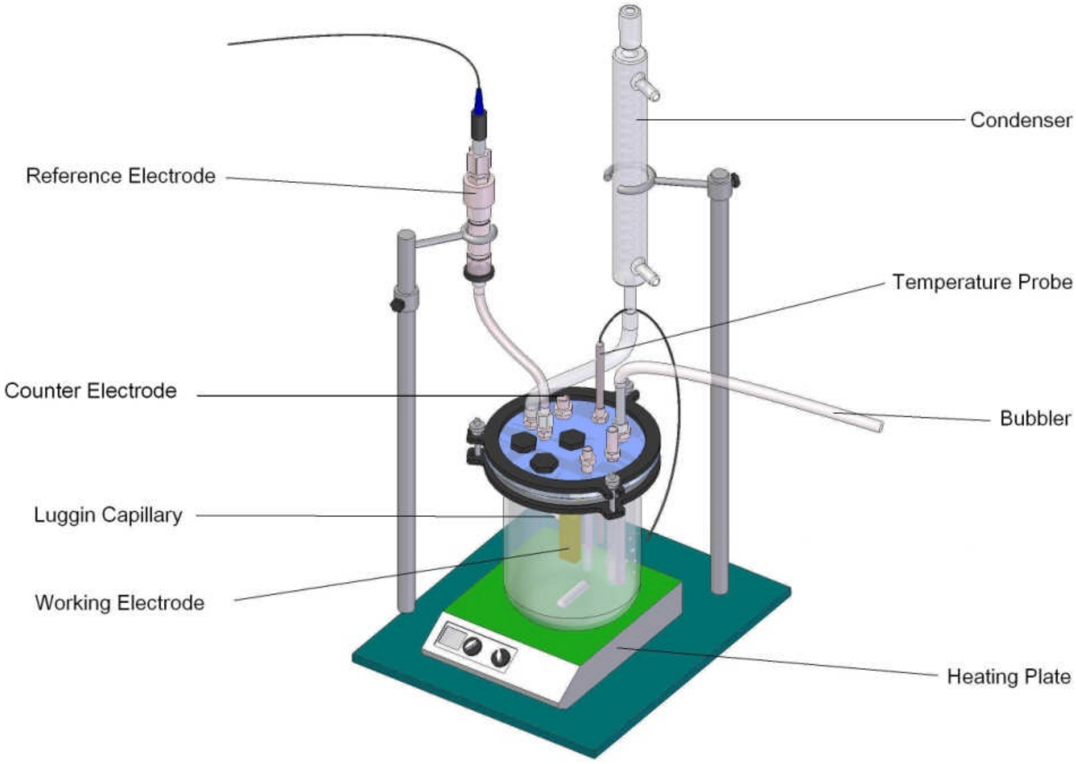

Figure 7. Electrochemical Glass-cell Set-up

Two groups of weld elements were sealed by epoxy in one weldment specimen as shown in Figure 8. One group was always uncoupled throughout the entire test period for linear polarization resistance and potential measurements to observe general intrinsic corrosion rate results without the influence of galvanic corrosion. To simulate the weldment service in reality, the other group was always coupled and would be used to measure the galvanic currents.

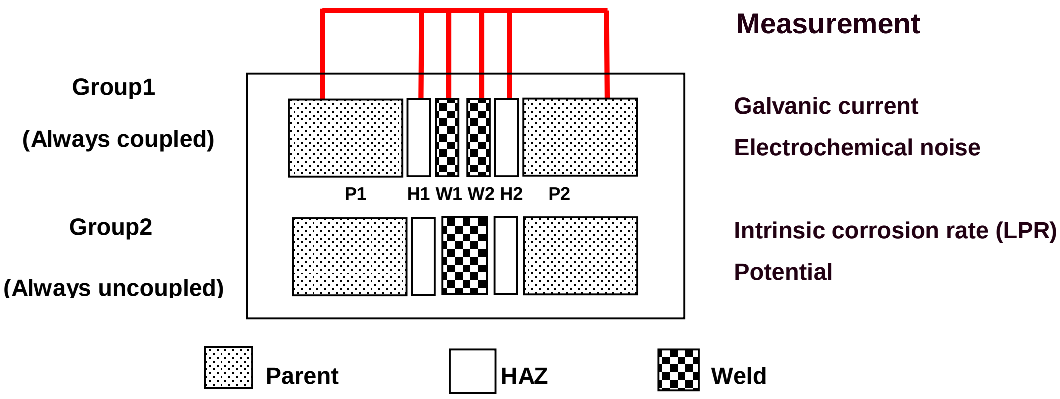

Figure 8. Schematic representation of sample showing coupled segments and uncoupled segments of the weldment with electrochemical measurement methods for each set of segments listed.

CHAPTER 5 MEASUREMENT TECHNIQUES

Electrochemical measurement techniques were used in this study. Linear polarization resistance (LPR) was used to measure the intrinsic corrosion of each segment of the weldment. EIS was used to measure the solution resistance which is a part of the resistance measured by LPR. Galvanic current measurement was applied to measure the galvanic current between each segment. Electrochemical noise was also applied to monitor if a localized corrosion event occurs.

Surface analysis techniques, including scanning electron microscopy (SEM), energy-dispersive X-ray spectroscopy (EDX), were used to identify the surface morphology and analyze the compositions of the corrosion products.

5.1 Linear polarization resistance (LPR)

Linear polarization resistance is a very effective technique that is used for the instantaneous measurement of the corrosion rate. In the LPR technique, a small potential (typically 5-20 mV depending on the stability of the potential in the system) is applied to a corroding steel sample in an aqueous solution. Then the resulting current response is measured. This small potential perturbation is usually applied step-wise, starting below the open circuit potential and ending above the open circuit potential. The linearized polarization resistance is then obtained by calculating the ratio of the applied potential and the resulting current. The corrosion rate of the steel sample can then be calculated from the polarization resistance by applying basic electrochemical theory.

LPR technique has been widely used in research laboratories as well as in industry for monitoring programs because of its reasonable accuracy, ease of use, simplicity and fast response. However, LPR also has its disadvantages[55]. In order to use the LPR technique, several assumptions have to be accepted. First of all, the corrosion attack has to be a uniform as LPR is not able to measure any localized corrosion. Second, the cathodic and anodic reactions involved in the corrosion process have to be under charge transfer (activation) control. In addition, the potential in the system has to be relatively stable.

5.2 Electrochemical impedance spectroscopy (EIS)

Electrochemical impedance spectroscopy (EIS) is another electrochemical measurement technique that can be used to measure the corrosion rate. Different from LPR which uses DC polarization, EIS technique measures the corrosion rate of the steel sample using AC polarization. In EIS technique, a small voltage typically between 5 to 50 mV, is applied to a steel specimen over a range of frequencies of 0.001 Hz to 100,000 Hz[51]. One can obtain the real and imaginary components of the impedance response of the system. From the impedance response, solution resistance, charge transfer resistance and mass transfer resistance can be separated by using a specific model of the process[51]. In this study, EIS was only used to measure the solution resistance which was subtracted from the polarization resistance measured by LPR.

5.3 Galvanic current

Unlike LPR and EIS that measure the corrosion rate of a single steel sample, galvanic current measurement technique actually measures the current flowing between two steel electrodes. Galvanic current measurement is especially helpful in studying the weldment corrosion due to the dissimilarity of each segment of the weldment.

The potential difference and the current flowing between two metals were measured during the galvanic current measurement. Potential difference between two disconnected electrodes is the indication of which metal will likely suffer increased corrosion, but it will not directly give the information of the magnitude of the increase, which can be indicated by galvanic current measurement. The general procedure of the galvanic current measurements is described below.

In a typical laboratory test, two metal samples are polished following the standard procedure and then put into the electrolyte, simulating the corrosion environment. Normally, the two metal samples are placed face to face that gives uniform current distribution so that the current density can be calculated easily. The electrical connection between two metal samples can be made externally through a resistor as illustrated in Figure 9[53]. A reference electrode placed in between two metal samples and an electrometer can be used to measure the potential difference. A resistor and a voltmeter are used to measure the current flowing between two metal samples. The resistor should be properly selected so that the IR drop cross the resistor is not more than 5 to 10 mV. A resistor with large resistance will result in a large voltage difference between two samples, which may not represent the real conditions. Too small of a resistor makes too small of an IR drop to accurately measure the galvanic current. A zero resistance ammeter can be used to overcome this difficulty. A schematic of a zero-resistance ammeter is shown in Figure 10[50]. The feedback resistor is relatively small and an optional amplifier is connected to magnify the current signal.

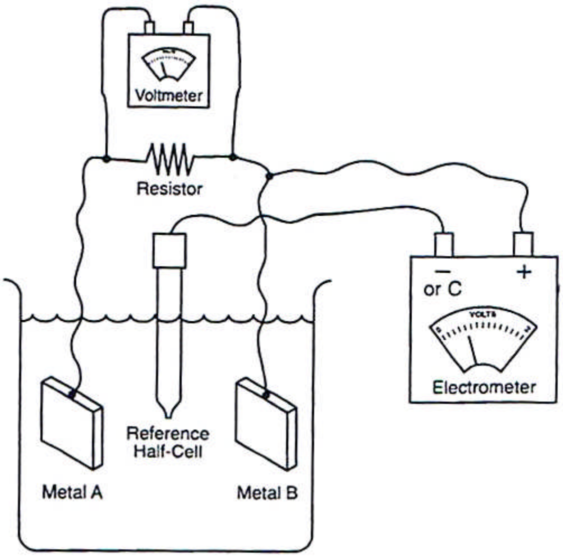

Figure 9. A schematic of a typical galvanic current measurement[50].

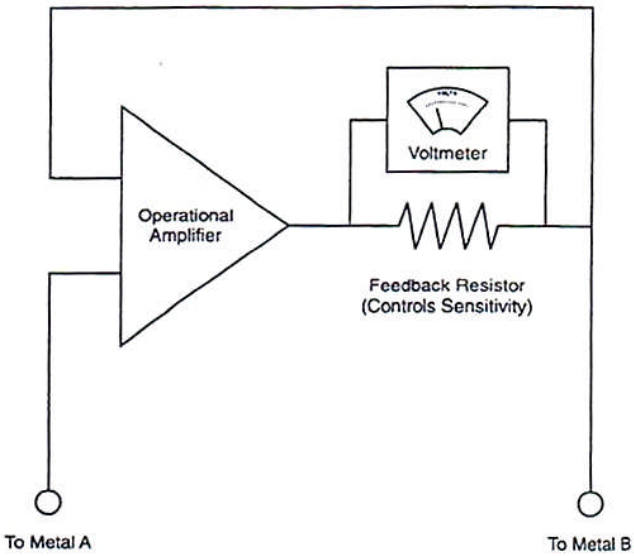

Figure 10. A schematic of zero resistance ammeters[50].

5.4 Electrochemical noise (EN)

Electrochemical noise (EN) is a relatively novel technique used in corrosion research. It typically refers to naturally occurring fluctuations in corrosion potential and current during the corrosion process. An electrochemical noise measurement instrument can monitor the electrochemical potential noise (EPN) and the electrochemical current noise (ECN)[56,57]. The monitoring of EPN and ECN is usually done at the same time. A sudden change of the corrosion potential noise may indicate a change in the state of the corrosion processes, while fluctuations in the corrosion current indicates a change of the corrosion kinetics.

A sudden fluctuation of potential and current noise, also called a transient is usually an indicator of the initiation of localized corrosion. Therefore, the electrochemical noise measurement technique has been used to differentiate between general and localized attack. The severity of localized attacks can also be measured by the intensity of the noise transients. This is the most important advantage over other electrochemical techniques.

Except for the detection of the localized corrosion, the combination of the measurement of EPN and ECN can also be used to derive the general corrosion rate by using statistical analysis of the data[56,57]. In this study, the electrochemical noise measurement technique was mainly used to detect the galvanic current and possible localized corrosion.

5.5 Scanning electron microscopy

Scanning electron microscopy (SEM) was applied to this study to observe the morphology of the corrosion products generated on the weldment specimen surface. SEM enabled a clear view of the specimen surface and a display of the morphology and critical features of the corrosion products on the specimen surface, which may play an important role in explaining the corrosion phenomena observed in this study.

SEM is a type of an electron microscope that can generate high quality and high magnification images of a sample surface by scanning with a high energy electron beam. The electrons interact with the atoms in the surface features of the samples. The electrons lose energy during the process of repeated random scattering and absorption on the specimen surface. The energy exchange between the electron beam and the sample can be detected by the specialized detector, which then creates signals that represent the information on the sample surface. The high resolution images of a sample surface are generated after the signals are processed. The signals are converted into a high resolution image after processing. An example of a SEM image of iron sulfide[58] is shown in Figure 11.

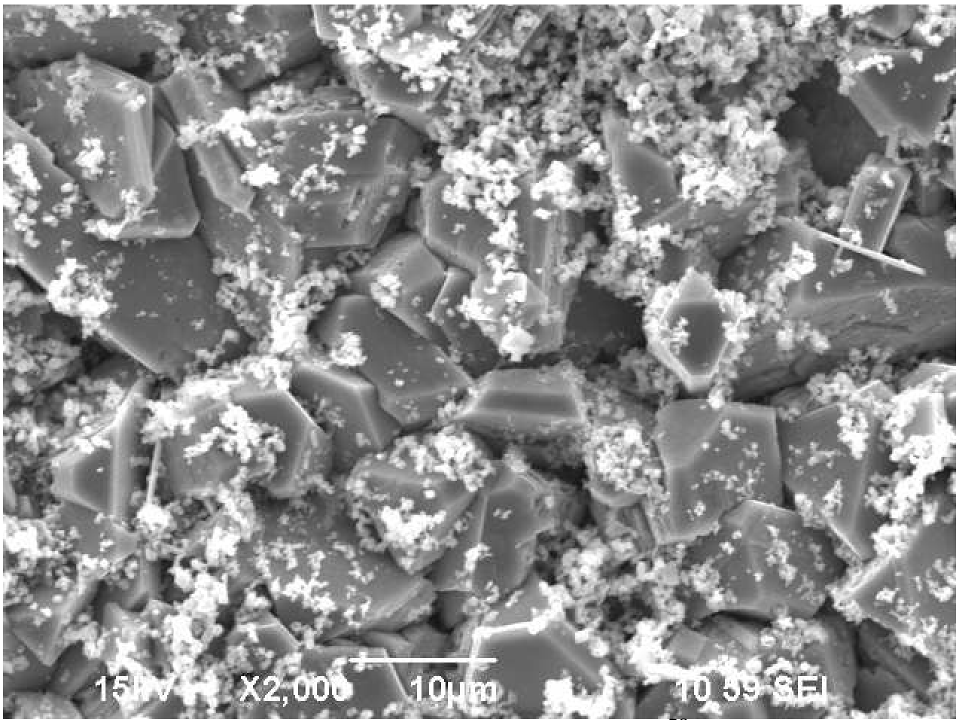

Figure 11. Example of a SEM image of an iron sulfide layer[58].

For conventional imaging in the SEM, the sample has to be electrically conductive. For a non-conductive or less conductive surface, the high energy electrons tend to accumulate on the sample surface resulting in a charging phenomenon. This may lead to a false image, image artifacts or unclear image. Therefore, in order to obtain a high quality SEM image, the non-conductive or even conductive surface needs to be gold coated before being scanned by SEM.

In this study, SEM provided a high quality visual image of the weldment specimen surface. It helped to better understand the corrosion phenomena occurring during the experimental studies.

5.6 Energy-dispersive X-ray spectroscopy (EDX)

Energy-dispersive X-ray spectroscopy is used for the elemental analysis or chemical characterization of a specimen. It is usually integrated into the SEM instrument and is commonly used in conjunction with SEM. SEM image and EDX analysis together are able to correlate the visual image and the elemental analysis. However, EDX cannot directly determine the actual chemical composition of the samples.

When an EDX measurement is started, a high-energy beam of electrons, or a beam of X-rays, bombard the surface of the sample being studied, which may lead to a huge impact to the atoms of the sample. The high energy incident beam may excite an electron in an inner shell. The excited electron may then escape from the inner shell and leave an electron hole. An electron from the outer shell then fills the hole left by the escaped electron. During this electron replacement process, a difference in energy between the outer shell and the inner shell may be released in the form of an X-ray, which can be measured by an energy-dispersive spectrometer. An energy difference between the high energy shell and low energy shell is unique for each specific element. By measuring the energy difference, the elemental composition of the sample may be detected. An example of EDX analysis is shown in Figure 12[59].

In this study, EDX analysis was used to determine the elemental composition of the corrosion products generated on the weldment sample surface.

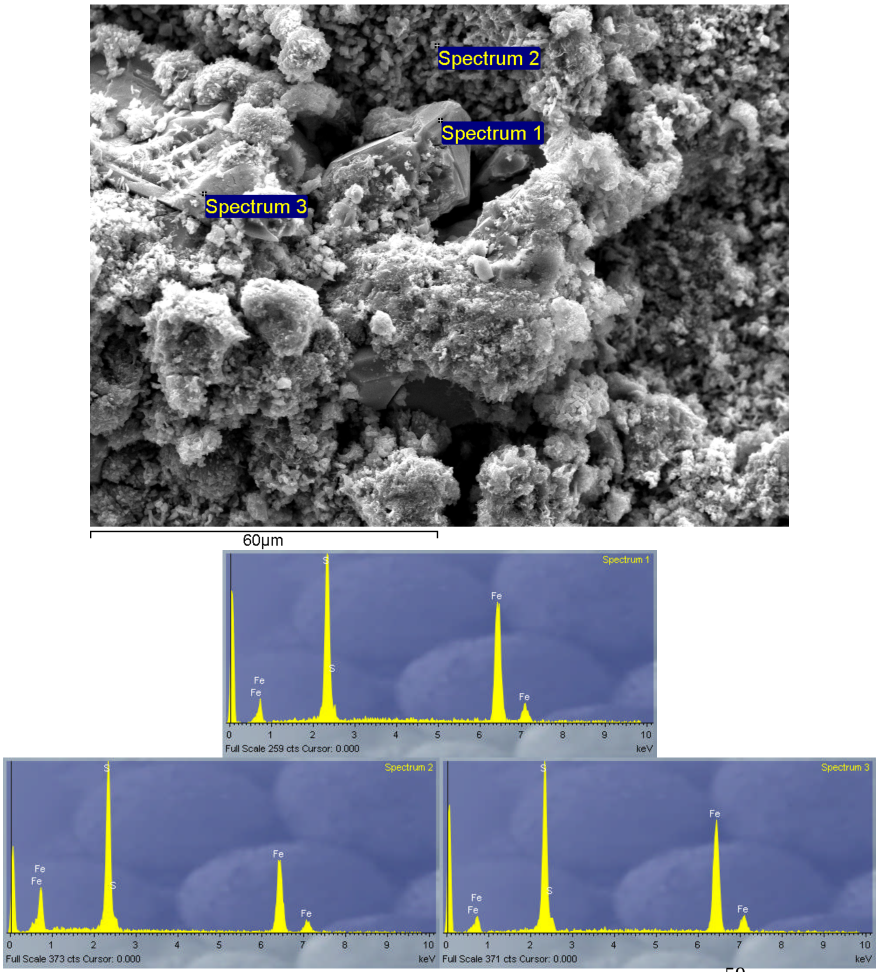

Figure 12. Example of SEM and EDX data for an iron sulfide layer[59].

CHAPTER 6 EXPERIMENTAL RESULTS AND DISCUSSION

According to the test strategy described in the previous sections, the experimental plan was executed in three main parts: (1) environmental effects in a sweet system, (ii) environmental effects in a sour system and (iii) the application of a micro-electrochemical cell. Numerous experiments have been performed to study the environmental effects on weldment corrosion. The results are explained in the following paragraphs.

6.1 Environmental effects on weldment corrosion in sweet system

Various environmental effects including temperature, chloride concentration, acetic acid, inhibitor, combined effect of acetic acid and inhibitor and iron carbonate film on weldment corrosion have been investigated in a CO_2 system. The intrinsic corrosion rate of each segment and galvanic current flowing between each segment were measured. Electrochemical noise measurement was also conducted to monitor the possible localized corrosion events. The specimen surface was inspected to support the noise data at different test conditions.

Considering the typical values of anodic Tafel slope (0.04 V/dec) for iron dissolution and cathodic Tafel slope (-0.12 V/dec) for proton and carbonic acid reduction, it would be expected that about 3/4 of the galvanic current relates to changes in the total corrosion rate. The total coupled corrosion rate can be obtained from the uncoupled intrinsic corrosion rate and the galvanic current rate/effect according to the following equations:

$$Coupled\ \ corrosion\ \ rate_{\ anode} = Uncoupled\ \ corrosion\ \ rate_{anode} + \frac{3}{4} Galvanic\ \ corrosion\ \ rate$$

$$Coupled\ \ corrosion\ \ rate_{\ cathode} = Uncoupled\ \ corrosion\ \ rate_{cathode} - \frac{3}{4} Galvanic\ \ corrosion\ \ rate$$

The derivation of the above equations is included in the Appendix.

6.1.1 The effects of temperature and chloride concentration

The effects of temperature and chloride concentration on the weldment corrosion were studied in the same series of tests. The results are summarized below.

6.1.1.1 Experiments done at 25^{o}C, pH 5.0, 1bar total pressure, and 1, 5, 10 wt% NaCl

Experimental data were interpreted in three categories: intrinsic corrosion rate, galvanic corrosion rate and surface analysis.

Intrinsic Corrosion Rates The LPR intrinsic corrosion rates of uncoupled parent, HAZ, and weld materials with time at 25^{o}C, different chloride concentrations (1, 5 or 10 wt% NaCl) are shown in Figure 13, Figure 14, and Figure 15 respectively. It appears that the intrinsic corrosion rate does not vary significantly for the various segments. The steady increase over time is due to the development of the iron carbide (cementite) layer which is actually the uncorroded portion of the steel. The chloride concentration effects on the intrinsic corrosion rate are summarized in

Table 7. It is clearly seen that the intrinsic corrosion rate of each segment did not change significantly when salt concentration was changed from 1 wt% to 5 wt%. However, when salt concentration was further increased to 10 wt%, corrosion rates of all three segments deceased. This may be due to the absorption of chloride ions on the steel

surface, thus slowing down the corrosion by limiting the surface area available to corrosive species[63].

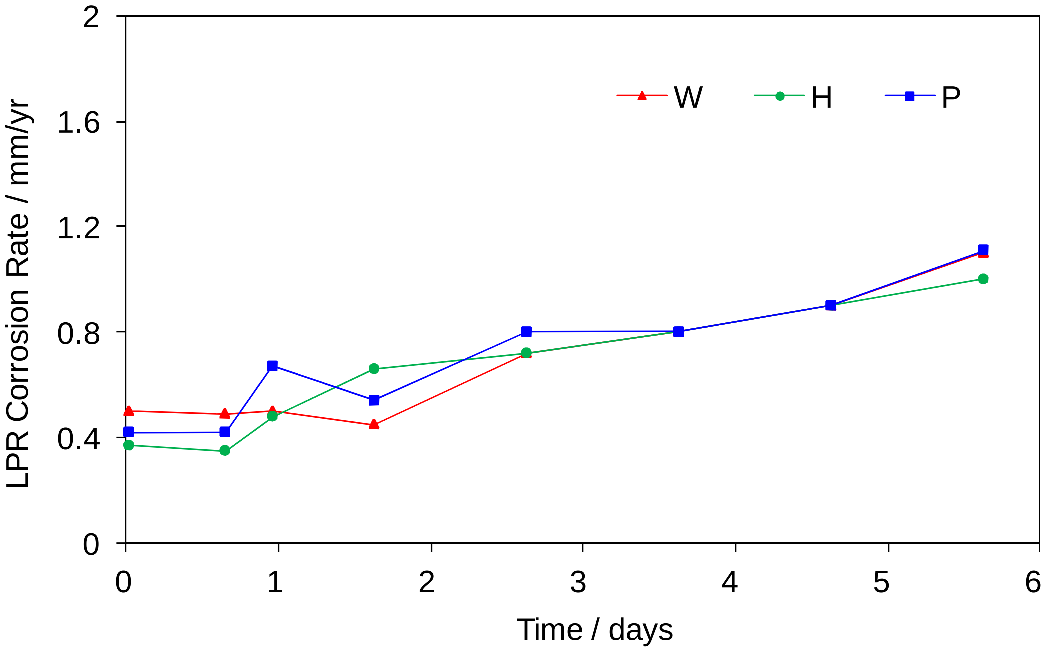

Figure 13. Intrinsic corrosion rate of uncoupled weldment vs. time at 1 wt% NaCl, 25ÜC.

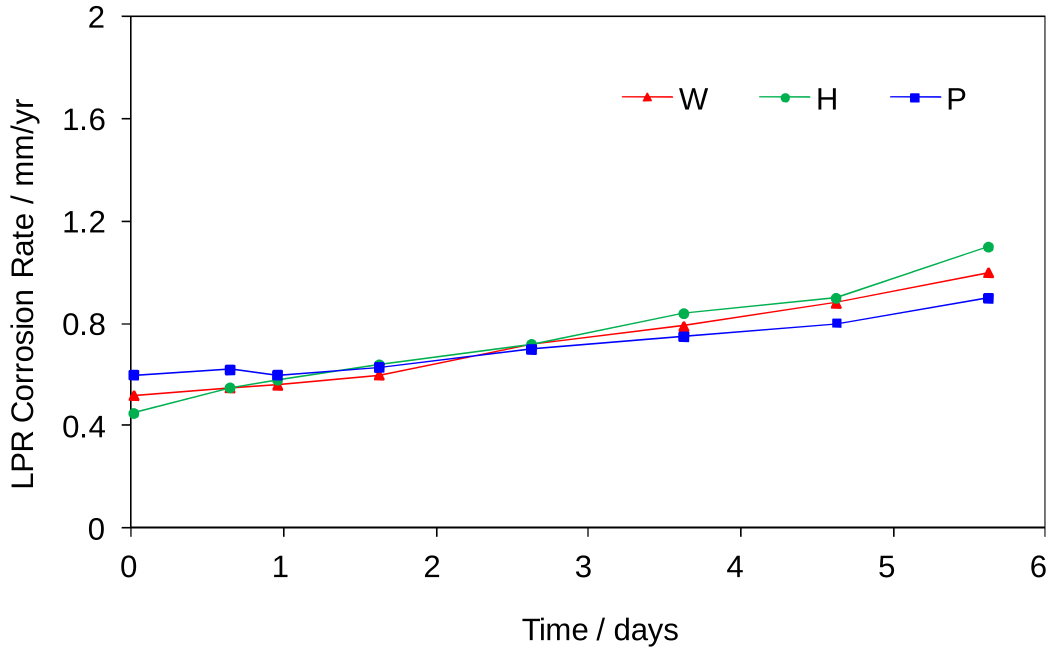

Figure 14. Intrinsic corrosion rate of uncoupled weldment vs. time at 5 wt% NaCl, 25Ü C.

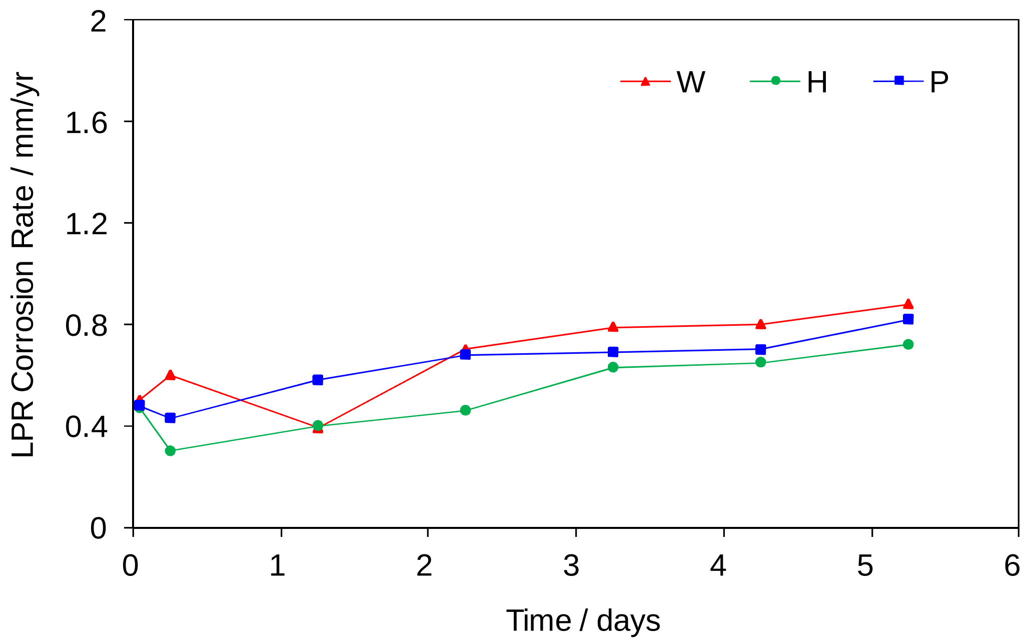

Figure 15. Intrinsic corrosion rate of uncoupled weldment vs. time at 10 wt% NaCl, 25Ü C.

Table 7. Average intrinsic corrosion rates of weldment segments at 25ºC (P = parent metal, H = heat affected zone metal, W = weld metal).

	1 wt% NaCl			5 wt% NaCl			10 wt% NaCl		
	P	H	W	P	H	W	P	H	W
Average intrinsic corrosion rate (mm/yr)	0.74	0.71	0.71	0.71	0.75	0.73	0.65	0.52	0.68

Galvanic Currents The galvanic current measurement results of coupled segments at different salt concentrations are shown in Figure 16, Figure 17, and Figure 18. According to the test results, it appears that parent and weld metal did not show consistent polarity. However, considering the total testing time (6 days), the weld metal tends to exhibit anodic behavior with respect to the other segments while the HAZ is the neutral section. For the same testing time, the parent steel was the more noble metal acting as a cathode. The test results also show that the galvanic current of the weld metal was about 4 µA and the galvanic current of the parent metal was around - 4µA. The increase of chloride concentration from 1 wt% to 5 wt% and 10 wt% does not appear to affect the magnitude and polarity of the galvanic currents.

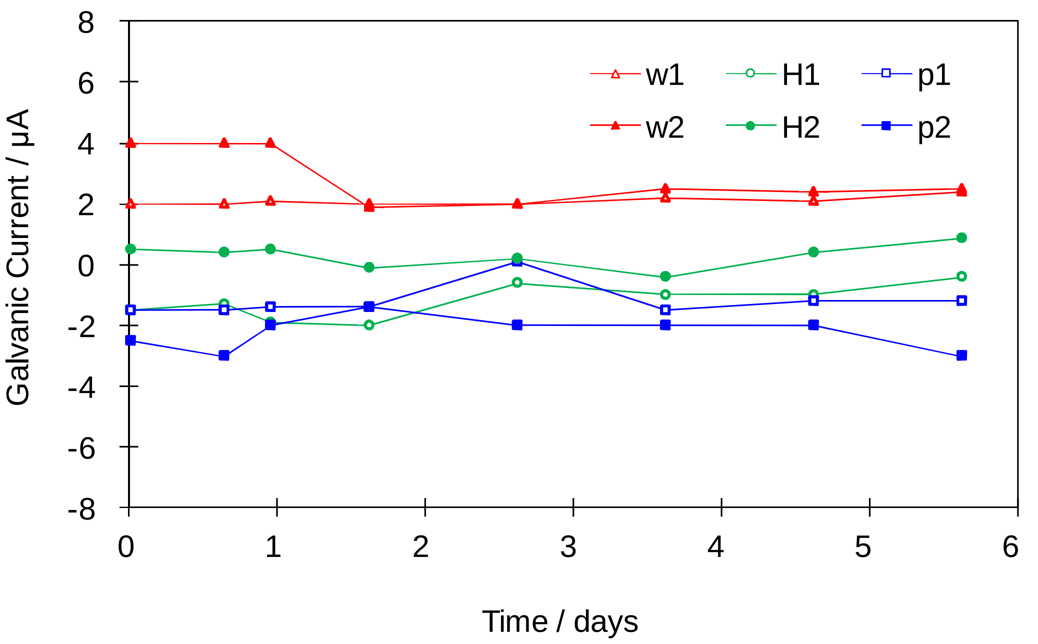

Figure 16. Galvanic current of coupled weldment vs. time at 1 wt% NaCl, 25ÜC.

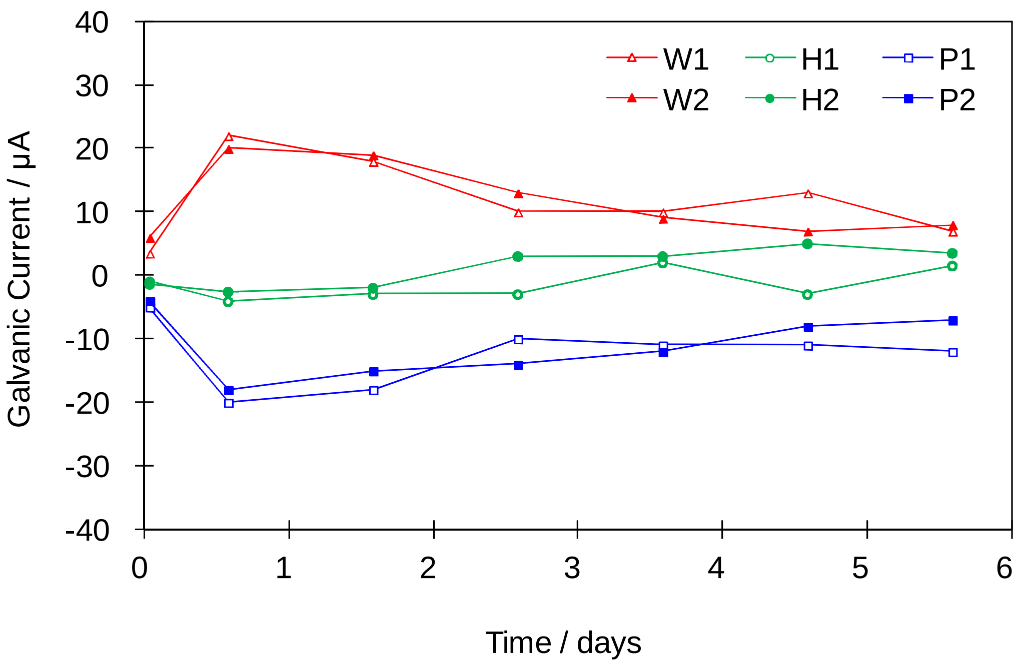

Figure 17. Galvanic current of coupled weldment vs. time at 5 wt% NaCl, 25ÜC.

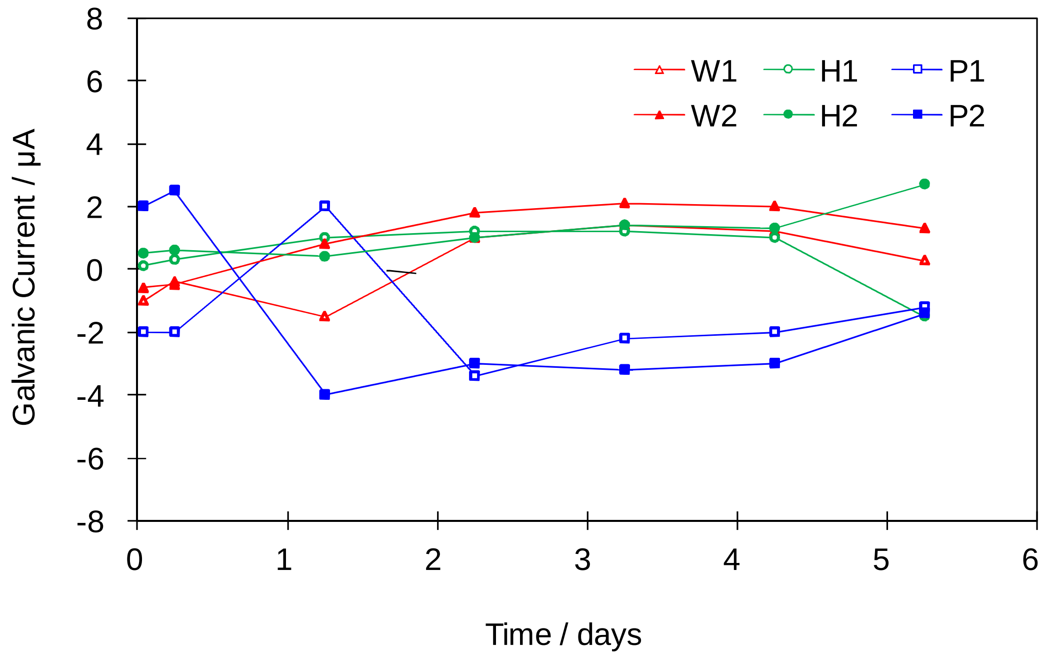

Figure 18. Galvanic current of coupled weldment vs. time at 10 wt% NaCl, 25Ŭ.

The galvanic effects on the total corrosion rate of each segment of weldment are also clarified by comparing them with the intrinsic corrosion rate results. The calculated total corrosion rates of the parent metal, the HAZ metal, and the weld metal at 1 wt% NaCl, 25Ŭ are shown in Figure 19, Figure 20, and Figure 21 respectively. It appears that the corrosion of parent metal as well as HAZ was mitigated by the galvanic effect. On the other hand, the galvanic effect accelerated the corrosion of weld metal. However, the magnitude of galvanic currents at all test conditions is relatively small; consequently, the galvanic current did not affect the total corrosion process significantly. As shown earlier, chloride ions did not show a considerable effect on the magnitude of galvanic current.

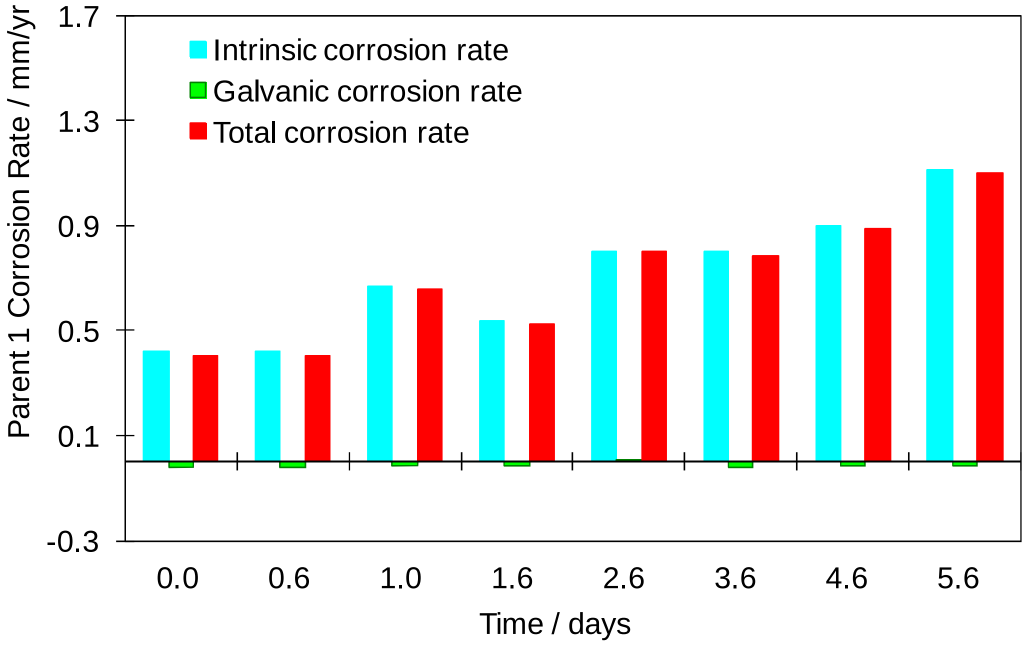

Figure 19. Corrosion rate of Parent 1 metal compared to the intrinsic corrosion rate and galvanic corrosion rate at 1 wt% NaCl, 25℃.

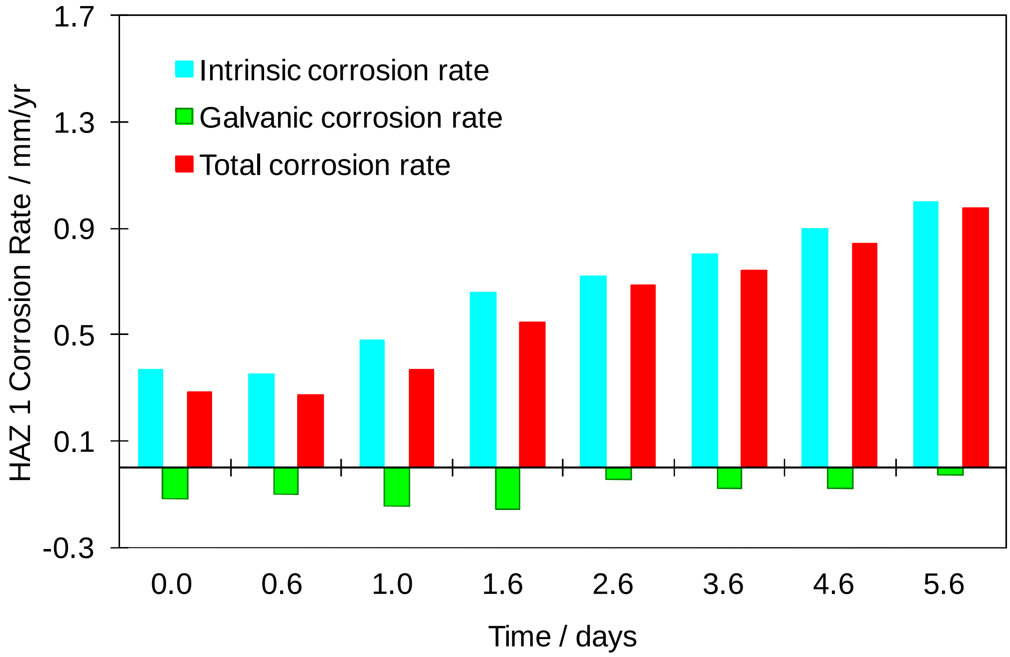

Figure 20. Corrosion rate of HAZ 1 metal compared to the intrinsic corrosion rate and galvanic corrosion rate1 wt% NaCl, 25℃.

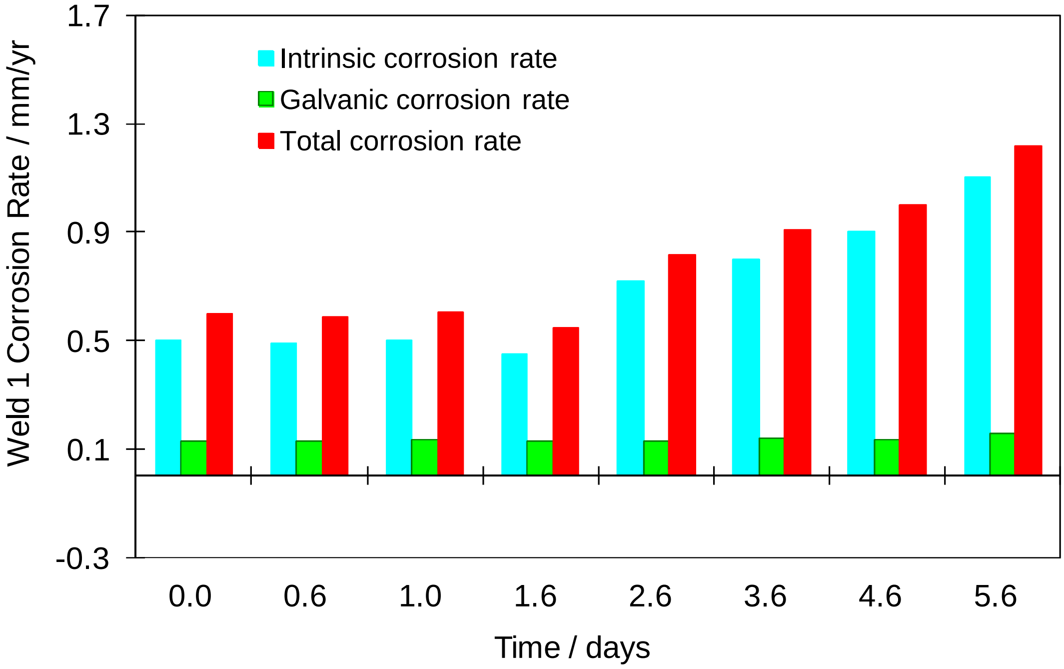

Figure 21. Corrosion rate of weld 1 metal compared to the intrinsic corrosion rate and galvanic corrosion rate at 1 wt% NaCl, 25ŬC.

Surface Analysis The specimen surface was scanned by SEM after the experiment. The surface morphologies of the parent, the HAZ, and the weld metal surface (with film) after different chloride concentration tests are shown in Figure 22, Figure 23, and Figure 24. No evidence of localized attack on each of the weldment segment surfaces was detected.

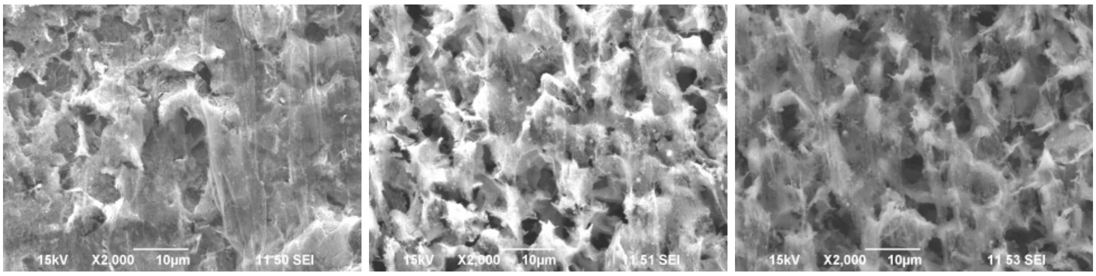

(a) Parent (b) HAZ (c) Weld

Figure 22. Surface morphology (with film) of parent, HAZ, and weld after 6 days at 1 wt% NaCl, 25°C.

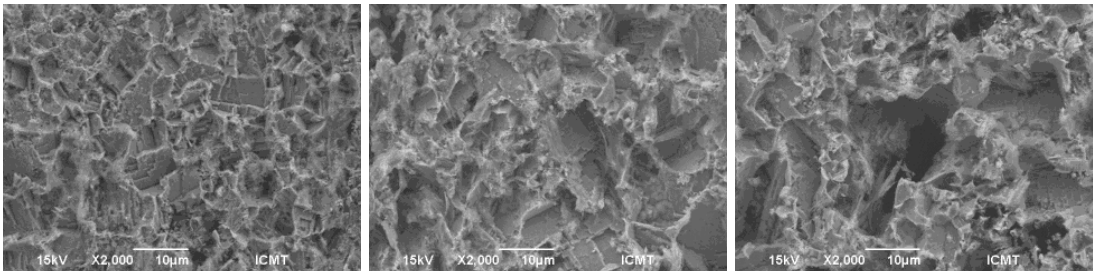

(a) Parent (b) HAZ (c) Weld

Figure 23. Surface morphology (with film) of Parent, HAZ, and Weld after 6 days at 5 wt% NaCl, 25°C.

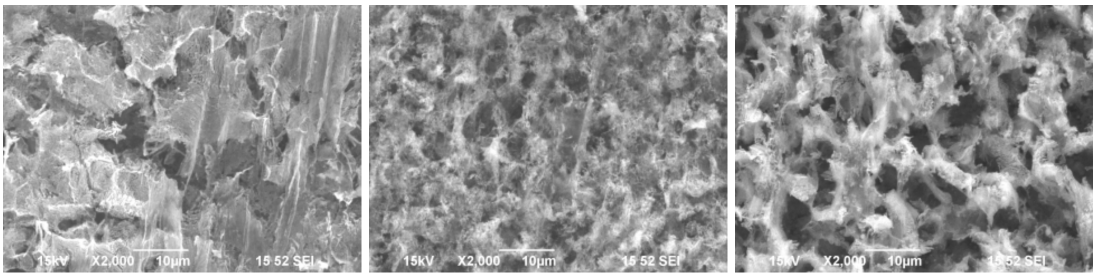

(a) Parent (b) HAZ (c) Weld

Figure 24. Surface morphology (with film) of parent, HAZ, and weld after 6 days at 10 wt% NaCl, 25°C.

6.1.1.2 60^{o}C, pH 5.0, 1bar total pressure, and 1, 5, 10 wt% NaCl

Similar experiments were conducted at 60^{o}C. The experimental results are shown below.

Corrosion rates The intrinsic corrosion rates of uncoupled parent, HAZ, and weld materials with time measured by LPR at 60°C, pH 5 and 1, 5 or 10 wt% NaCl are shown in Figure 25, Figure 26, and Figure 27 respectively. The results suggest that the intrinsic corrosion rates of parent, HAZ, and weld material are of the same magnitude under the same test conditions. The chloride effects on intrinsic corrosion rate are shown in Table 8. Different from the results at 20°C, it appears that an increase of chloride concentration from 1 wt% to 5 wt% at 60°C significantly increased the intrinsic corrosion rates of all segments. When the chloride concentration further increased from 5 wt% to 10 wt%, the acceleration of corrosion rate did not persist. The experimental results suggest that the interaction of the chloride ions with the steel surface at high temperature may be significantly different from the interaction at low temperatures.

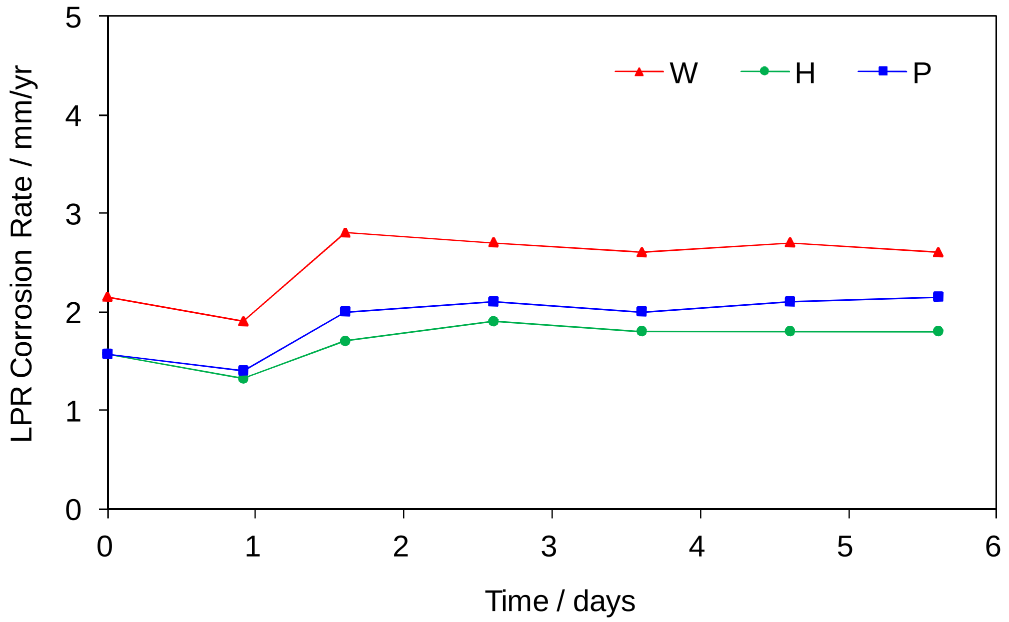

Figure 25. LPR corrosion rate of uncoupled weldment vs. time at 1 wt% NaCl, 60ŬC.

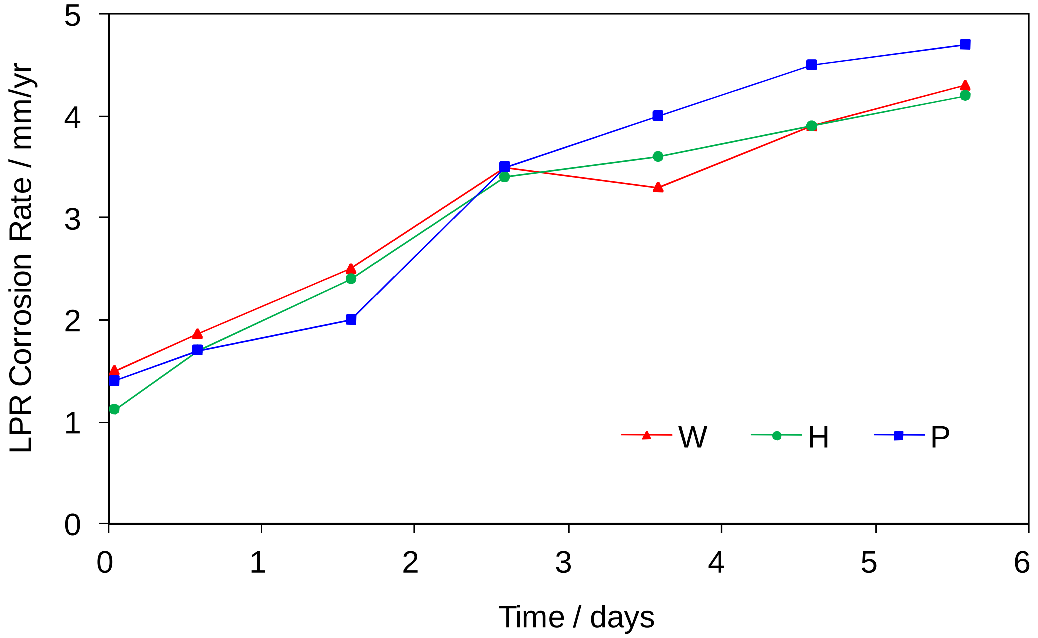

Figure 26. LPR corrosion rate of uncoupled weldment vs. time at 5 wt% NaCl, 60Ű̈C.

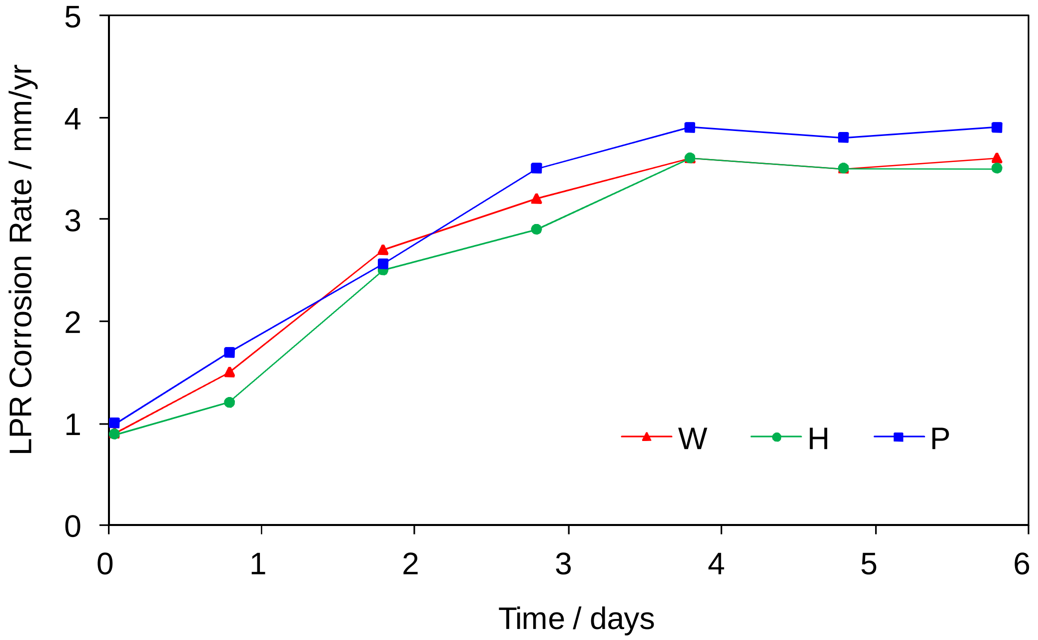

Figure 27. LPR corrosion rate of uncoupled weldment vs. time at 10 wt% NaCl, 60Ű̈C.

Table 8. Average intrinsic corrosion rates of weldment segments at 60ΆC.

	1 wt% NaCl			5 wt% NaCl			10 wt% NaCl		
	P	H	W	P	H	W	P	H	W
Average intrinsic corrosion rate (mm/y)	1.93	1.72	2.53	3.26	3.07	3.10	3.05	2.72	2.86

Galvanic Currents The galvanic currents flowing between each segment at 60°C were also measured. The results at different salt concentrations are shown in Figure 28, Figure 29 and Figure 30. According to the test results, the galvanic current on weld metal was always positive, which suggests that the weld metal acting as anode was always more active than the HAZ and the parent metal. The HAZ appears to be the neutral section and the parent metal was the section that was cathodically protected. The result also shows that the magnitude of galvanic current on weld metal increased from 4 μA to around 20 μA when temperature was increased from 25°C to 60°C. However, the chloride ion concentration does not appear to have a significant effect on the magnitude of the galvanic current and the metal polarity at 60°C, which was observed at 20°C as well.

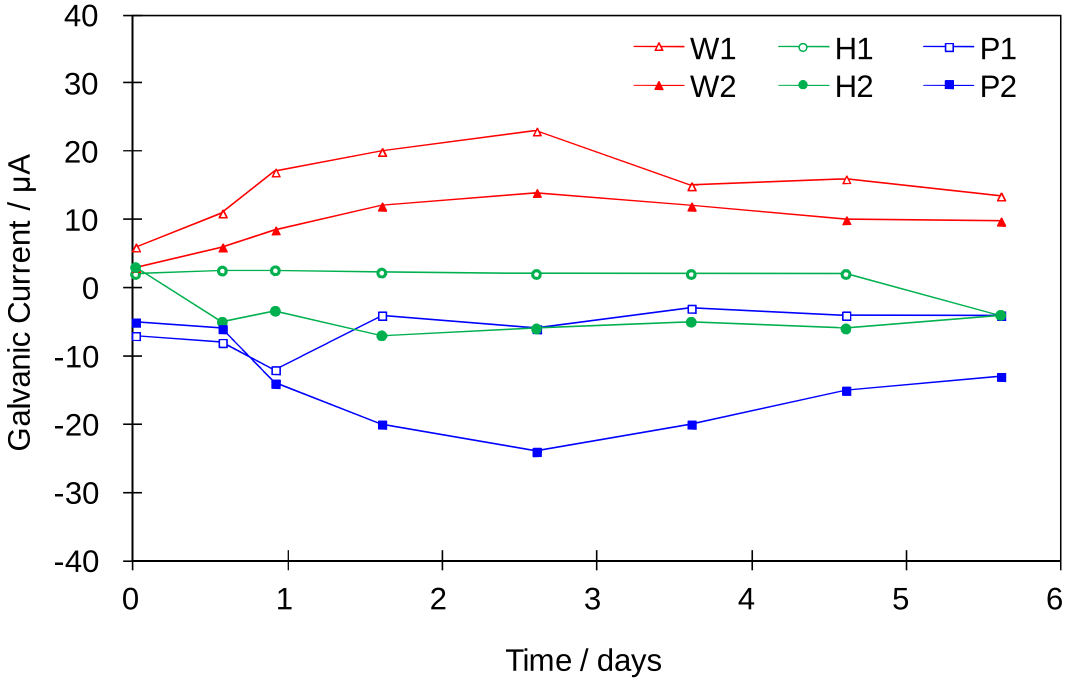

Figure 28. Galvanic current of coupled weldment vs. time at 1 wt% NaCl, 60ŬC.

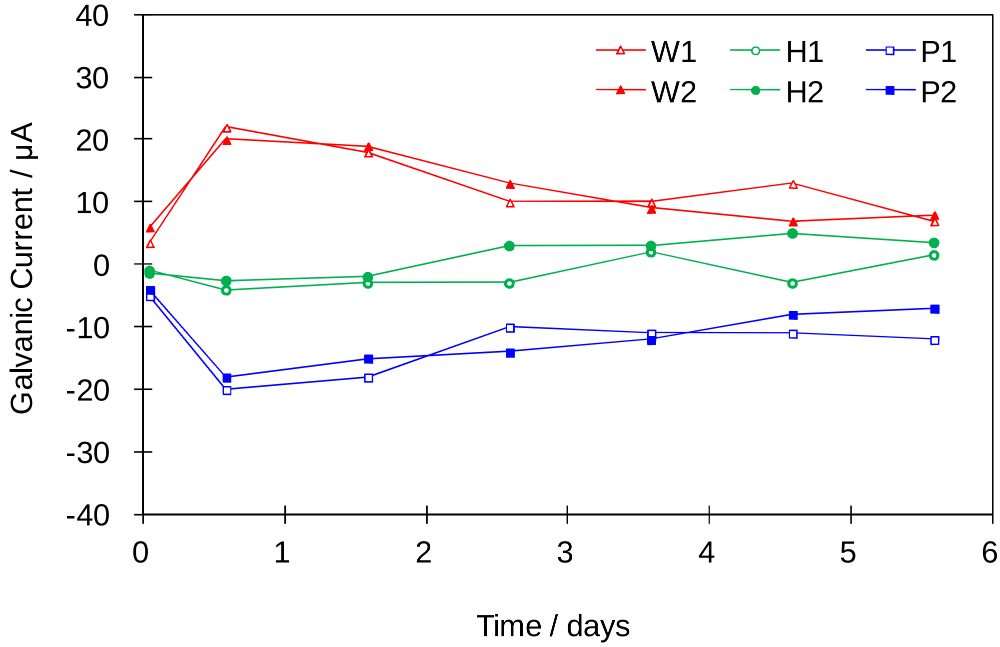

Figure 29. Galvanic current of coupled weldment vs. time at 5 wt% NaCl, 60ŬC.

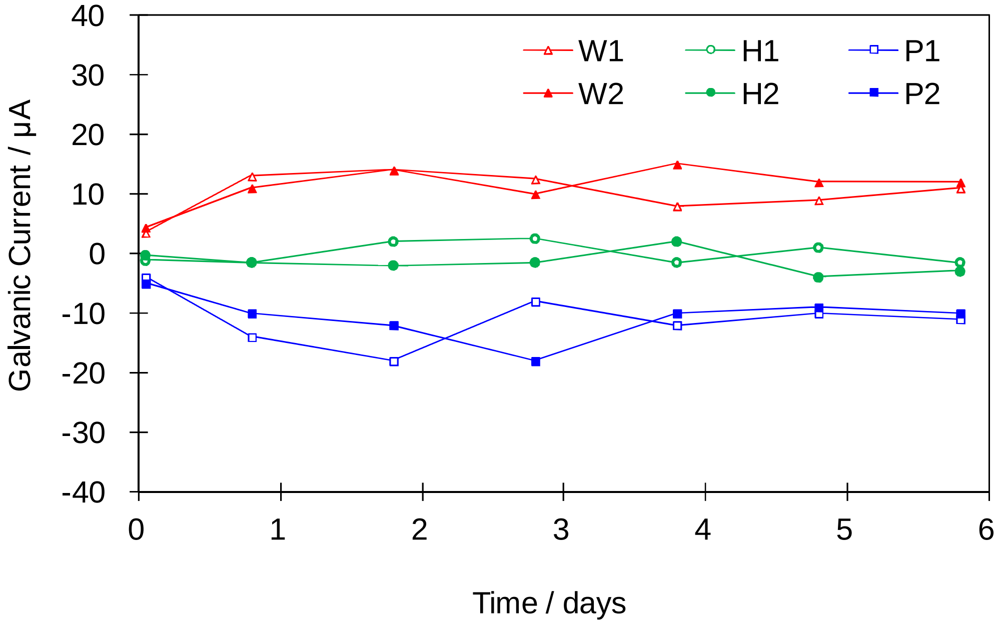

Figure 30. Galvanic current of coupled weldment vs. time at 10 wt% NaCl, 60 ℃.

The total corrosion rates of each segment of weldment which combines the intrinsic and the galvanic corrosion rate at 1 wt% NaCl and 60℃ are shown in Figure 31, Figure 32, and Figure 33. Apparently, the total corrosion rate of the parent metal was reduced by the galvanic effect. The galvanic current significantly accelerated the total corrosion rate of the weld metal.

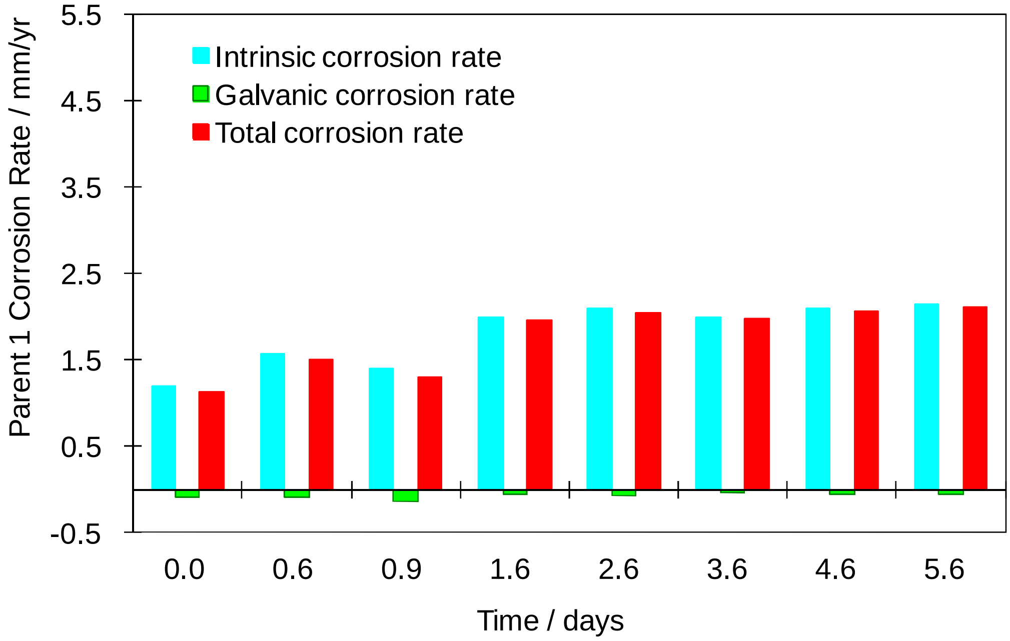

Figure 31. Corrosion rate of parent 1 metal compared to the intrinsic corrosion rate and galvanic corrosion rate at 1 wt% NaCl, 60ŬC.

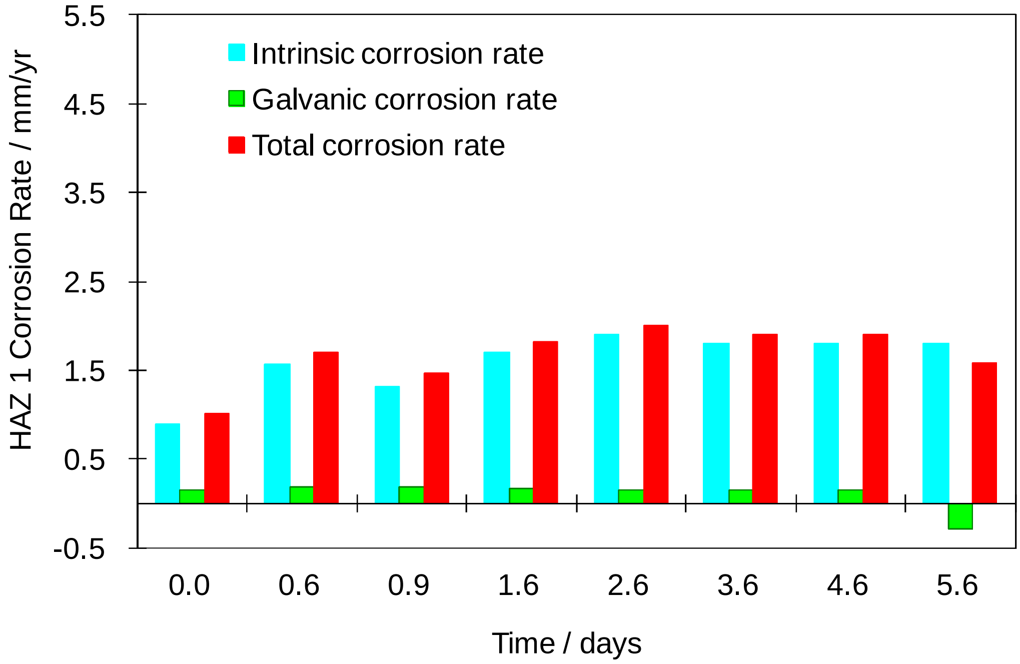

Figure 32. Corrosion rate of HAZ 1 metal compared to the intrinsic corrosion rate and galvanic corrosion rate at 1 wt% NaCl, 60ŬC.

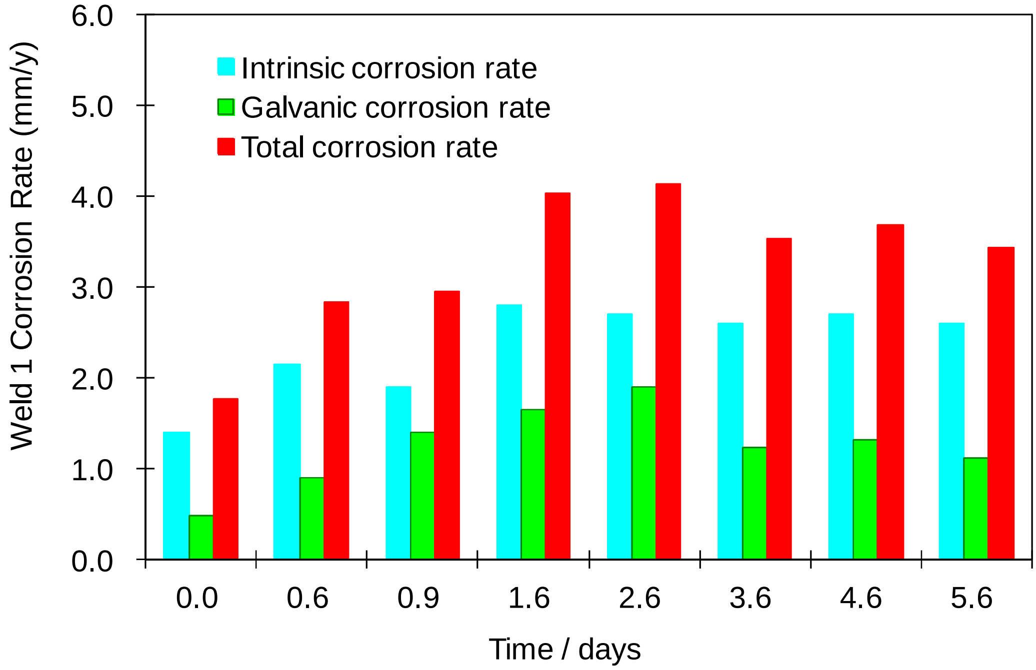

Figure 33. Corrosion rate of weld 1 metal compared to the intrinsic corrosion rate and galvanic corrosion rate at 1 wt% NaCl, 60Ŭ.

Surface Analysis The surface morphologies of parent, HAZ, and weld metal (with corrosion products) after experiments at different chloride concentrations are shown in Figure 34, Figure 35, and Figure 36. A crystallized corrosion product was detected on the specimen surface under the condition of 1 wt% NaCl, 60Ŭ. The EDX analysis as shown in Figure 37 confirms it to be iron carbonate. However, when the salt concentration was increased to 5 and 10 wt%, the formation of iron carbonate on the coupon surface was hardly observable by SEM. The iron carbonate layer was then removed by Clarke solution. The surface morphology is shown in Figure 38. Localized corrosion was not observed on the surfaces of all segments. Based on the experimental results, even when the galvanic effects were accelerated by an increase of temperature, localized corrosion event was still not observed at all chloride concentrations.

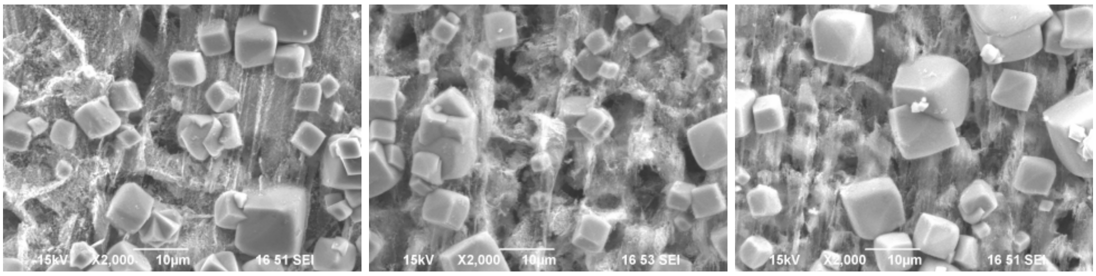

(a) Parent (b) HAZ (c) Weld

Figure 34. Surface morphology (with corrosion products) of parent steel, HAZ, and weld after 6 days at 1 wt% NaCl, 60ŬC.

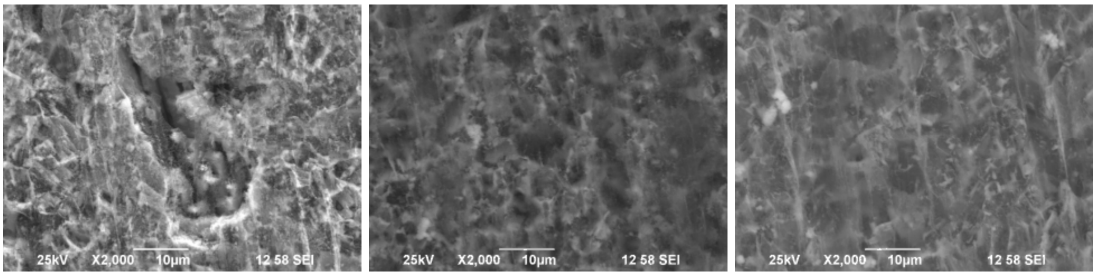

(a) Parent (b) HAZ (c) Weld

Figure 35. Surface morphology of parent steel, HAZ, and weld after 6 days at 5 wt% NaCl, 60ŬC.

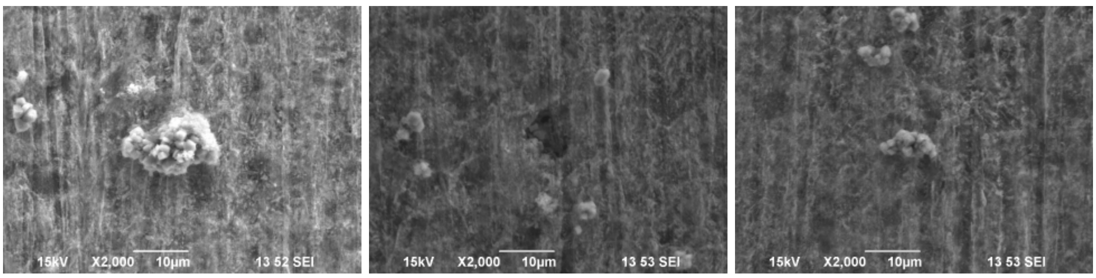

Figure 36. Surface morphology of parent steel, HAZ, and weld after 6 days at 10 wt% NaCl, 60ŬC.

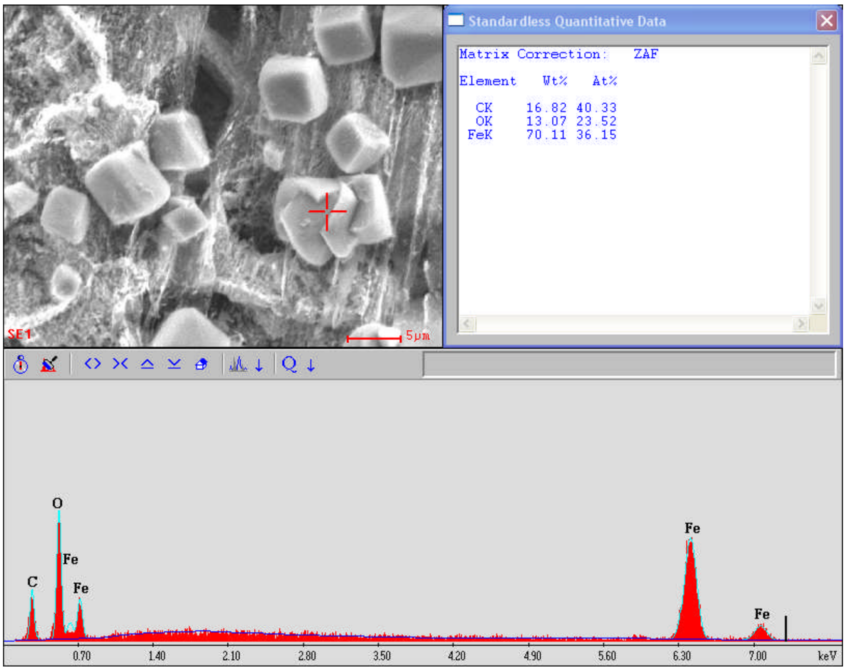

Figure 37. EDX results of crystals on parent steel after 6 days at 1 wt% NaCl, 60ŬC.

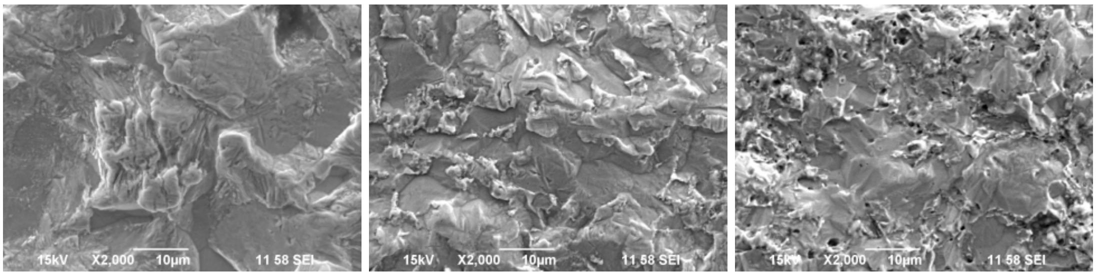

(a) Parent (b) HAZ (c) Weld

Figure 38. Surface morphology (without crystals) of parent steel, HAZ, and weld after 6 days at 1 wt% NaCl, 60ŬC.

6.1.1.3 Summary

Temperature and chloride ion concentration effects were studied in this series of experiments. An increase of temperature from $25^{o}C$ to $60^{o}C$ significantly increased the intrinsic corrosion rate of each segment. The magnitude of galvanic current flowing through each segment was also increased by an increase of temperatures.

At 25^{o}C, an increase of chloride concentration from 5 wt% to 10 wt% reduced the intrinsic corrosion rate of each segment. This may be due to the absorption of chloride ions on the steel surface acting as a mass transfer barrier. However, when the temperature was increased to 60^{o}C, the effects of chloride ion concentration on the intrinsic corrosion rate were opposite, i.e., the intrinsic corrosion rate was increased with an increase of chloride concentration.

The intrinsic corrosion rate of each segment appears to have no significant difference from each other under the same experimental conditions. The weldment metal always appears to be anodic with respect to HAZ and parent metal.

No localized corrosion was observed at all test conditions.

6.1.2 The effects of acetic acid

The effects of acetic acid on weldment corrosion were investigated by adding 100 ppm of un-dissociated acetic acid to the solution. This series of experiments were only conducted at 60^{o}C to promote localized corrosion. Sodium chloride concentration was 1 wt% to minimize the interference by the chloride concentration effect. Electrochemical noise measurements were also conducted in the experiments to detect possible localized corrosion.

6.1.2.1 Experiential results

Intrinsic corrosion rate The intrinsic corrosion rates of uncoupled parent, HAZ, and weld materials with time at 100 ppm acetic acid condition are shown in Figure 39. The intrinsic corrosion rate of all segments does not appear to be different. This was the same as observed in the previous experiments. The experimental results also show that the intrinsic corrosion rate of each segment with the addition of acetic acid was around 3 mm/yr, which is much higher that the corrosion rate without acetic acid which was at 2 mm/yr. This suggests that the addition of acetic acid significantly accelerated the overall intrinsic corrosion rates of all segments. Since the pH and the partial pressure of CO_2 remain the same as the previous test, it also suggests that the acetic acid was directly involved in the corrosion reactions.

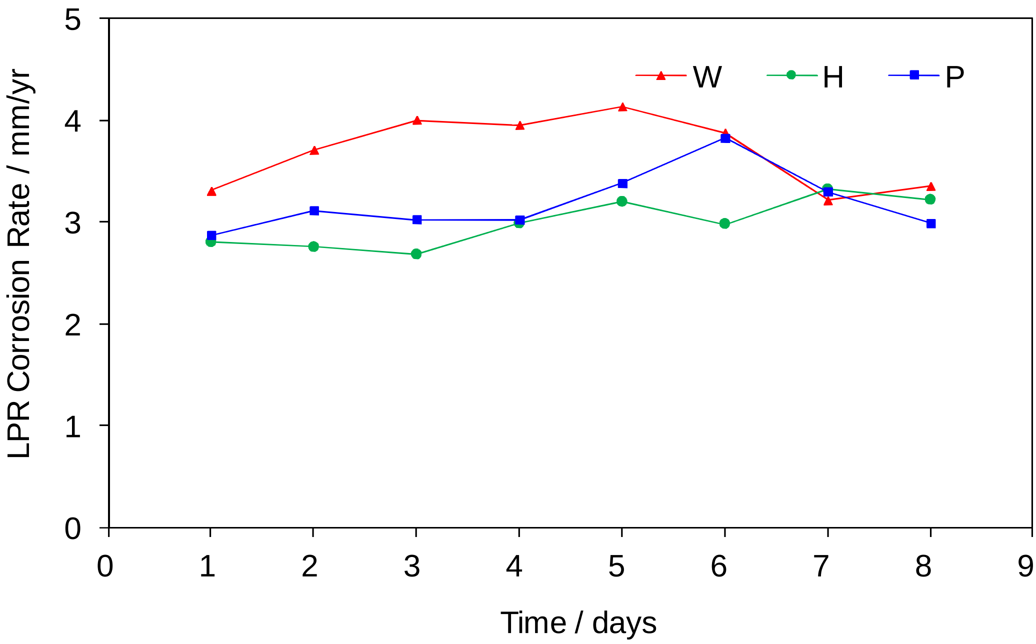

Figure 39. LPR corrosion rate vs. time in 1 wt% NaCl, 100 ppm un-dissociated acetic acid solution (60^{o}C, 0.8 bar P_{CO2}, pH 5.0, 1 wt% NaCl).

Galvanic current The results of the galvanic current measurement from the first day to the eighth day are shown in Figure 40. The same metal polarity was observed. Weld metal was corroded more due to the galvanic effects. HAZ remains neutral and the parent metal was cathodically protected. The galvanic current of weld metal was as high as 30 μA, which is 10 μA higher than the galvanic current without the addition of acetic acid. Therefore, the addition of 100 ppm acetic acid not only increased the intrinsic corrosion rate but also increased the galvanic current flowing between the segments.

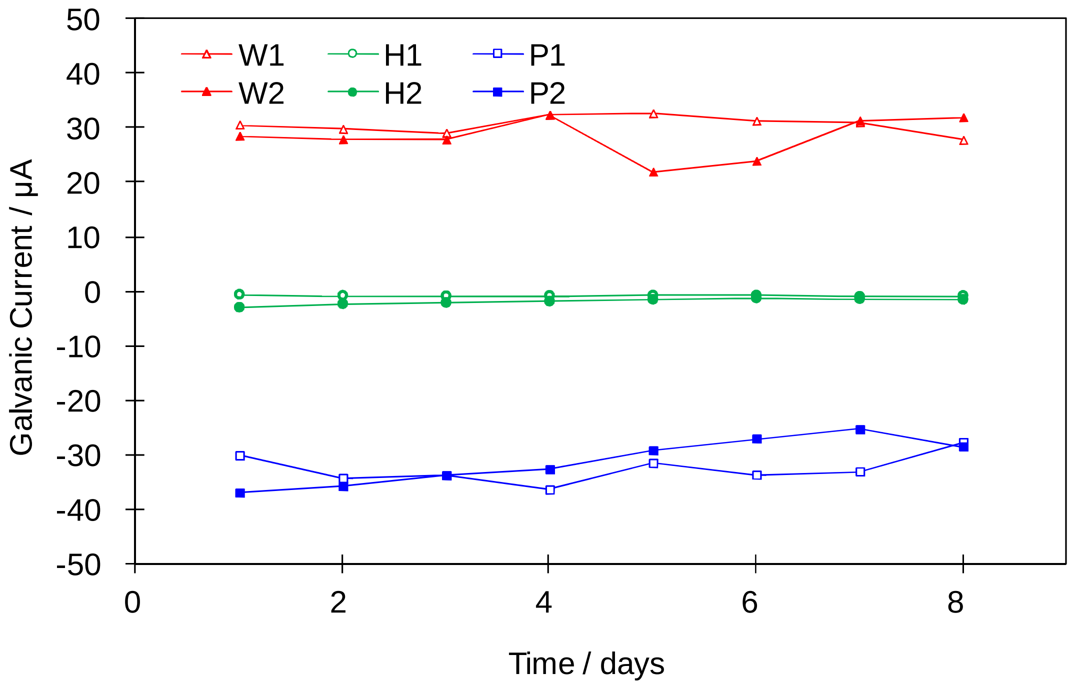

Figure 40. Galvanic currents vs. time in 1 wt% NaCl, 100 ppm undissociated acetic acid solution in 8 days.

Electrochemical noise Electrochemical noise measurement was conducted in this series of experiments to detect localized corrosion. The measurement was performed on each segment, but only the noise data of weld metal is reported due to the similarity of all the test data. Figure 41 to Figure 47 show the potential and current noise data at different time periods. It is clearly seen that no event of transient was observed during the whole test period. This is an indication of general corrosion.

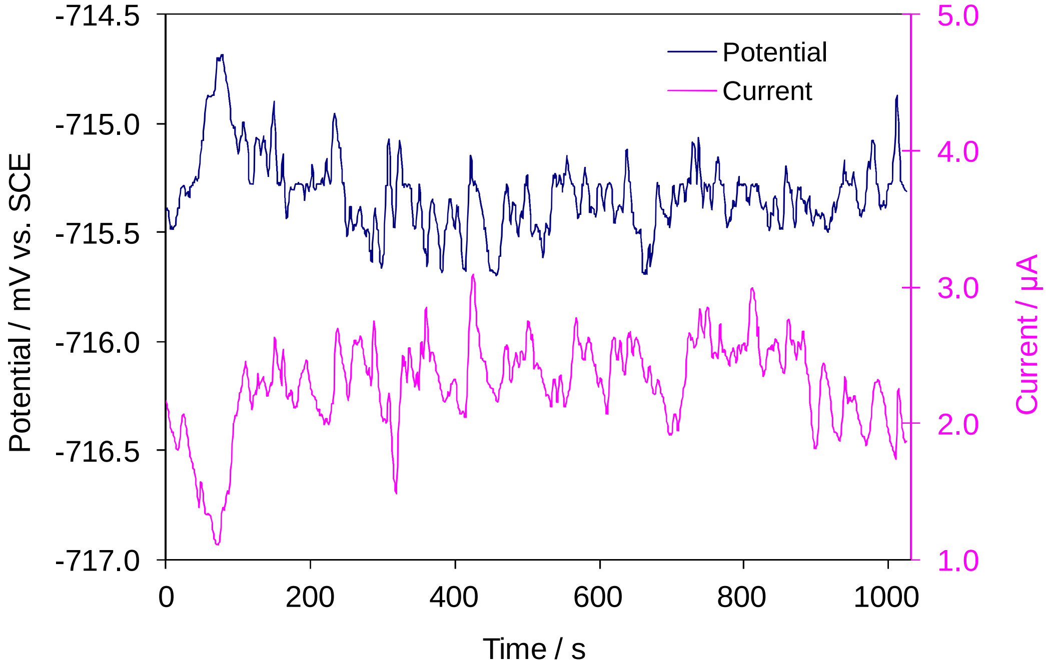

Figure 41. Potential noise and current noise of weld metal vs. time in 1 wt% NaCl, 100 ppm undissociated acetic acid solution (2 day).

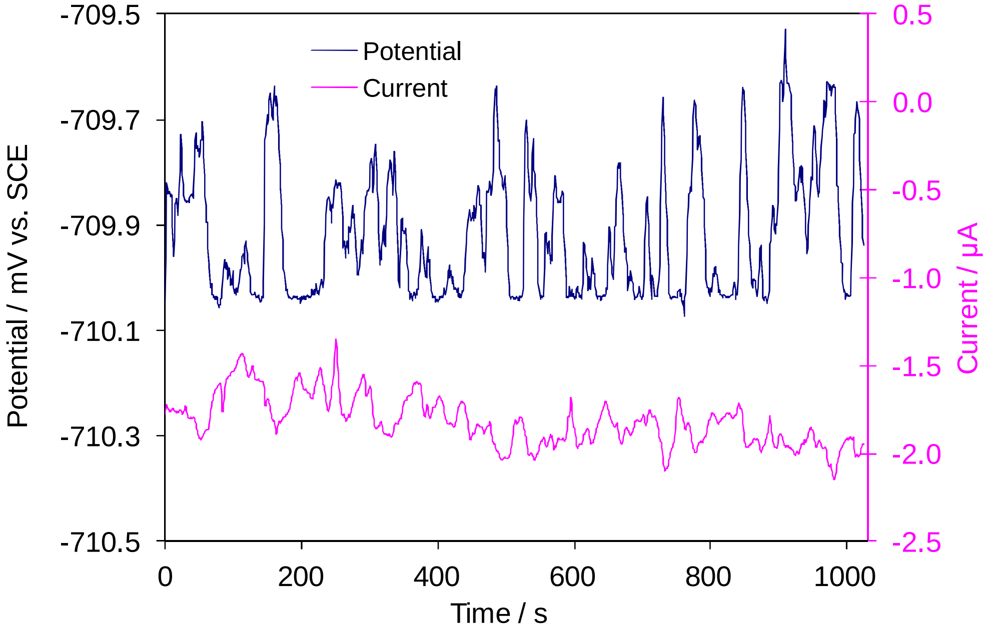

Figure 42. Potential noise and current noise of weld metal vs. time in 1 wt% NaCl, 100 ppm undissociated acetic acid solution (3 days).

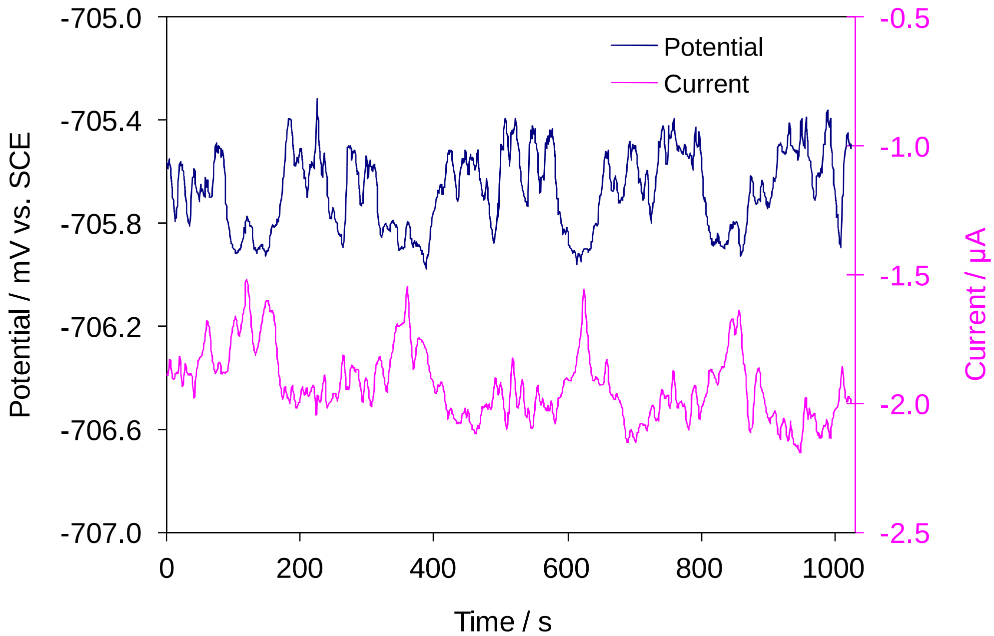

Figure 43. Potential noise and current noise of weld metal vs. time in 1 wt% NaCl, 100 ppm undissociated acetic acid solution (4 days).

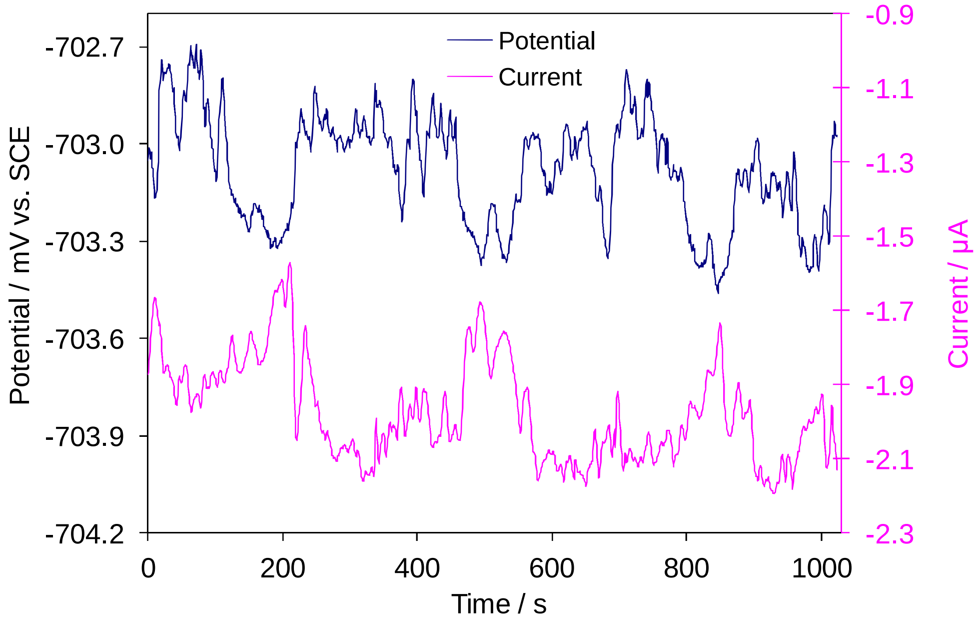

Figure 44. Potential noise and current noise of weld metal vs. time in 1 wt% NaCl, 100 ppm undissociated acetic acid solution (5 days).

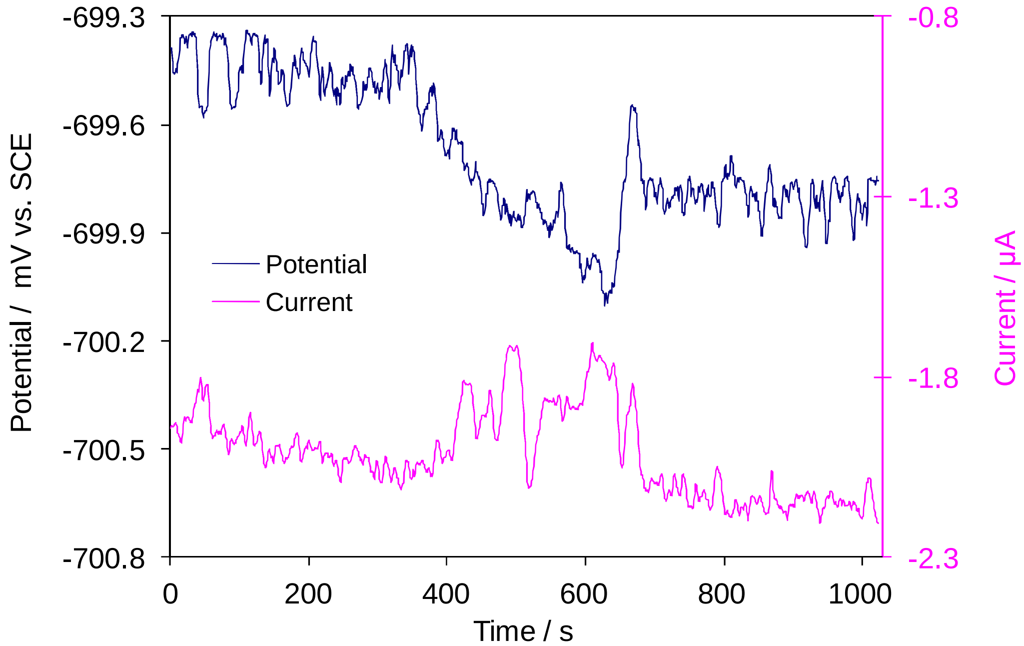

Figure 45. Potential noise and current noise of weld metal vs. time in 1 wt% NaCl, 100 ppm undissociated acetic acid solution (6 days).

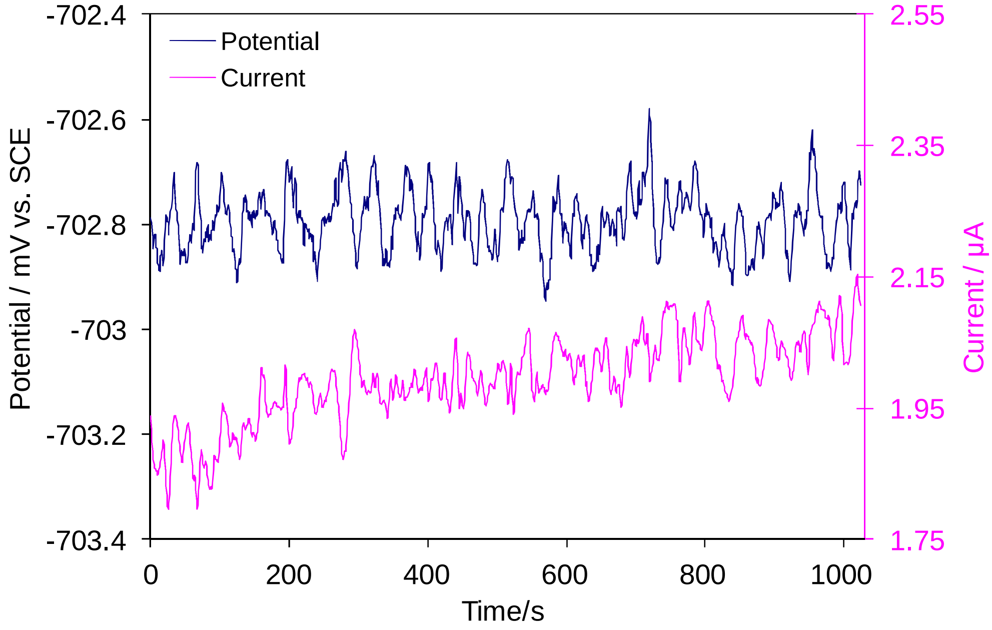

Figure 46. Potential noise and current noise of weld metal vs. time in 1 wt% NaCl, 100 ppm undissociated acetic acid solution (7 days).

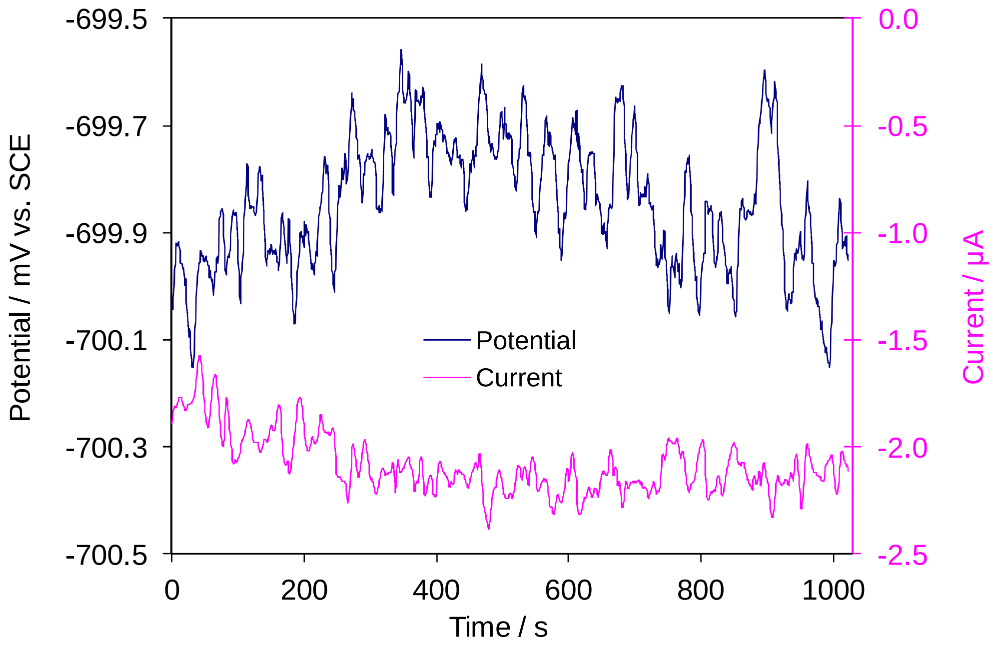

Figure 47. Potential noise and current noise of weld metal vs. time in 1 wt% NaCl, 100 ppm undissociated acetic acid solution (8 days).

Electrochemical potential and current noise data from time domain were converted to frequency domain by using Fast Fourier Transfer method and plotted in Figure 48 and Figure 49 respectively. It appears that the potential and current power spectrum densities at all time periods stay at the same energy level and the slopes are also the same. This suggests that no special events (localized corrosion) occurred during the whole experimental period.

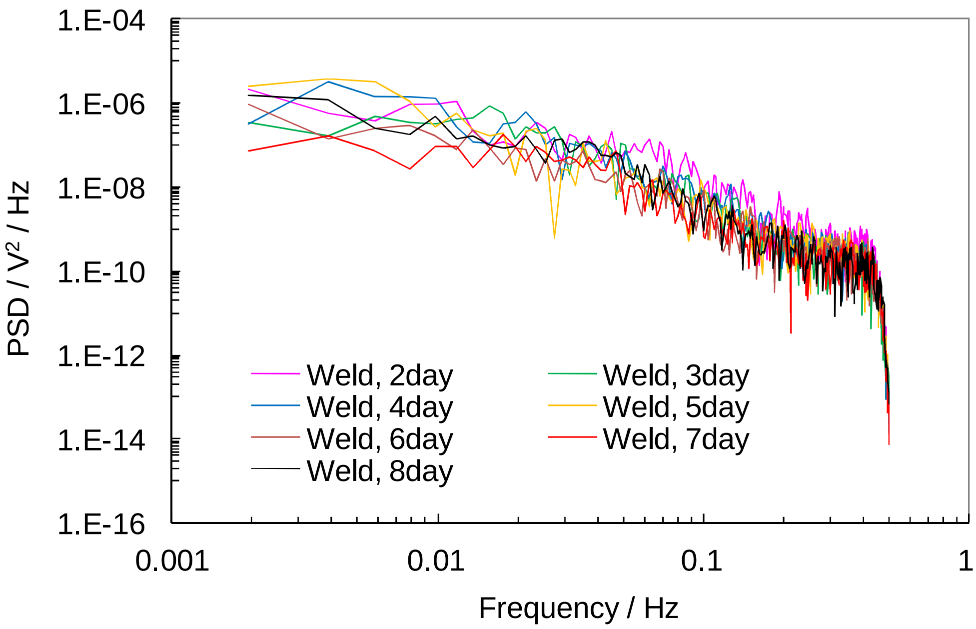

Figure 48. Variation of potential power spectra density (FFT) with time in 1 wt% NaCl, 100 ppm undissociated acetic acid solution.

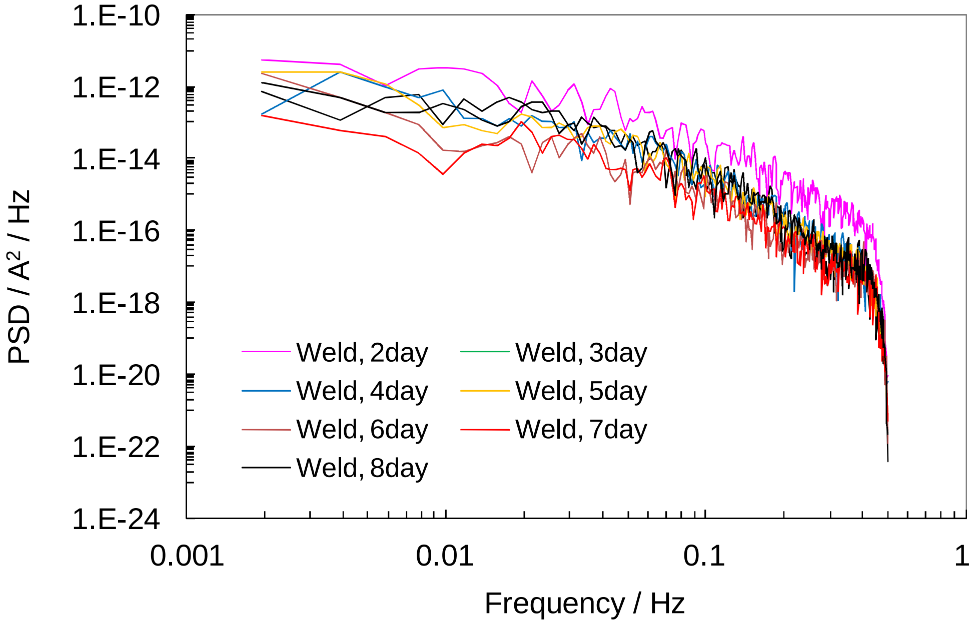

Figure 49. Variation of current power spectra density (FFT) with time in 1 wt% NaCl, 100 ppm undissociated acetic acid solution.

Surface Analysis The specimen surface was scanned by SEM to detect possible localized corrosion. The SEM surface images of the parent metal, the HAZ metal, and the weld metal after experiments are shown in Figure 50, Figure 51, and Figure 52. From the images, it appears that the general corrosion is the dominant corrosion mechanism under the test conditions. No localized corrosion was detected from the SEM images. The surface analysis is consistent with the electrochemical noise data.

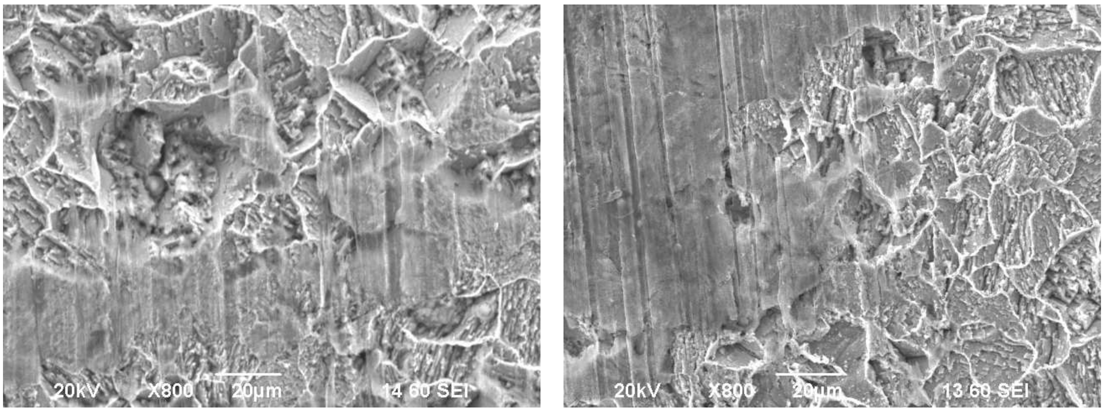

Figure 50. Morphologies of parent material (SEM) after corrosion (8 days) in 1 wt% NaCl, 100 ppm undissociated acetic acid solution.

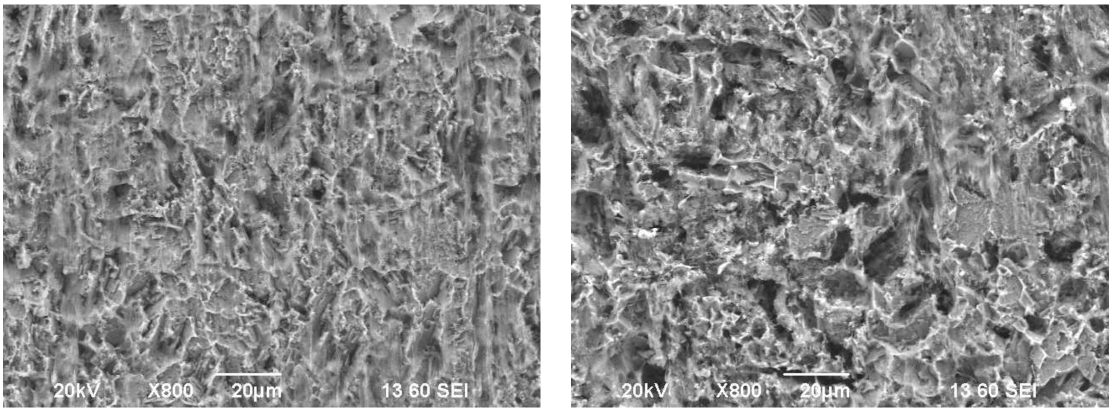

Figure 51. Morphologies of HAZ material (SEM) after corrosion (8 days) in 1 wt% NaCl, 100 ppm undissociated acetic acid solution.

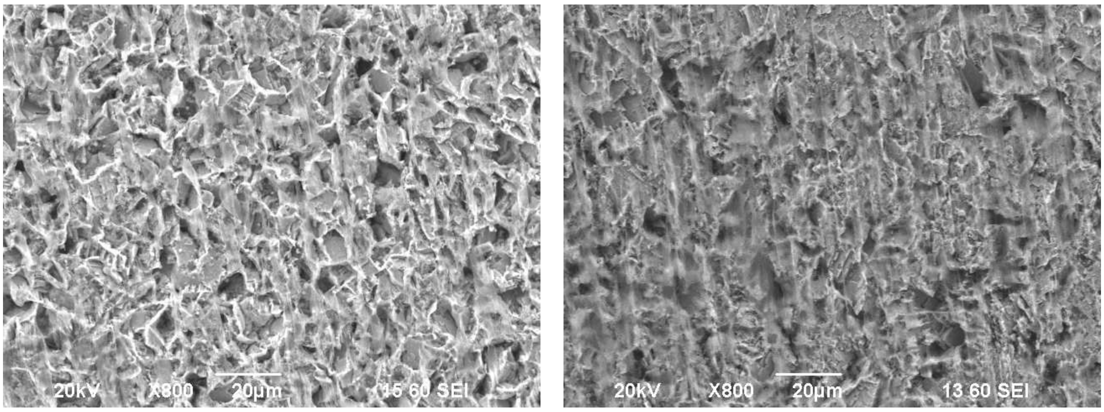

Figure 52. Morphologies of weld material (SEM) after corrosion (8 days) in 1 wt% NaCl, 100 ppm undissociated acetic acid solution.

6.1.2.2 Summary

The effect of the addition of acetic acid on the weldment corrosion was studied in this set of experiments. It was discovered that the addition of acetic acid significantly increased the intrinsic corrosion rates of all segments of the weldment.

The magnitude of galvanic current on weld metal was increased as well when 100 ppm acetic acid was injected into the system. However, the metal polarity stayed the same: weld was anodic, HAZ was neutral and parent was cathodic.

Even when the galvanic current flowing through each segment increased, localized corrosion was still not detected on the surfaces of any segments.

6.1.3 The effects of corrosion inhibitor

Corrosion inhibitor is frequently applied in oil and gas field situations to inhibit the corrosion rate. The non-uniform inhibitor film distribution on the steel surface may result in severe localized corrosion. In this set of experiments, 20 ppm of a generic corrosion inhibitor was injected into the test solution. The experiment was only conducted at 60^{o}C.

6.1.3.1 Experimental results

Intrinsic corrosion rate The intrinsic corrosion rates of the uncoupled parent, the HAZ and the weld materials with time under the condition of 60^{o}C, pH 5.0 and 1 wt% NaCl are shown in Figure 53. The corrosion rates of all segments are all of the same magnitude at about 1 mm/yr. After about 15 hours of measurements, 20 ppm corrosion inhibitor was injected. The corresponding intrinsic corrosion rates of all segments immediately decreased and finally stabilized at about 0.05 mm/yr. This suggests that a protective inhibitor layer was formed on the weldment surfaces.

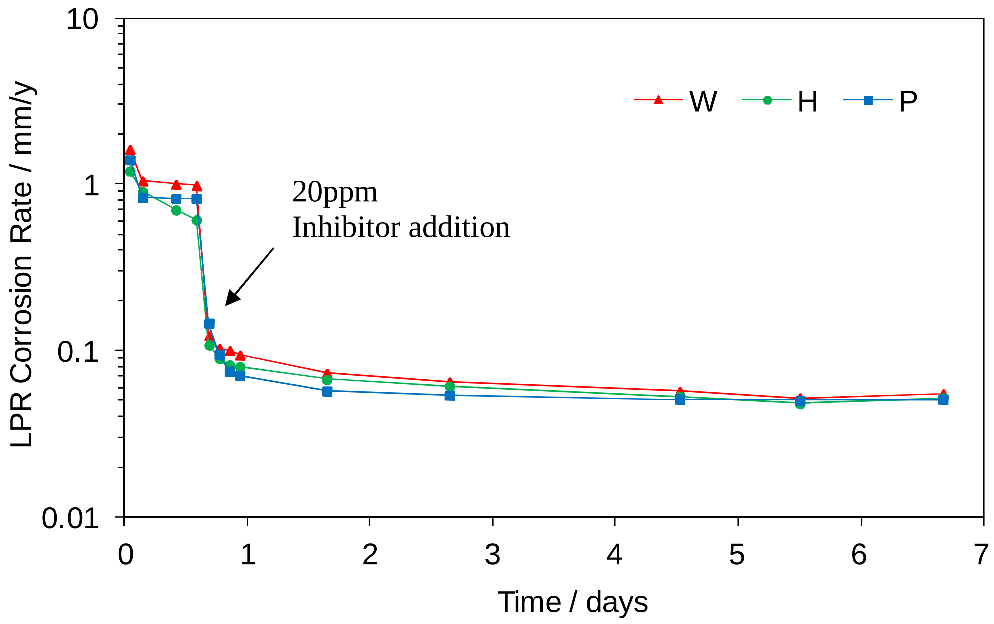

Figure 53. LPR corrosion rate of uncoupled weldment vs. time (60°C, 0.8 bar pCO_2, pH 5.0, 1 wt% NaCl).

Galvanic current The results of spontaneous galvanic current measurement on coupled segments are shown in Figure 54. According to the result, it is clearly seen that the galvanic current on the weld metal was suppressed from 6 µA to less than 2 µA by the addition of 20 ppm of corrosion inhibitor. It has also been observed that through the whole test period, the weld metal always had the positive galvanic current. Vice versa, the parent metal always appeared to be cathodic with respect to the other two sections of the weldment. HAZ remained neutral all the time. This was observed in all the previous experimental results.

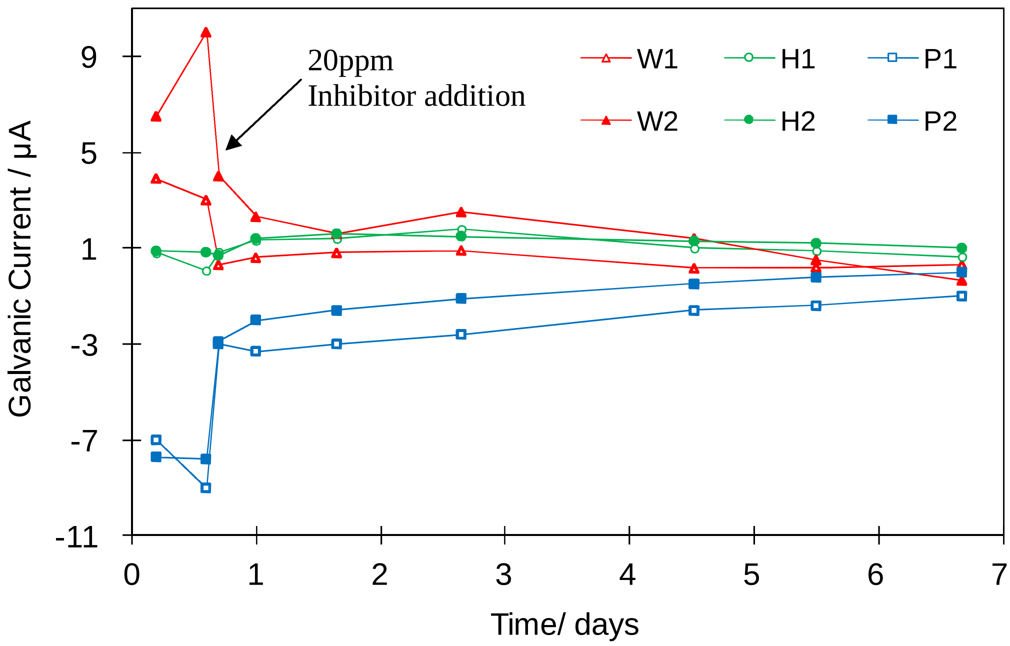

Figure 54. Galvanic current of coupled weldment vs. time.

The total corrosion rate considering both intrinsic and galvanic corrosion rates is calculated for all segments and is shown in Figure 55, Figure 56, and Figure 57. From the results, it is seen that the galvanic current was contributing ~ -0.07 mm/yr for each parent, ~0.002 mm/yr for each HAZ and ~0.06 mm/y for each weld material before adding inhibitor. The galvanic effects when compared with the total corrosion rate are not significant. After 20 ppm inhibitor was injected, the galvanic currents of all segments decreased to a negligible value and stabilized at a low level.

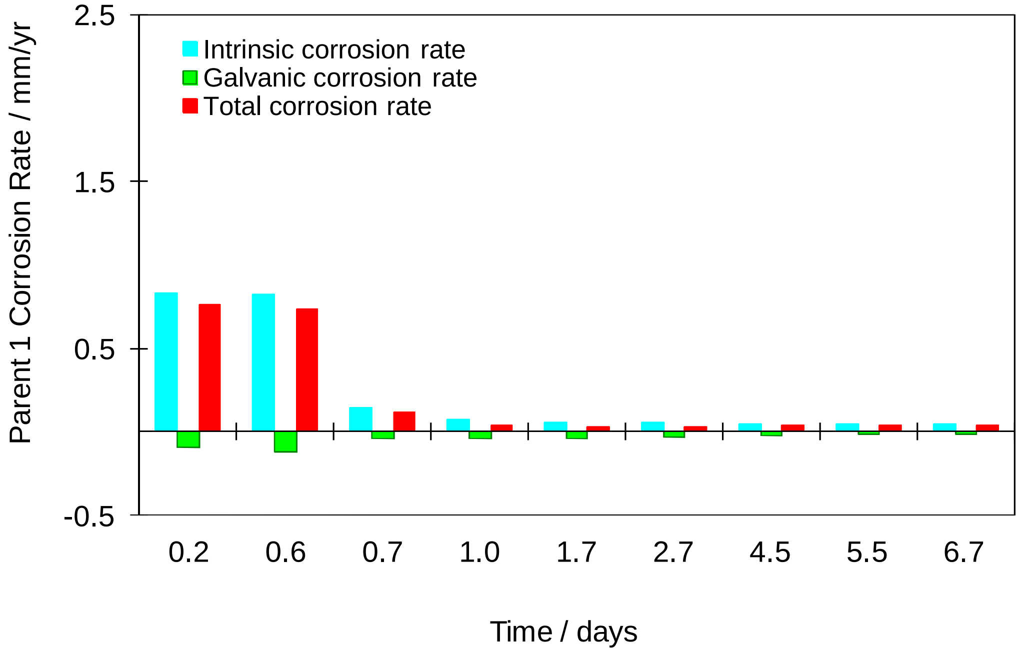

Figure 55. Corrosion rate of parent 1 metal compared to the intrinsic corrosion rate and galvanic corrosion rate at 1 wt% NaCl, 60ºC. 20 ppm inhibitor.

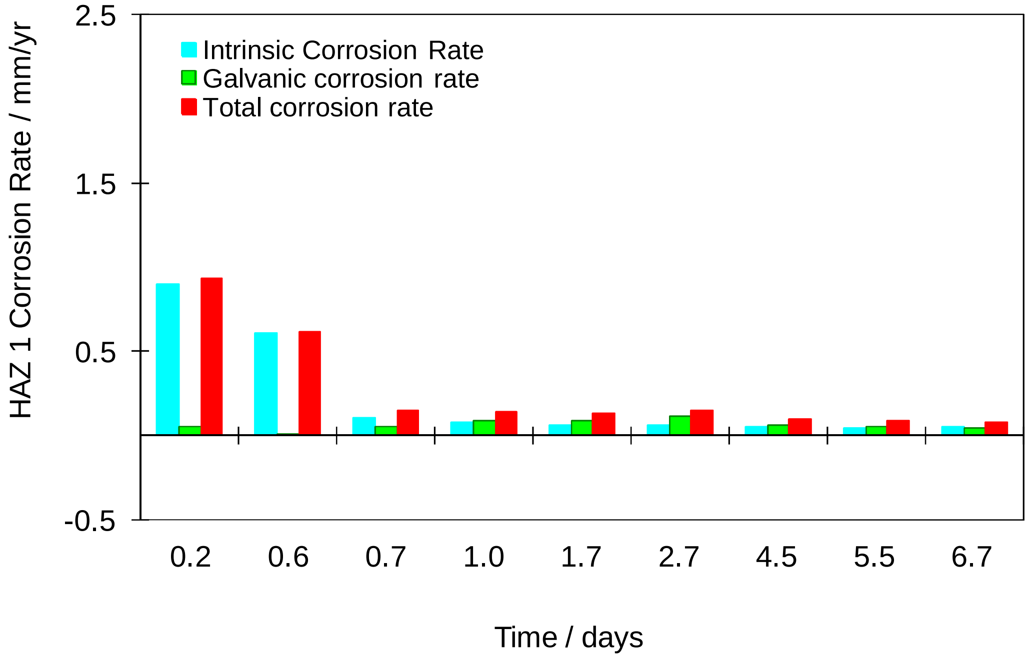

Figure 56. Corrosion rate of HAZ 1 metal compared to the intrinsic corrosion rate and galvanic corrosion rate at 1 wt% NaCl, 60ºC. 20 ppm inhibitor.

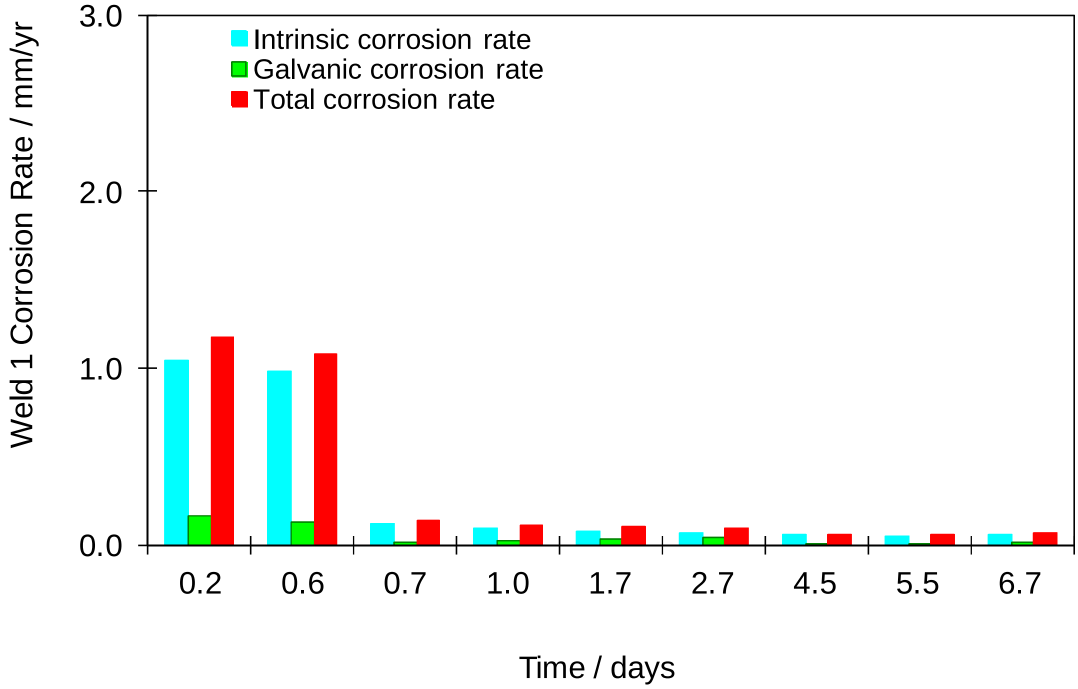

Figure 57. Corrosion rate of weld 1 metal compared to the intrinsic corrosion rate and galvanic corrosion rate at 1 wt% NaCl, 60ºC. 20 ppm inhibitor.

Electrochemical noise Electrochemical noise measurement was performed on the coupled weldment during the whole experimental period. There was no significant difference between the electrochemical noise data of each segment, therefore, only the noise data generated from the weld metal is reported. The potential and current noise data from the weld metal at different time periods are shown from Figure 58 to Figure 61.The signature of localized corrosion which is a sudden increase and slow decrease (transient) was not observed from potential noise or current noise data in the time domain. From the noise data in the time domain, it seems most likely that localized corrosion did not occur under the test conditions. However, this assumption needs to be confirmed by observing the metal surface by SEM.

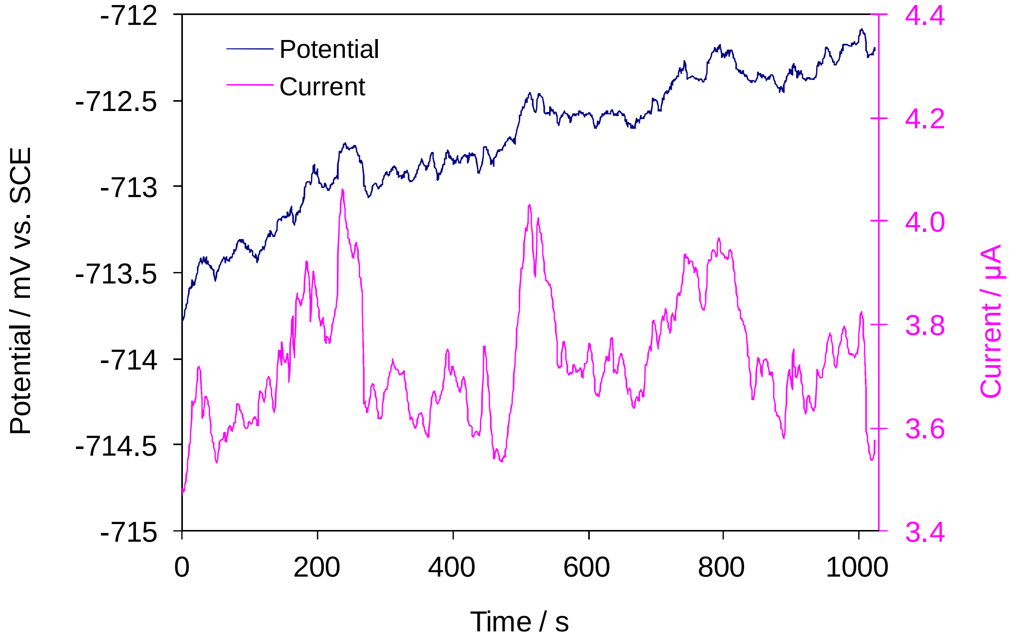

Figure 58. Potential noise and current noise of coupled weld mental vs. time without inhibitor addition (1days).

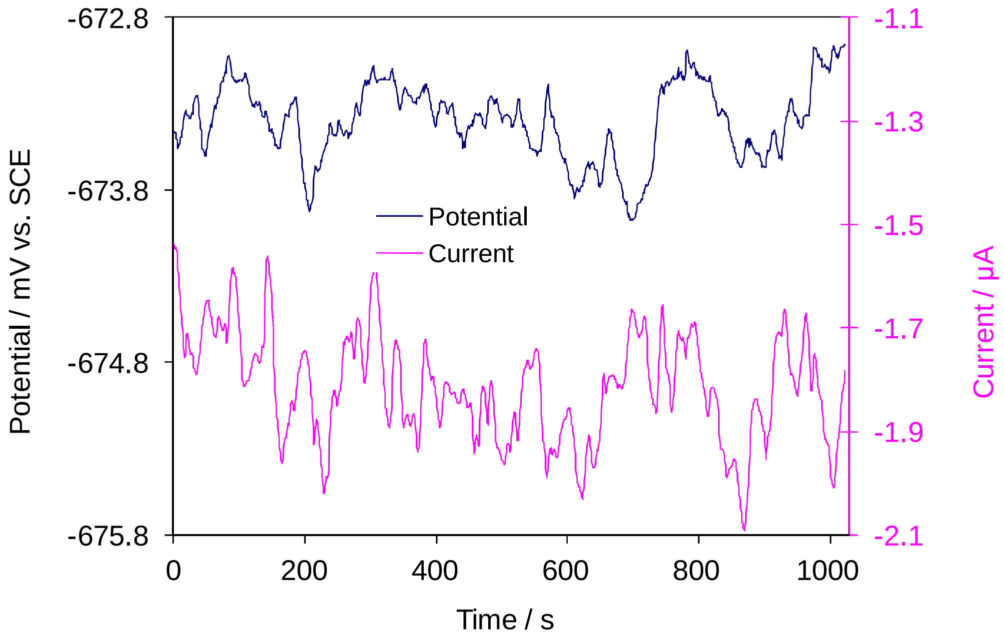

Figure 59. Potential noise and current noise of coupled weldment vs. time with inhibitor addition (3 days).

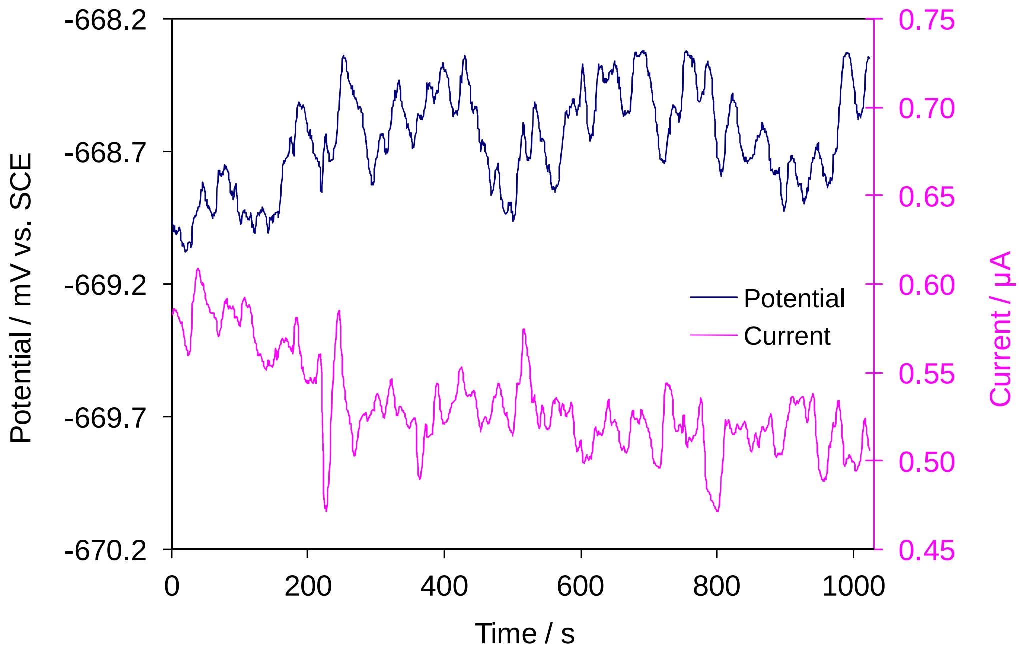

Figure 60. Potential noise and current noise of coupled weldment vs. time with inhibitor addition (5 days).

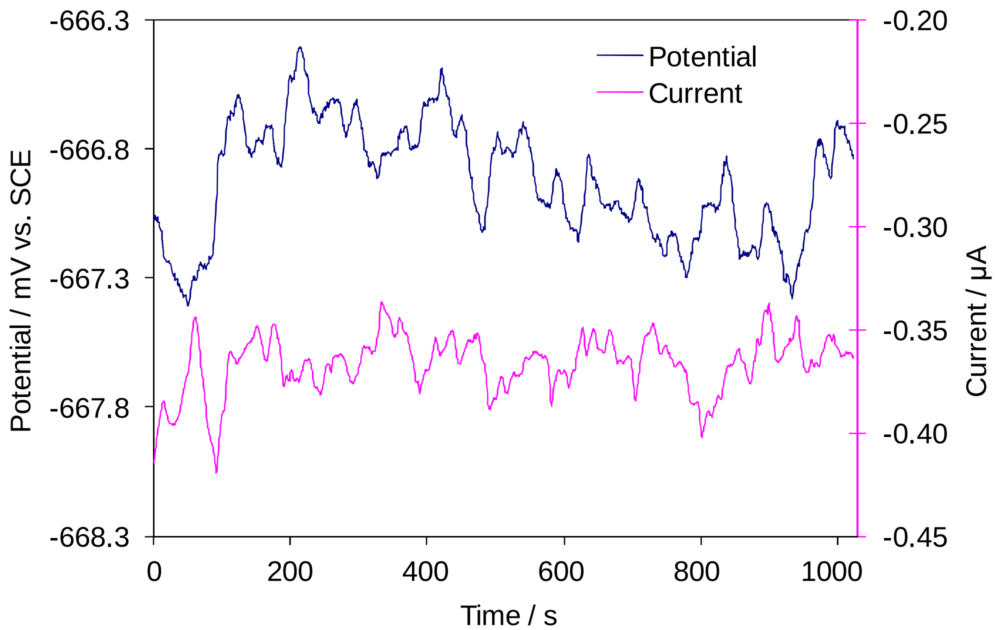

Figure 61. Potential noise and current noise of coupled weldment vs. time with inhibitor addition (7 days).

The results of power spectrum density (PSD) converted from the electrochemical potential and current noise data from time domains are shown in Figure 62 and Figure 63 respectively. It appears that the potential and current power spectrum densities at all time periods stay at the same energy level and the slopes are also the same. The power spectrum density data further confirms that no localized corrosion occurred during the experiment.

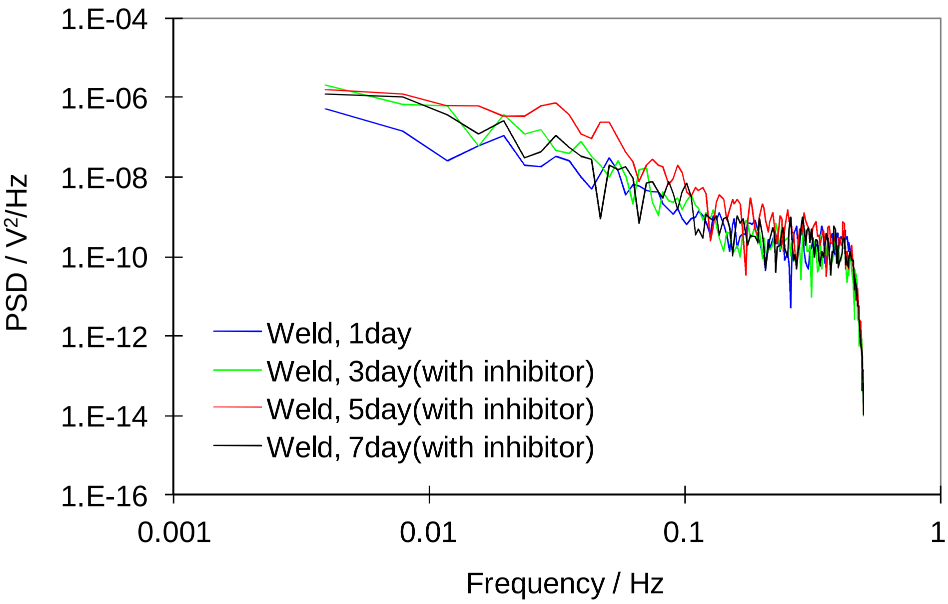

Figure 62. Variation of potential power spectra density (FFT) of coupled weldment with time, with corrosion inhibitor and without acetic acid.

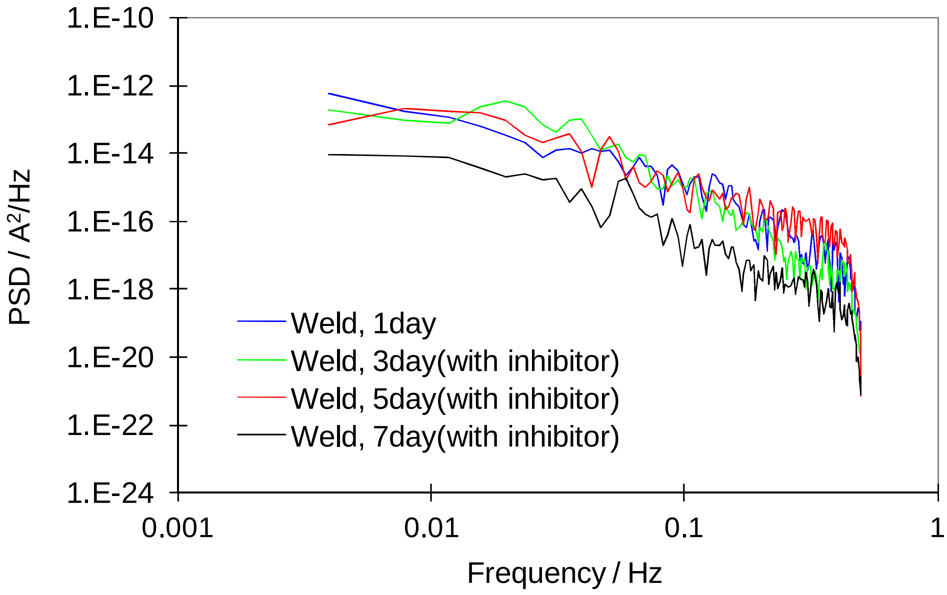

Figure 63. Variation of current power spectra density (FFT) of coupled weldment with time, with corrosion inhibitor and without acetic acid.

Surface analysis The weldment specimens were taken out of the test solution after the seven day experimental period. The corrosion products were removed by Clarke's solution and then the specimen surfaces were scanned by SEM. The SEM images of each segment surfaces are shown in Figure 64, Figure 65 and Figure 66. Clearly, no localized corrosion was detected.

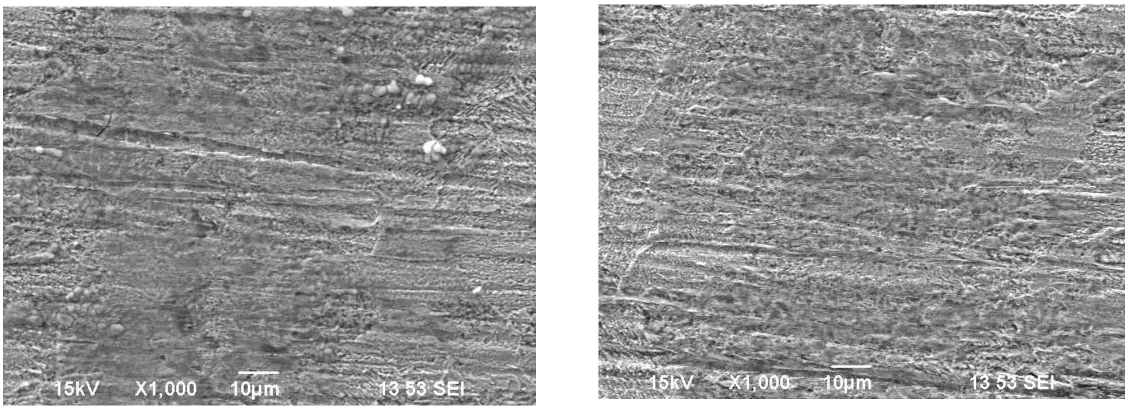

Figure 64. Morphologies of parent material (SEM) of coupled weldment after corrosion with corrosion inhibitor and without acetic acid.

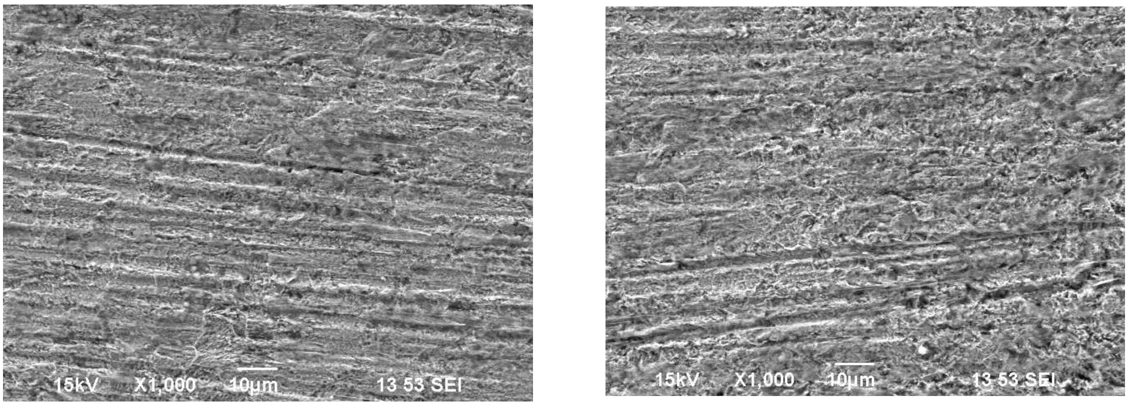

Figure 65. Morphologies of HAZ material (SEM) of coupled weldment after corrosion with corrosion inhibitor and without acetic acid.

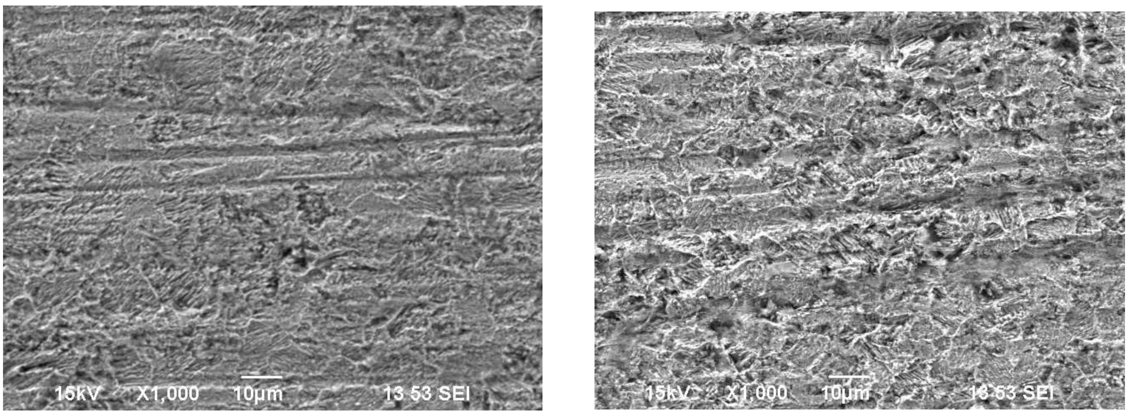

Figure 66. Morphologies of weld material (SEM) of coupled weldment after corrosion with corrosion inhibitor and without acetic acid.

6.1.3.2 Summary

20 ppm corrosion inhibitor was injected into the system to investigate the effects of corrosion inhibitor on weldment corrosion. The experimental results suggest that the addition of a corrosion inhibitor suppressed both the intrinsic corrosion rate and the galvanic corrosion rate. The addition of a corrosion inhibitor did not change the polarities of the weld metal, the HAZ, and the parent metal as they were determined in the previous experiments.

6.1.4 The combined effects of acetic acid and corrosion inhibitor

It has been seen from the previous experimental results that the addition of acetic acid significantly increased the intrinsic and galvanic corrosion rate. It would be interesting to see what would occur when acetic acid and corrosion inhibitor are both present in the same system. Therefore, in this set of experiments, acetic acid and corrosion inhibitor were both injected into the test solution.

6.1.4.1 Experimental results

Intrinsic corrosion rate The LPR measurement was conducted on the uncoupled parent, the HAZ, and the weld materials during the whole experimental period. The intrinsic corrosion rate data are shown in Figure 67. At 20 hours, 100 ppm of acetic acid was injected into the test solution. It is clearly seen that the addition of 100 ppm of acetic acid increased the total general corrosion rate of all three materials especially for weld metal. At 40 hours, right after the 20 ppm corrosion inhibitor was added into the solution, the intrinsic corrosion rates of all segments immediately dropped and stabilized at 0.05 mm/yr at the end of the experiment. Basically, the results from this set of experiments show the same synergic effects as the previous experiments: acceleration effect of acetic acid and retardation effect of corrosion inhibitor.

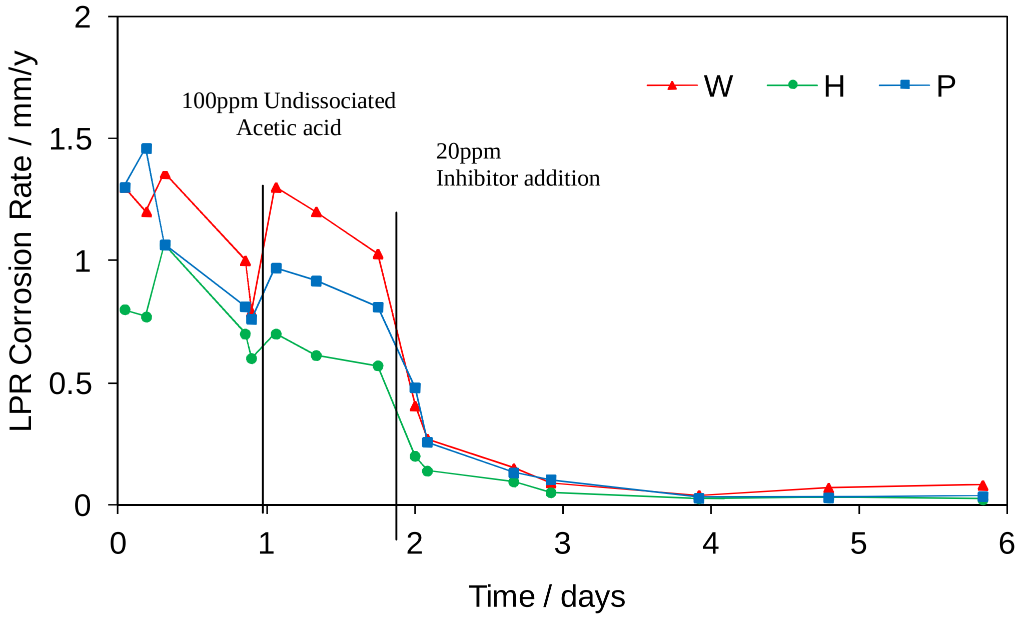

Figure 67. LPR corrosion rate vs. time (60°C, 0.8 bar pCO_2, pH 5, 1 wt% NaCl) with 100 ppm undissociated acetic acid solution.

Intrinsic corrosion rate The galvanic current measurement results for the coupled segments are shown in Figure 68. The metal polarities remain the same as before: the weld material acted as an anode, the HAZ was the neutral section and the parent section acted as a cathode. The addition of 100 ppm undissociated acetic acid increased the magnitude of the galvanic current. However, after 20 ppm of corrosion inhibitor was injected into the test solution, the magnitude of the galvanic current dropped to a negligible value.

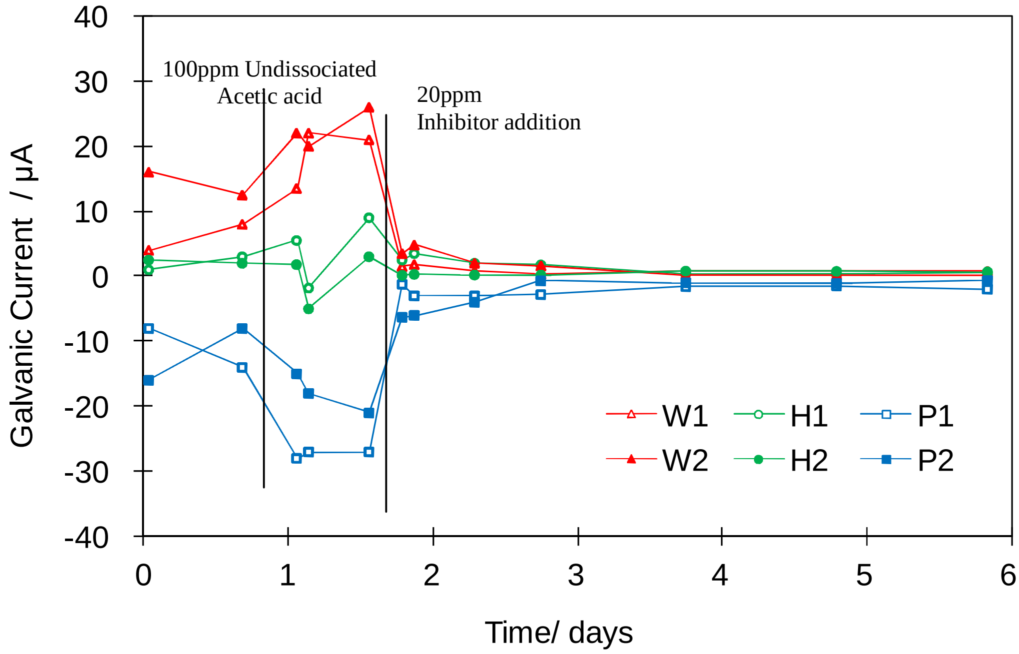

Figure 68. Galvanic current of coupled weldment vs. time with 100 ppm undissociated acetic acid solution.

Electrochemical noise The electrochemical noise data for the weld metal at different experimental periods are shown in Figure 69 to Figure 72. No clear transients which represent localized corrosion events were observed during the whole experimental period.

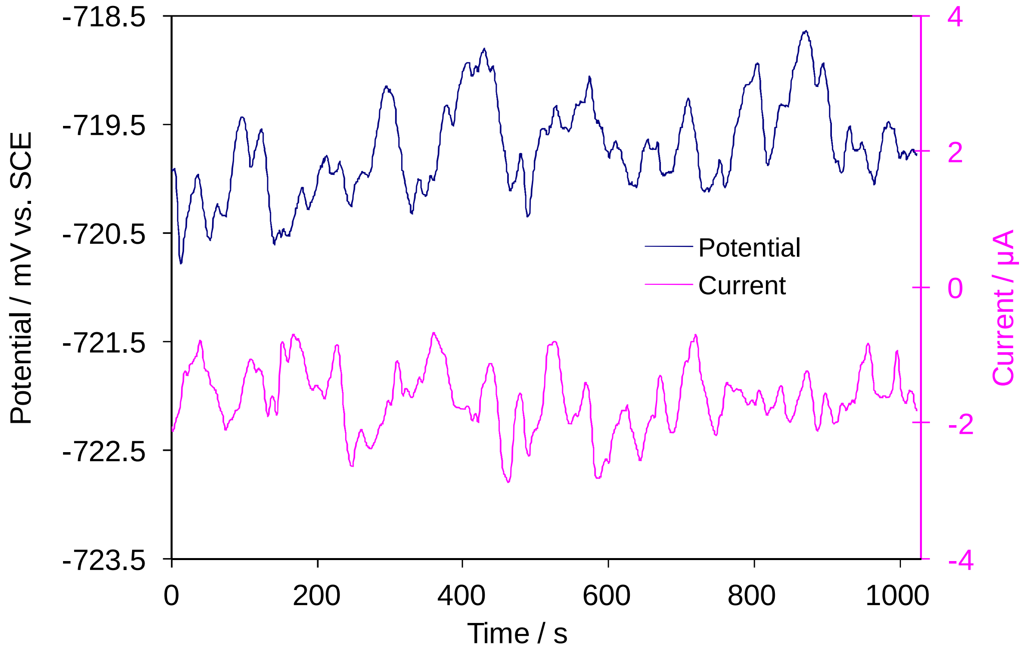

Figure 69. Potential noise and current noise of coupled weld vs. time without acetic acid and corrosion inhibitor (1 day).

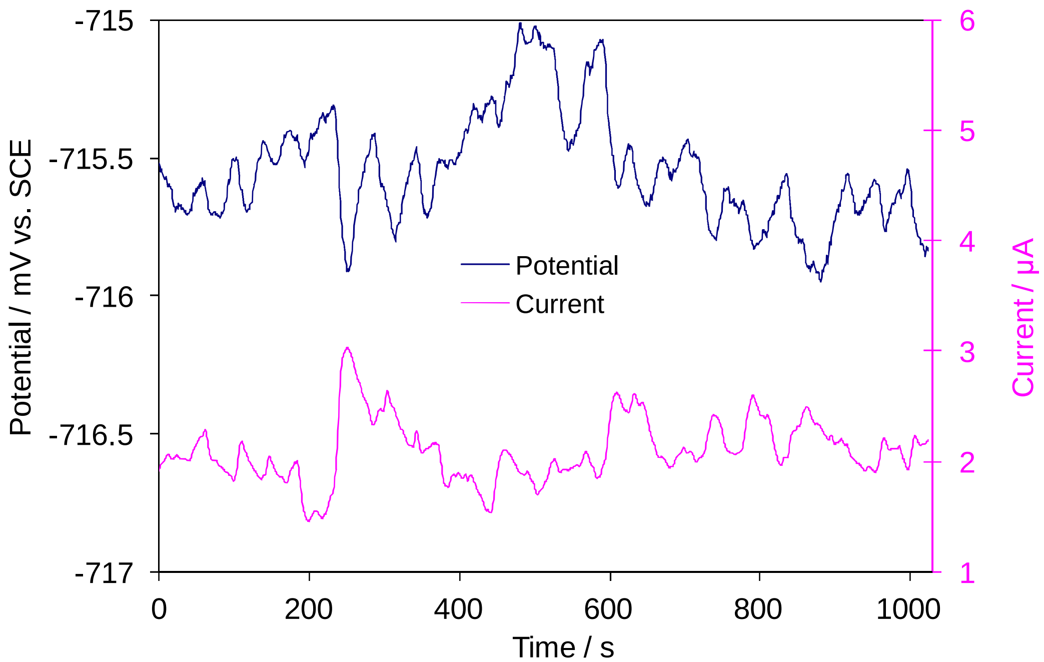

Figure 70. Potential noise and current noise of coupled weld vs. time in 100 ppm undissociated acetic acid solution (1.5 days).

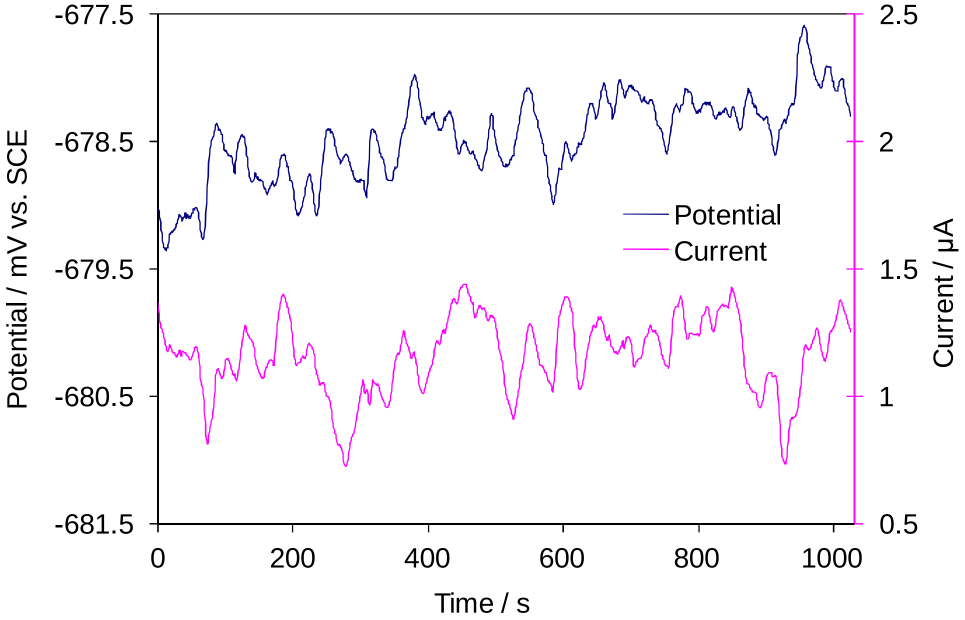

Figure 71. Potential noise and current noise of coupled weld vs. time in 100 ppm undissociated acetic acid solution with 20 ppm corrosion inhibitor (4 days).

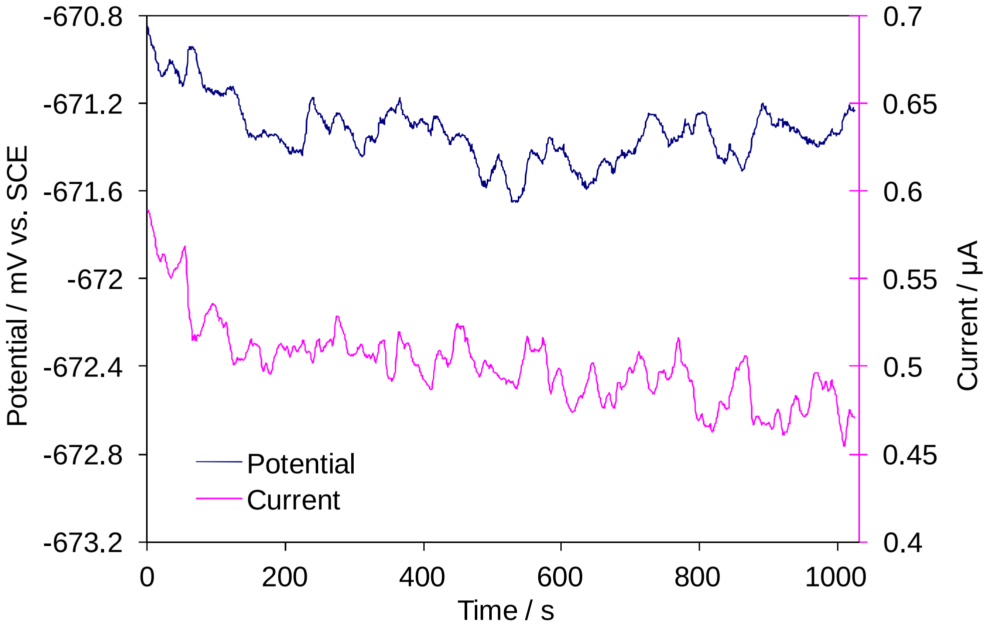

Figure 72. Potential noise and current noise of coupled weld vs. time in 100 ppm undissociated acetic acid solution with 20 ppm corrosion inhibitor (6 days).

The electrochemical noise data in the frequency domain (potential and current power spectrum density) are illustrated in Figure 73 and Figure 74. It can be seen from the experimental results that the energy levels of both potential PSD and current PSD with respect to time are all of the same magnitude. This suggests that most likely the corrosion mechanism under the test condition was uniform corrosion.

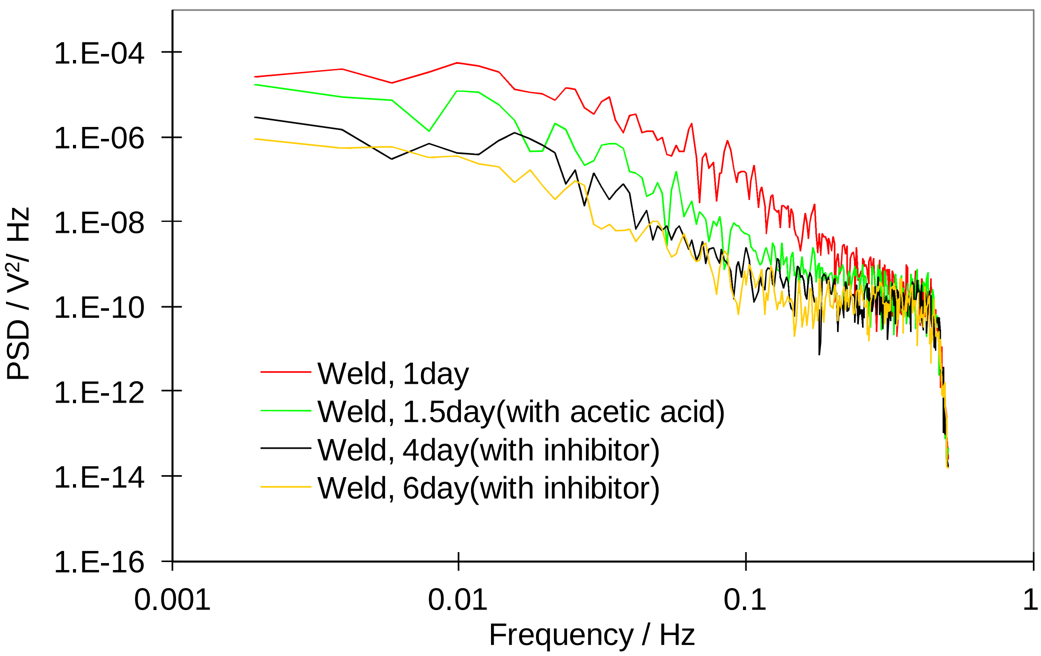

Figure 73. Variation of potential power spectra density (FFT) of coupled weld with time.

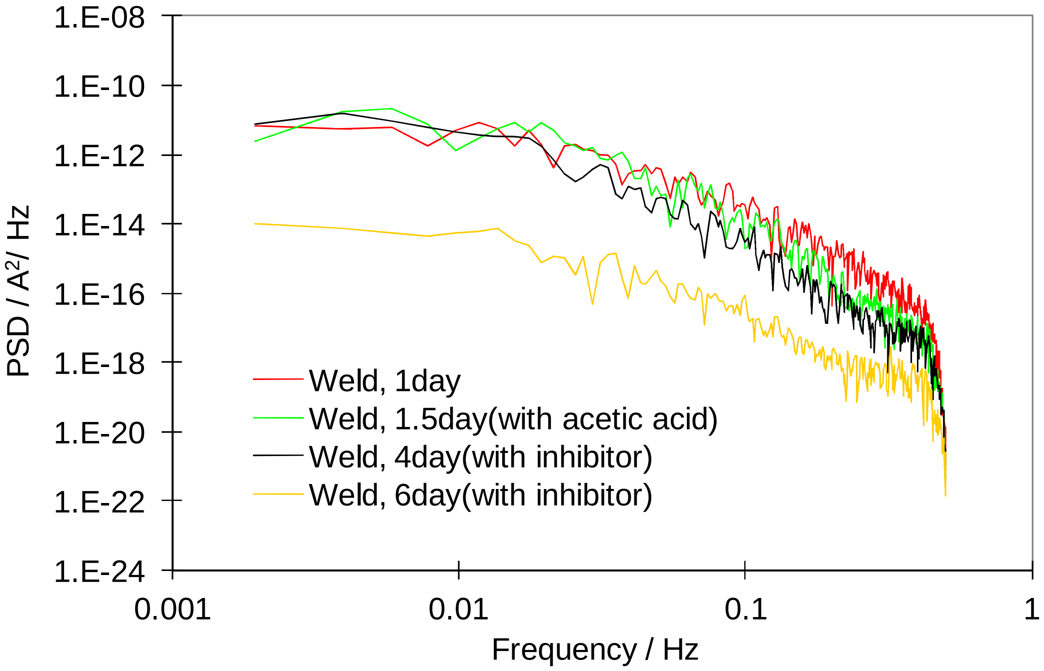

Figure 74. Variation of current power spectra density (FFT) of coupled weld with time.

The specimen surfaces were scanned by SEM to confirm the assumption derived from the electrochemical noise data. The SEM images of the surface of the parent material, the HAZ, and the weld metal after removing the corrosion products are shown in Figure 75, Figure 76, and Figure 77 consecutively. Localized corrosion was not detected on the weldment surfaces. The SEM results are consistent with the electrochemical noise data.

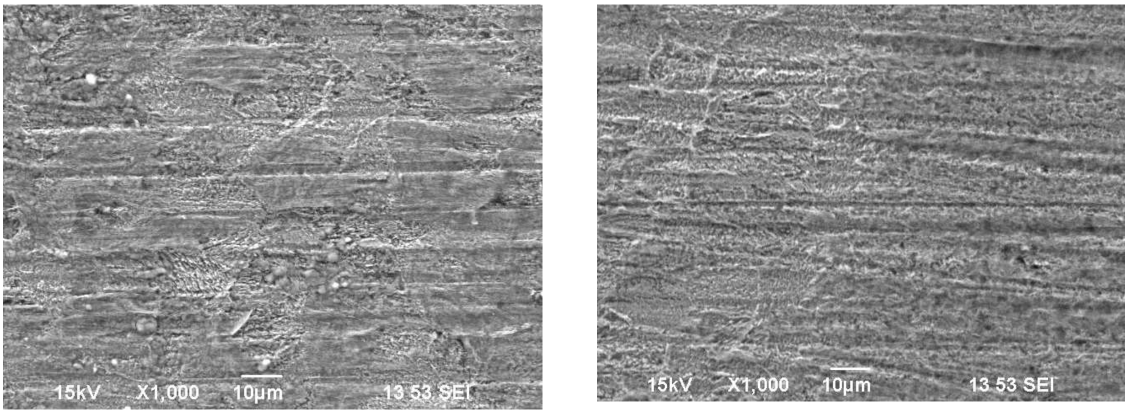

Figure 75. Morphologies of parent material (SEM) of coupled weldment after corrosion in 100 ppm undissociated acetic acid solution with 20ppm corrosion inhibitor.

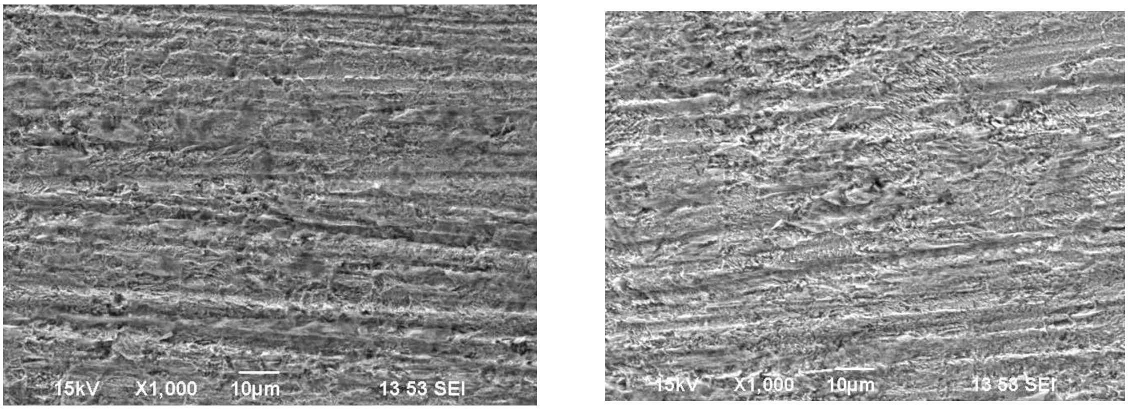

Figure 76. Morphologies of HAZ material (SEM) of coupled weldment after corrosion in 1 wt% NaCl, 100 ppm undissociated acetic acid solution with 20ppm corrosion inhibitor.

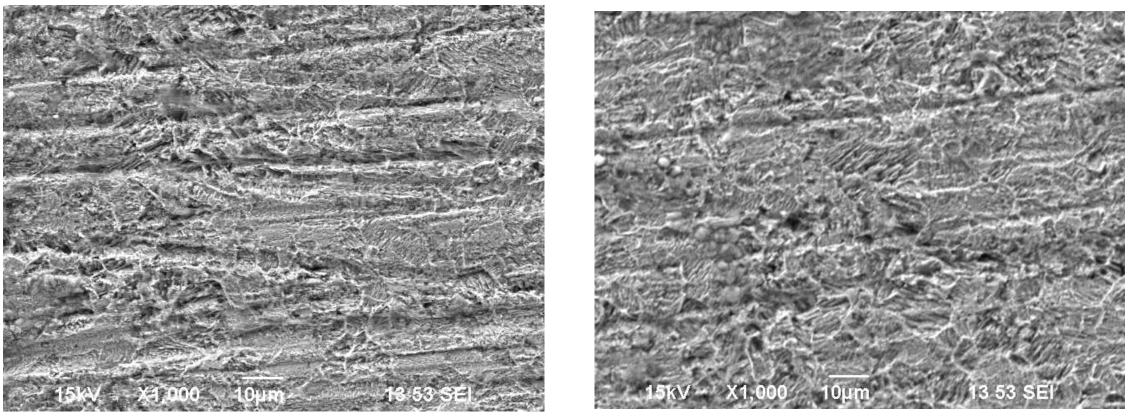

Figure 77. Morphologies of weld material (SEM) of coupled weldment after corrosion in 1 wt% NaCl, 100 ppm undissociated acetic acid solution with 20ppm corrosion inhibitor.

6.1.4.2 Summary

In this series of experiments, 100 ppm acetic acid and 20 ppm corrosion inhibitor were added into the system in succession to study the combined effects of acetic acid and corrosion inhibitor on the weldment corrosion. The experimental results suggest that the corrosion inhibitor is the controlling factor on the intrinsic corrosion and the galvanic corrosion rate. The interaction between the acetic acid and the corrosion inhibitor did not lead to a localized corrosion of the weldment.

6.1.5 The effects of iron carbonate layer

When the concentration of iron carbonate reaches the solubility limit, it will precipitate and finally deposit on the steel surface. The spontaneous formation of an iron carbonate layer on the steel surface is commonly seen in the oil and gas field. When the iron carbonate layer is partially removed due to the change of local conditions, there is a high possibility that localized corrosion can occur. Therefore, it is important to determine the role of iron carbonate on weldment corrosion.

In this set of experiments, the super-saturation of iron carbonate was controlled during the whole experimental period by adjusting the pH of the test solution. The corrosion testing was conducted in three stages. In the iron carbonate formation stage, the super-saturation of iron carbonate was initially controlled at 200 for 2.3 days by adding the $FeCl_2 \cdot 4H_2O$. After a protective layer was formed, the pH was adjusted again to maintain the saturation of iron carbonate at 0.04 for 4 hours. At the last stage, the saturation of iron carbonate was maintained in the so called “gray zone” (0.5~2) until the experiment was finished.

6.1.5.1 Experimental results

Saturation of iron carbonate In this experiment, the saturation of iron carbonate was controlled and adjusted throughout the whole experiment. Figure 78 shows the calculated saturation values with time for iron carbonate. The saturation of iron carbonate was kept high at the beginning of the test and then it slowly dropped toward one due to the formation of iron carbonate layer on the weldment surface. After the protective layer was formed, iron carbonate was adjusted to under-saturation at 0.04 to let the precipitated layer be partially dissolved. Then the saturation was maintained close to saturation, i.e. in the "grey zone".

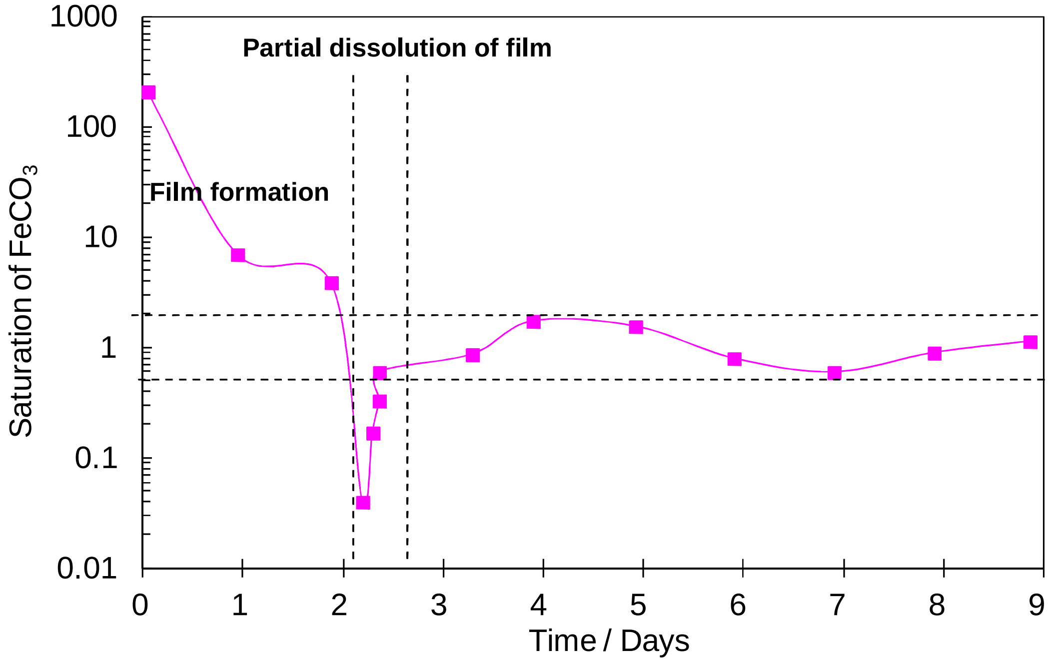

Figure 78. Saturation of $FeCO_3$ with time.

Intrinsic corrosion rate The intrinsic corrosion rates of uncoupled parent, HAZ, and weld materials measured by LPR are shown in Figure 79. The corrosion rate results are in a good agreement with the saturation of iron carbonate. The initial corrosion rate started high at about 1 mm/yr. After the saturation of iron carbonate was adjusted to 200, the intrinsic corrosion rates of all segments immediately decreased due to the formation of iron carbonate layer. When the iron carbonate in solution was adjusted to under-saturation, the corrosion rate started to increase because of the partial dissolution of the iron carbonate layer. Then saturation of iron carbonate was maintained in the range of 0.5 to 2, which resulted in a relatively high corrosion rate at around 0.5 mm/yr.

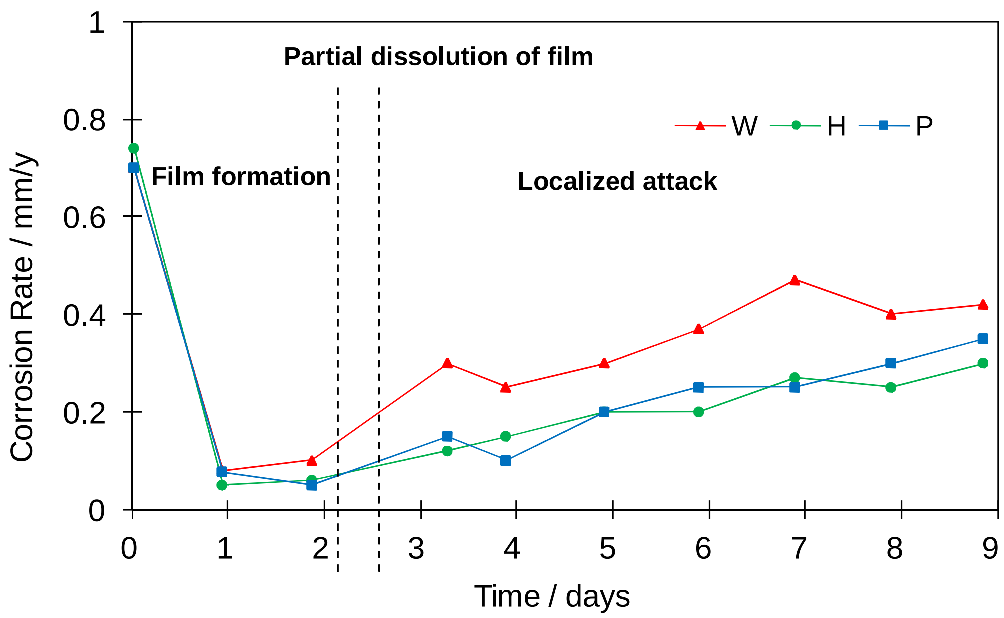

Figure 79. LPR corrosion rate of uncoupled weldment vs. time.

Galvanic current The results of galvanic current measurement for coupled segments are shown in Figure 80. According to the previous test results, it appeared that the weld material was the more active material, acting as an anode. The HAZ was the neutral section. The parent section was the more noble material acting as a cathode and was protected. In general, the magnitude of the galvanic current was small for standard weld tested. In this experiment, the change of galvanic current followed the trend of intrinsic corrosion rate with respect to time. The formation of iron carbonate layer also reduced the magnitude of galvanic current. However, it is unusual that all segments did not show consistently anodic or cathodic behavior. For instance, the W2 weld metal switched its polarity several times during the first seven days, but became an anode by the end of the test. Interestingly, the same materials, P1 and P2, exhibited different polarity behavior. P1 showed cathodic behavior and P2 showed anodic behavior.

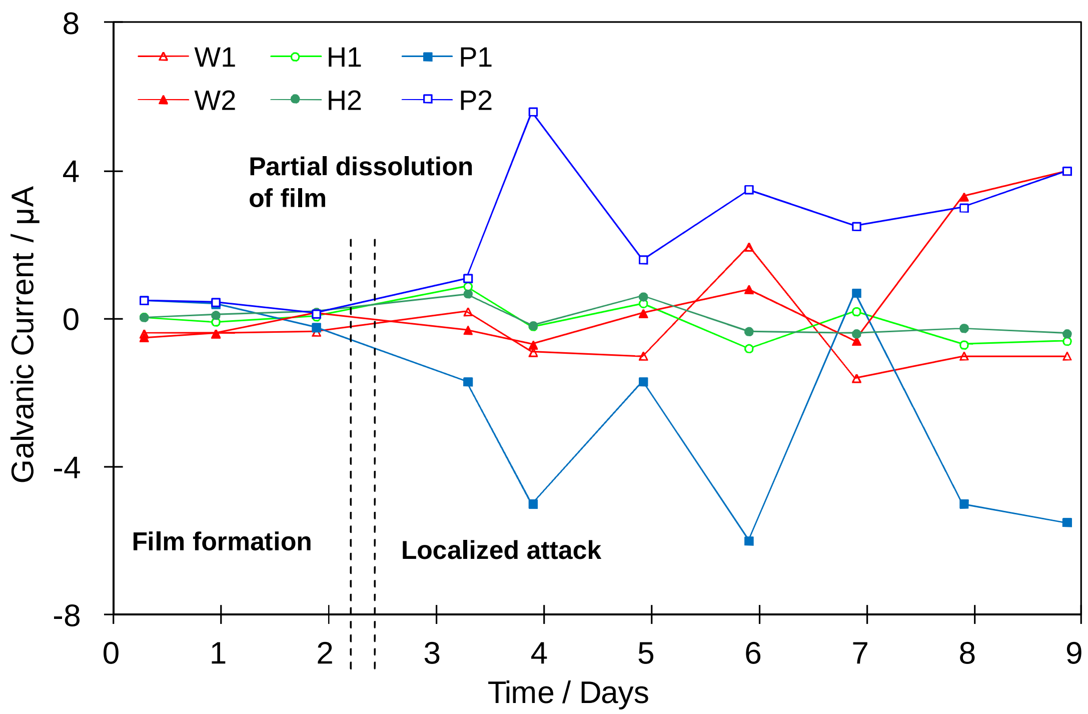

Figure 80. Galvanic current of coupled weldment vs. time.

Electrochemical noise The electrochemical noise measurements were conducted for all segments of the weldment. The potential and current noise data of the parents, the HAZs, and the welds at different experimental periods are shown from Figure 81 to Figure 95. From the noise data for parent metal (Figure 81 to Figure 84), it is clearly seen that during the first five days, no transients were observed. On the sixth day, the noise signal of sudden decrease followed by an exponential decay was observed in the time domain (Figure 83). This is a sign of the initiation of metastable pitting.

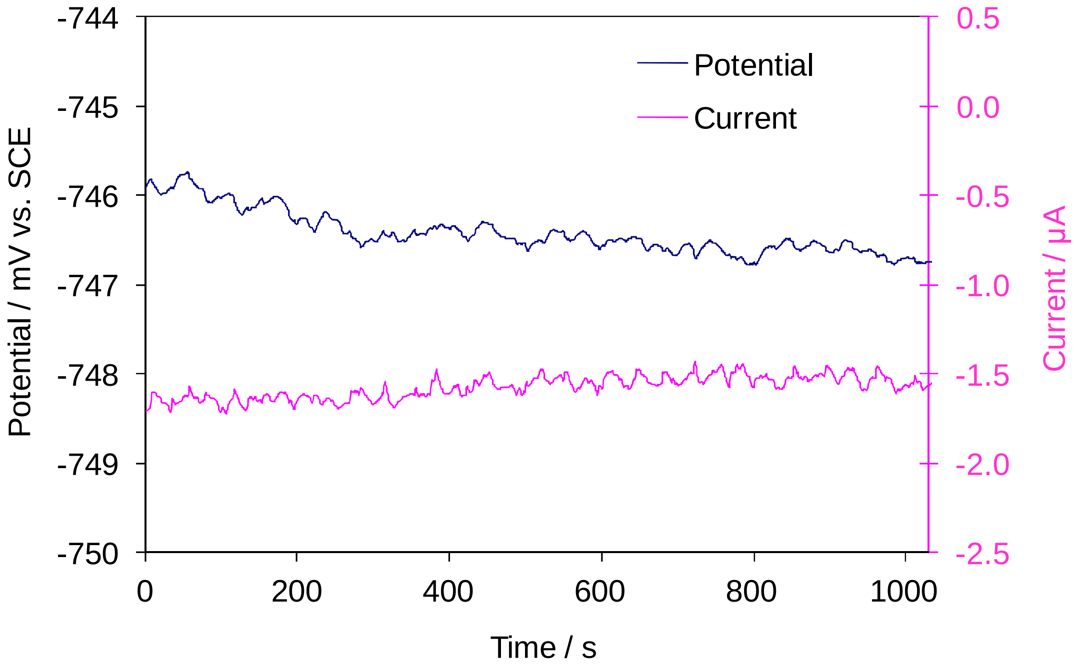

Figure 81. Potential and current noise raw data of parent metal at 3days.

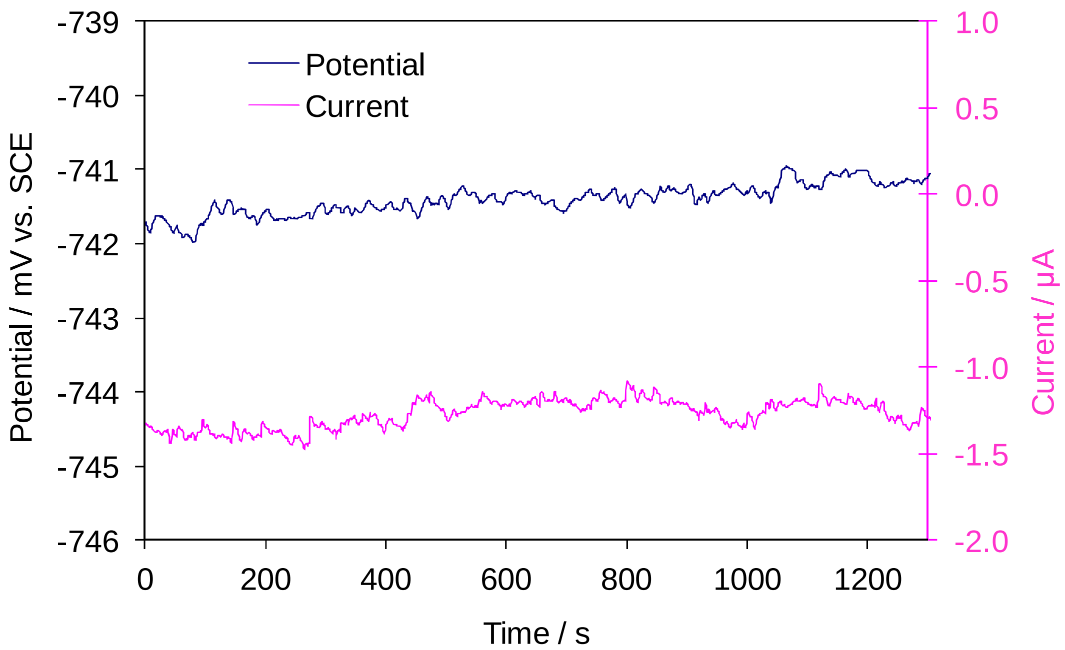

Figure 82. Potential and current noise raw data of parent metal at 5 days.

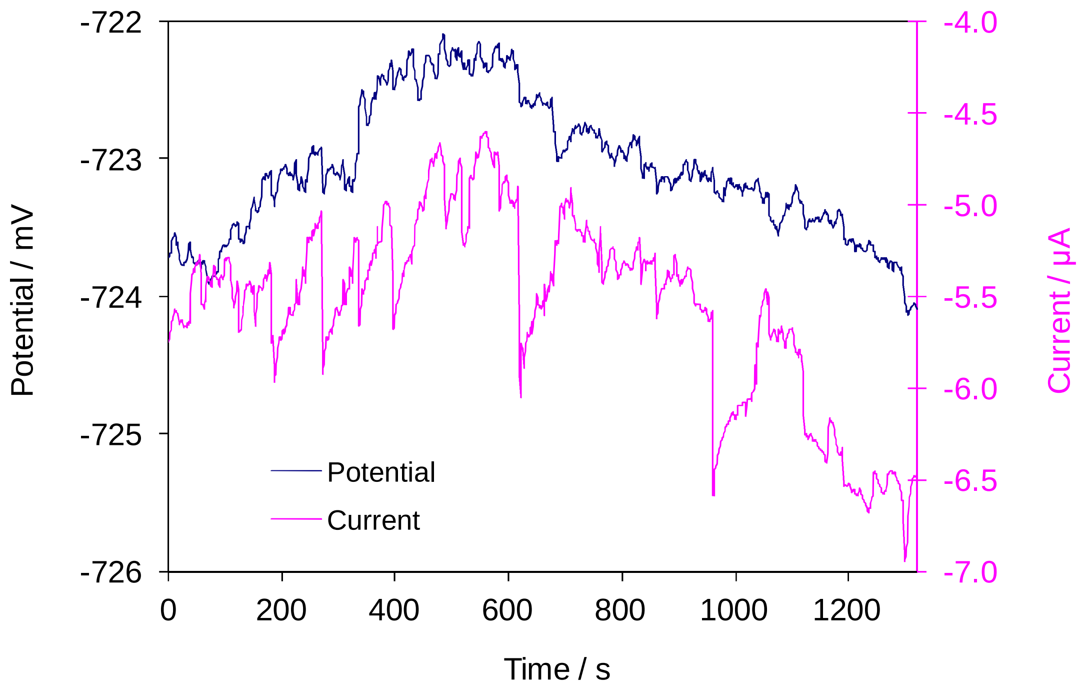

Figure 83. Potential and current noise raw data of parent metal at 6days.

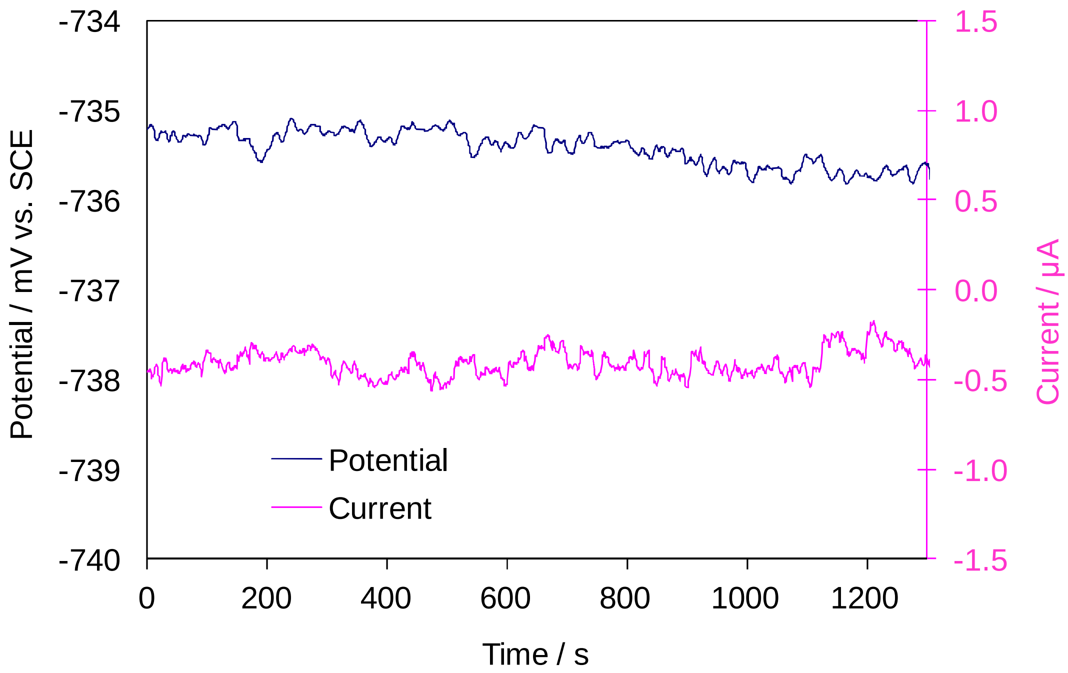

Figure 84. Potential and current noise raw data of parent metal at 7days.

Figure 85 shows the current power spectrum density data for the parent metal. Obviously, the energy level of the PSD at sixth day is much higher than the rest, which suggests that an unusual event occurred at that time and most likely to be the localized corrosion event. The PSD data is very consistent with the noise date in time domain.

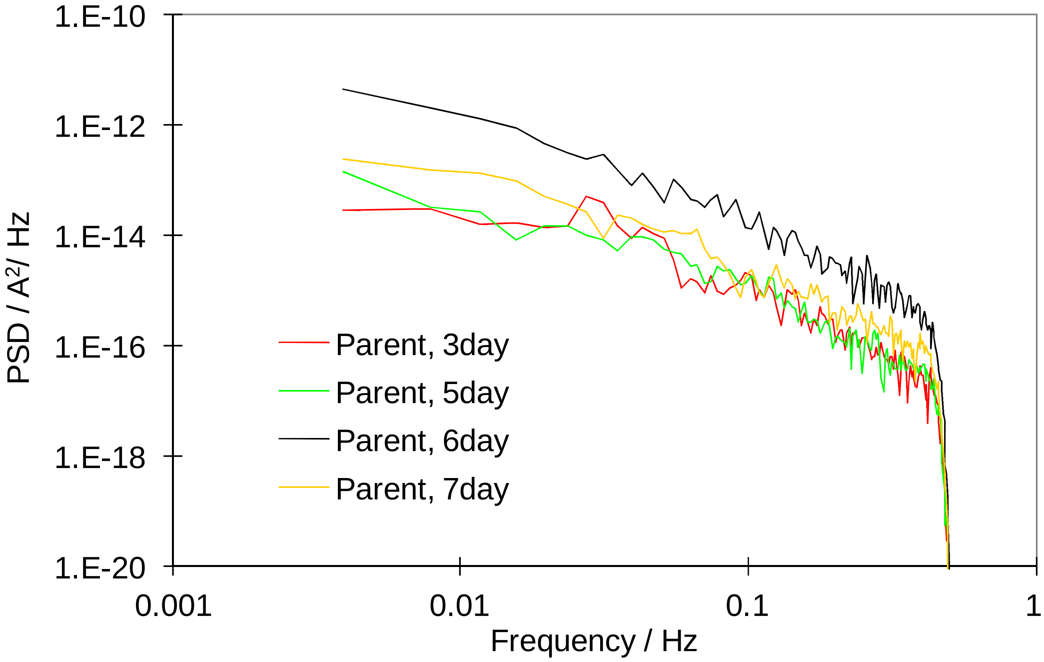

Figure 85. Current power spectrum density of parent metal with time.

For HAZ metal, similar transients were observed at the fifth (Figure 87), sixth (Figure 88), and seventh day (Figure 89). It is worth noting that the shapes of the transients were different. Localized corrosion may also have occurred on the HAZ surface.

The noise data in time domain was then converted to frequency domain and the PSD data for HAZ is shown in Figure 90. Apparently, the energy levels of the PSD at fifth, sixth and seventh day are in the same magnitude and are higher than the one at the first day. Both noise and PSD data suggest that HAZ may undergo the localized corrosion.

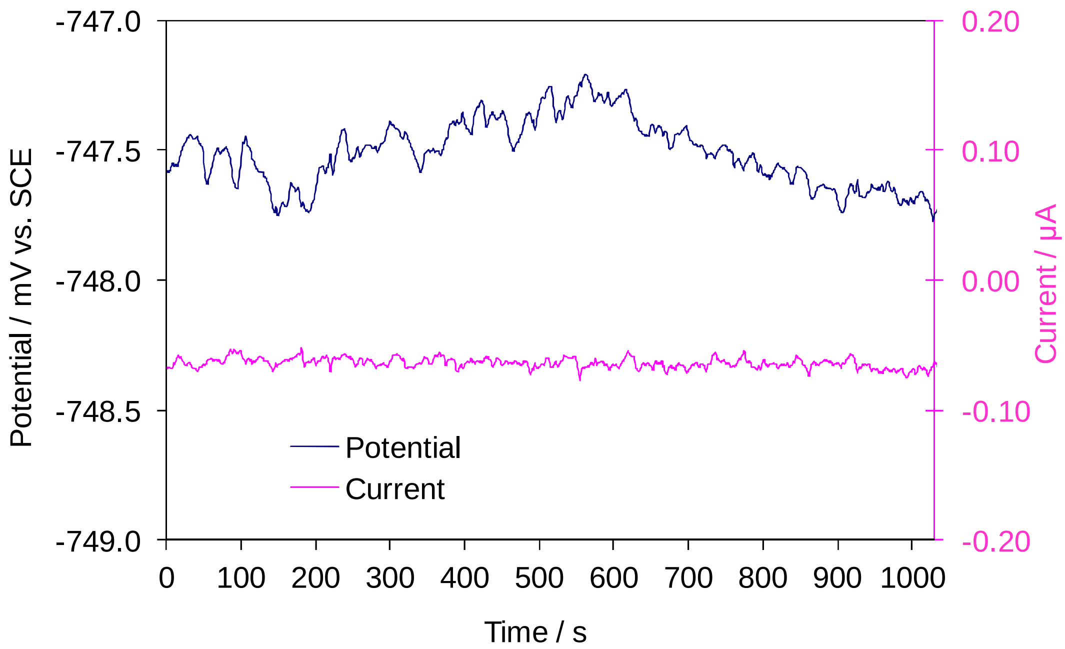

Figure 86. Potential and current noise raw data of HAZ metal at 3days.

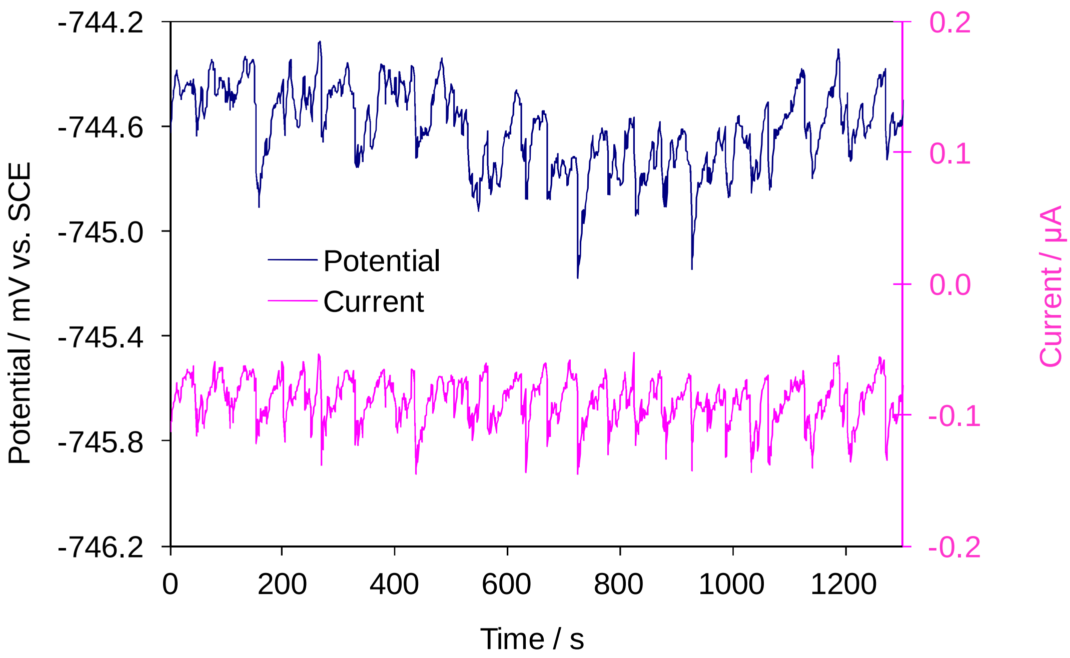

Figure 87. Potential and current noise raw data of HAZ metal at 5days.

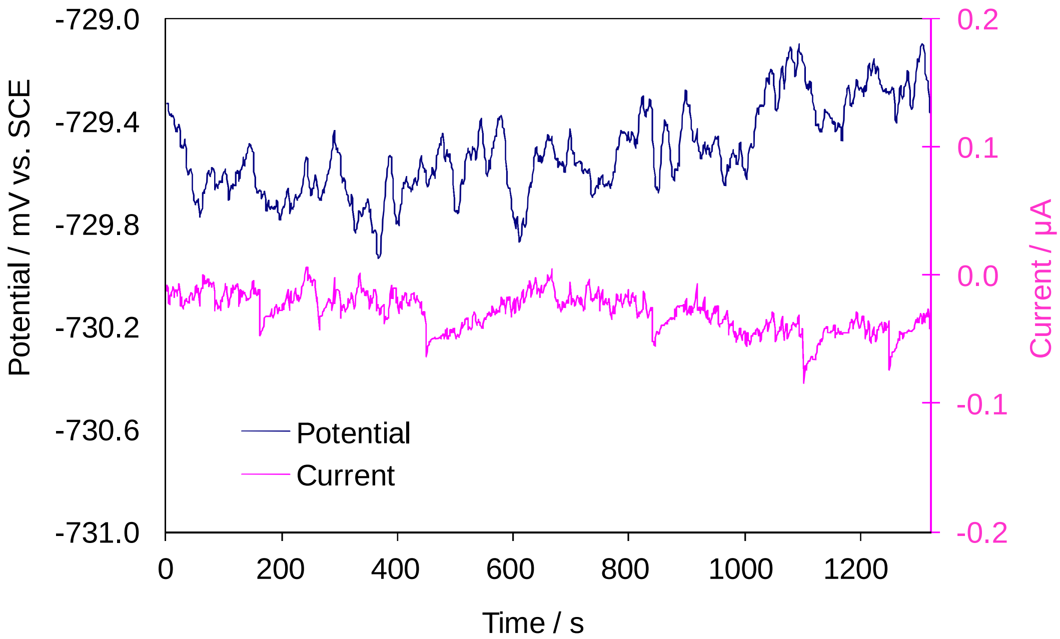

Figure 88. Potential and current noise raw data of HAZ metal at 6days.

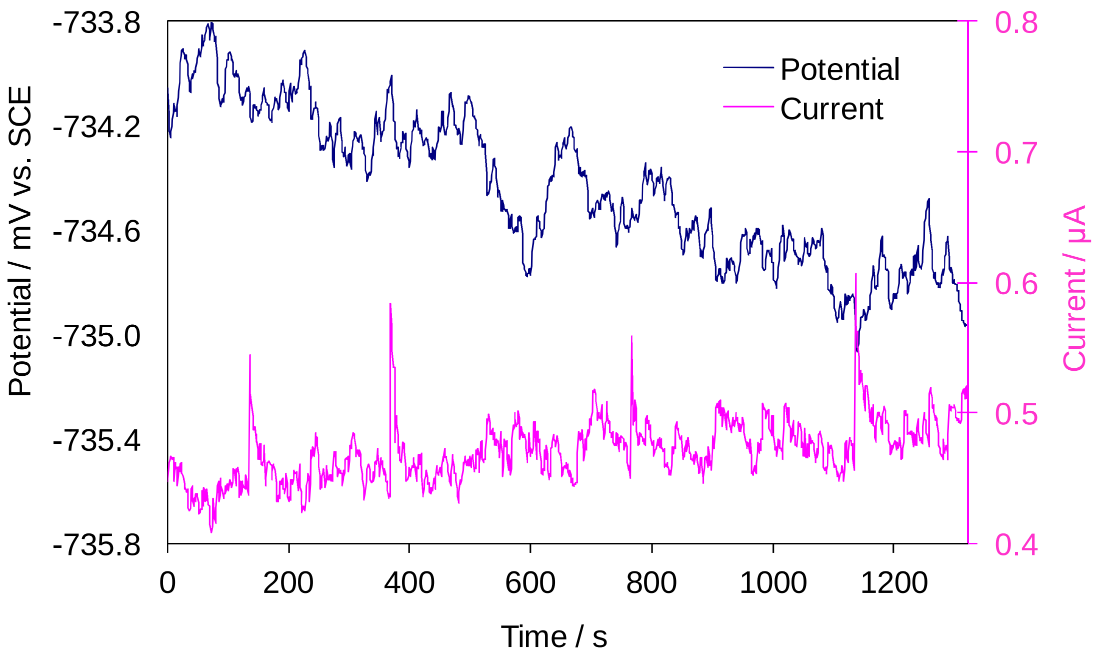

Figure 89. Potential and current noise raw data of HAZ metal at 7days.

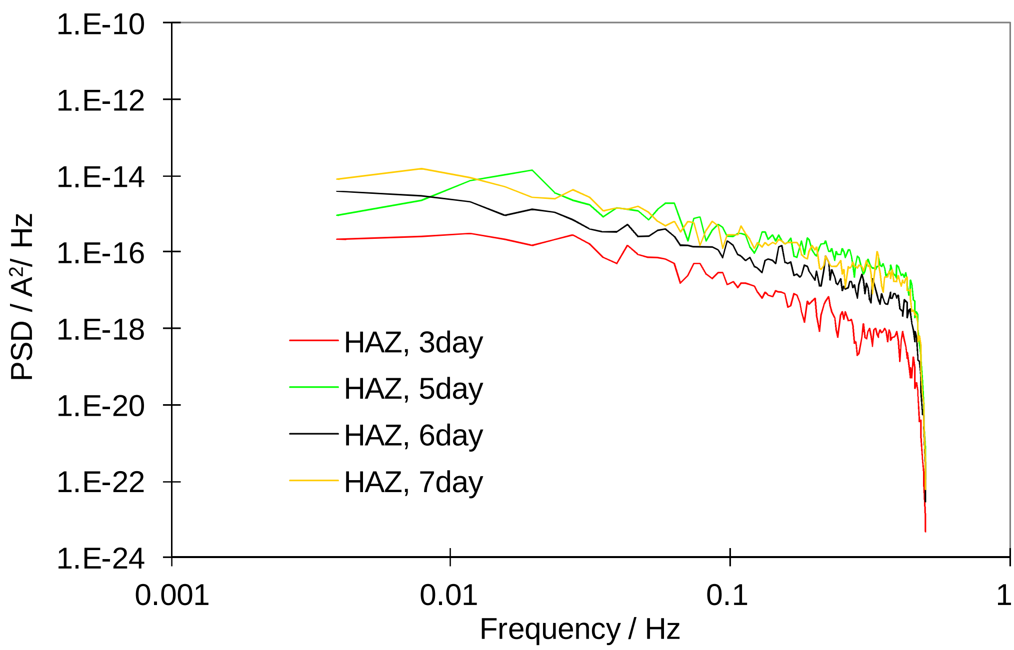

Figure 90. Current power spectrum density of HAZ metal with time.

The potential and current noise of the weld metal were measured as well and are shown from Figure 91 to Figure 94. Clear transient was observed from the noise data on the sixth day. The shape of the transient for weld metal is similar to the one observed for parent metal. This indicates that the same corrosion event may have occurred to parent and weld metal at the same time period.

The current power spectrum density data for weld metal shown in Figure 95 is consistent with the noise data in time domain. The magnitude of the PSD at the sixth day is much higher than the rest.

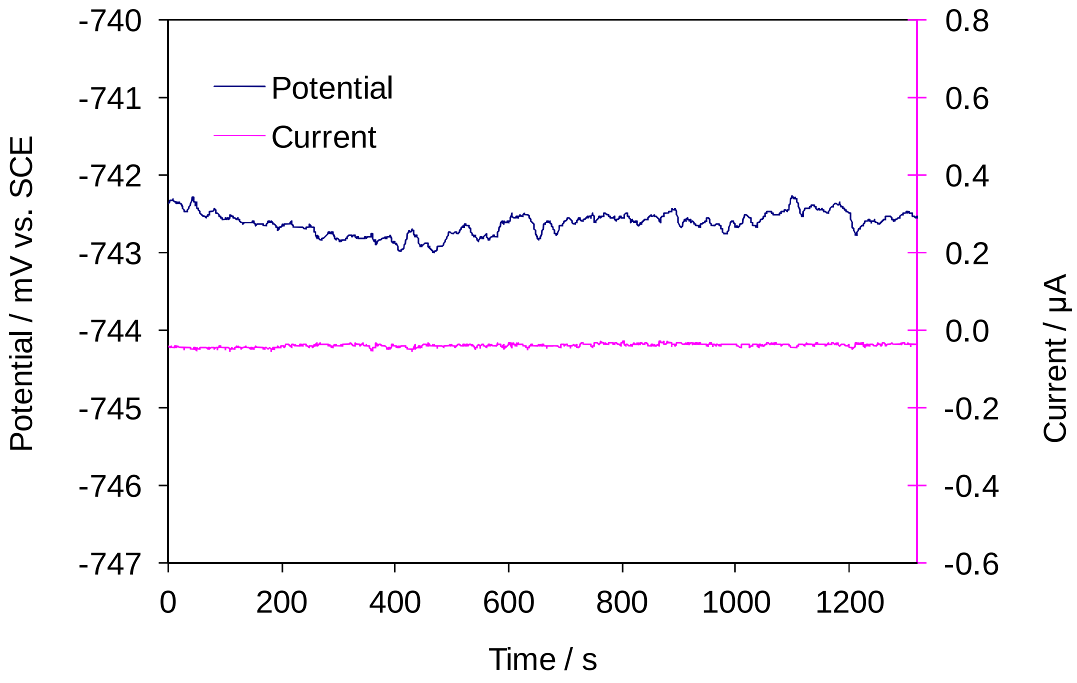

Figure 91. Potential and current noise raw data of Weld metal at 3 days.

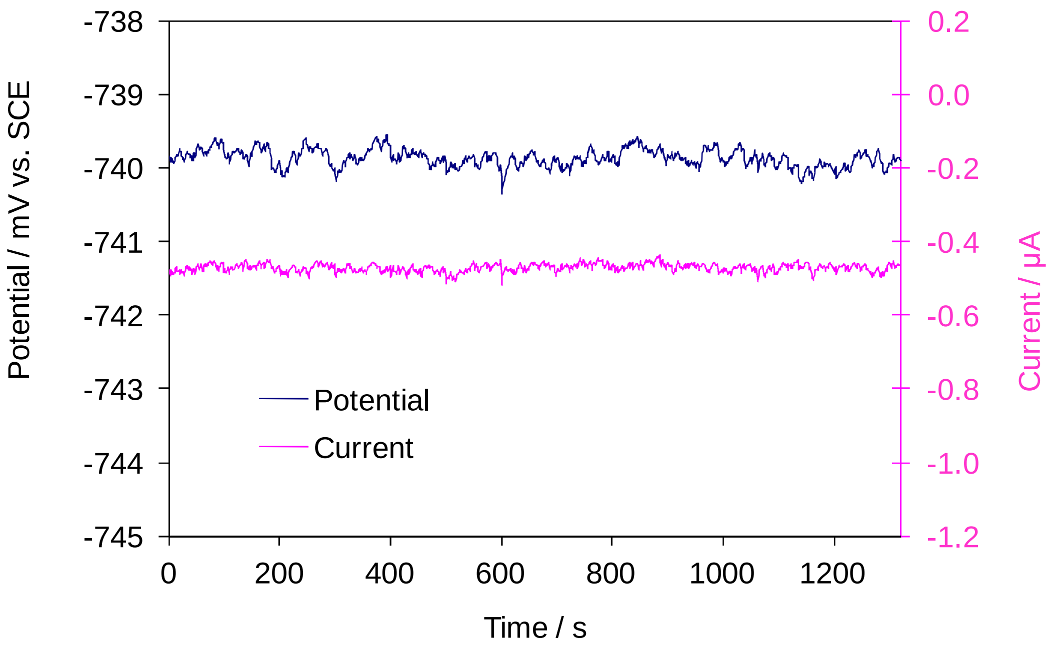

Figure 92. Potential and current noise raw data of Weld metal at 5 days.

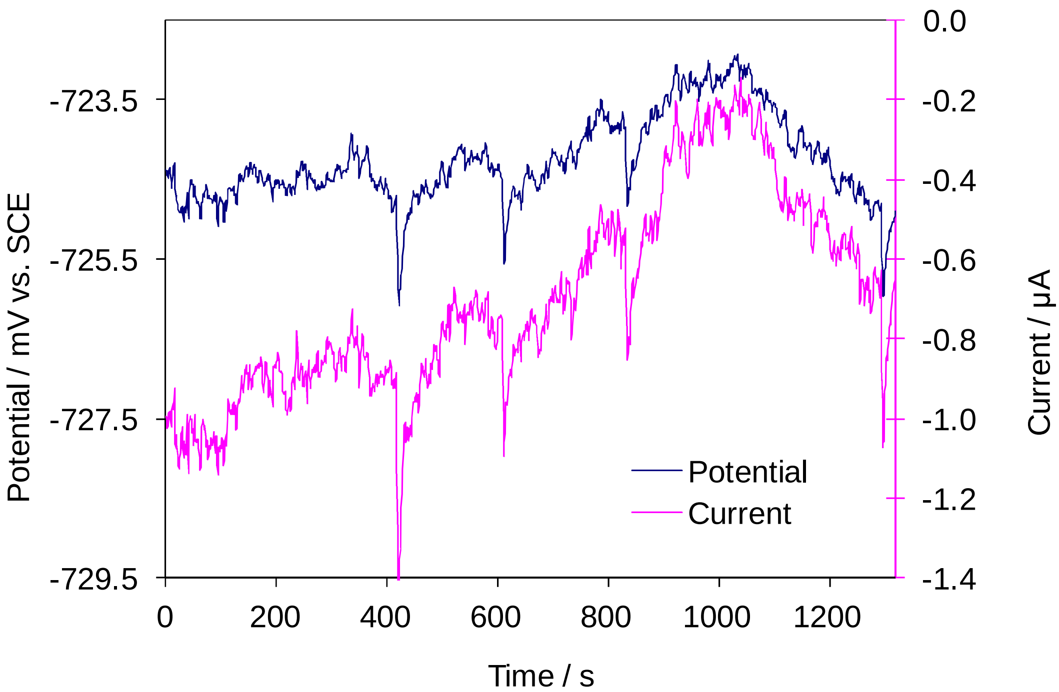

Figure 93. Potential and current noise raw data of Weld metal at 6 days.

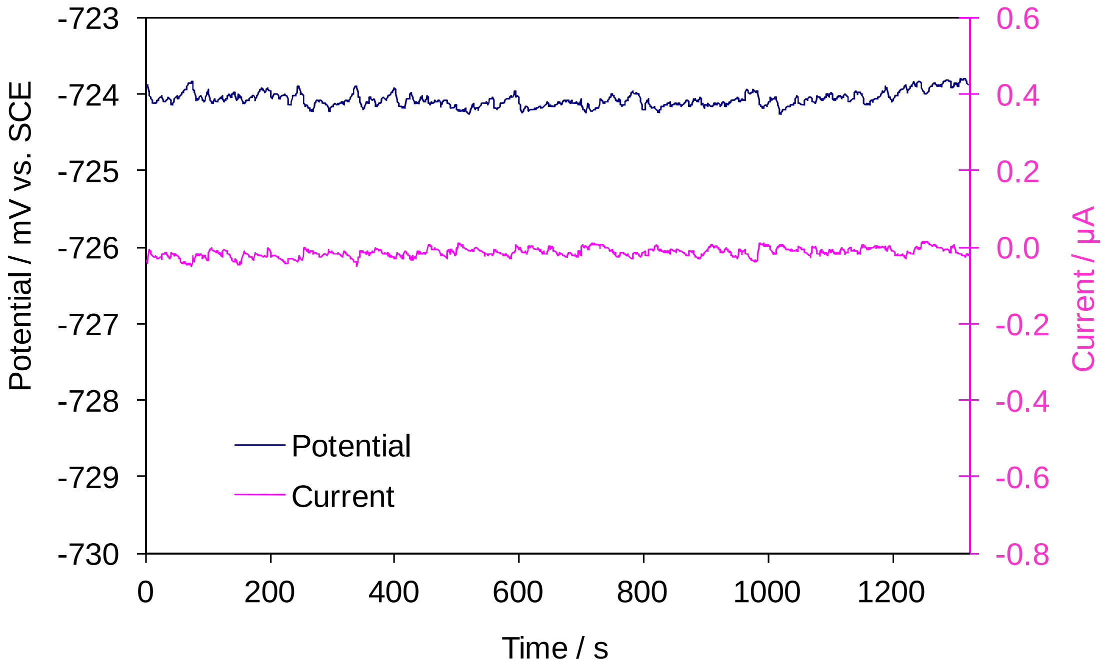

Figure 94. Potential and current noise raw data of Weld metal at 7days.

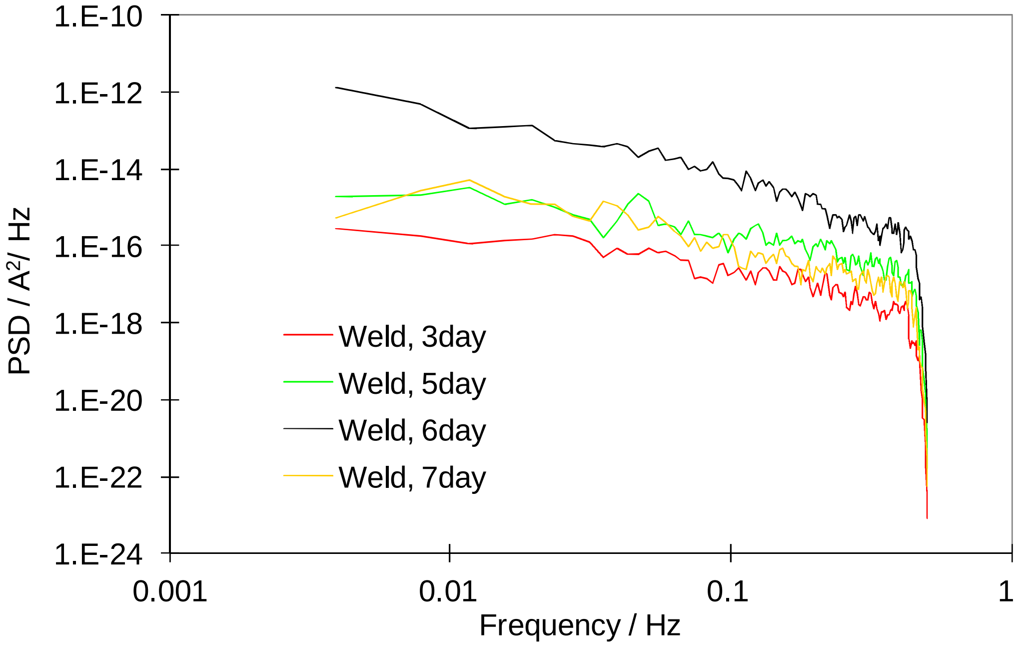

Figure 95. Current power spectrum density of Weld metal with time.

Surface analysis The weldment specimen during different test periods was scanned by SEM. A SEM image of parent metal at the iron carbonate formation stage is shown in Figure 96. The dense and highly crystallized iron carbonate layer was formed on the surface of parent metal. The protectiveness of the iron carbonate layer has been proven from the intrinsic corrosion rate data.

Figure 97 shows the SEM images of parent metal at the beginning of the “grey zone” stage. The clear message from this image is that the parent metal surface was partially covered by the crystallized iron carbonate layers.

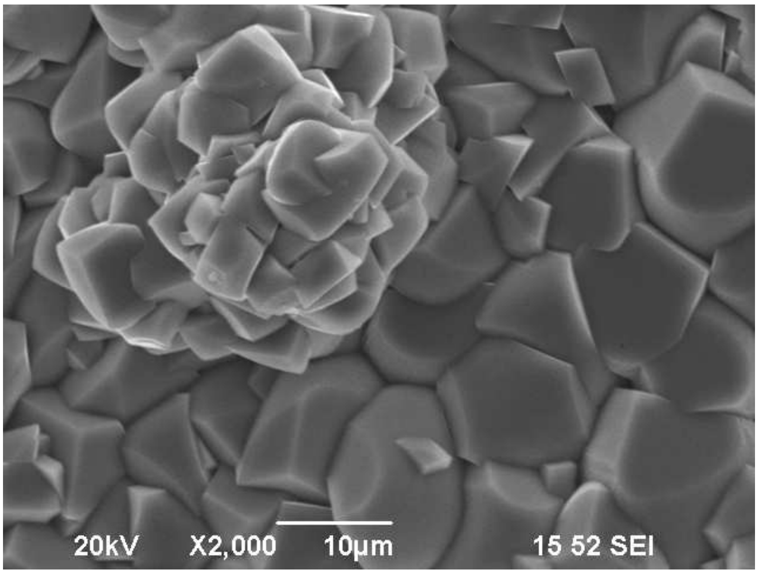

Figure 96. Surface morphology of parent at film formation stage.

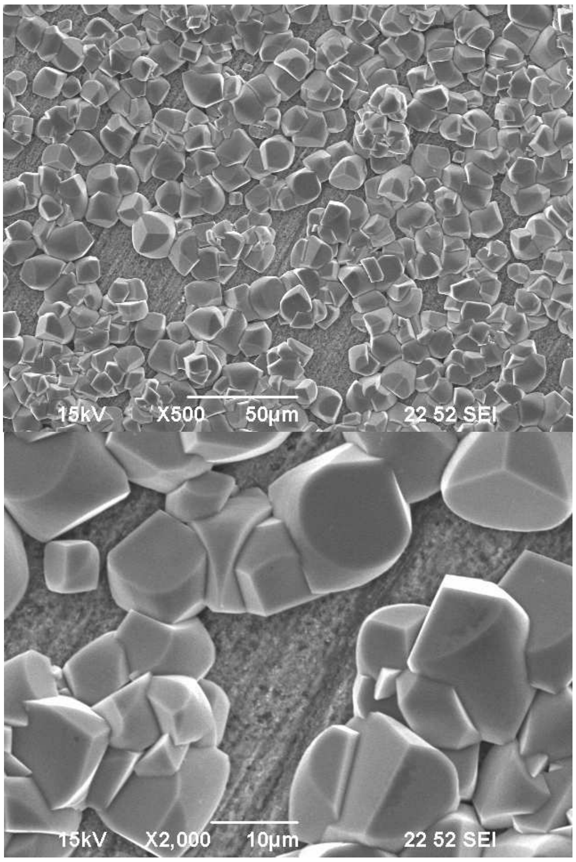

Figure 97. Surface morphology of parent surface after 2.5 days.

At the end of the experiment, all of the segments of the weldment specimen were scanned by SEM. Figure 98 shows the SEM images of the segments with the corrosion products. It has been observed that the iron carbonate was scattered on the specimen surface and appeared to be not protective.

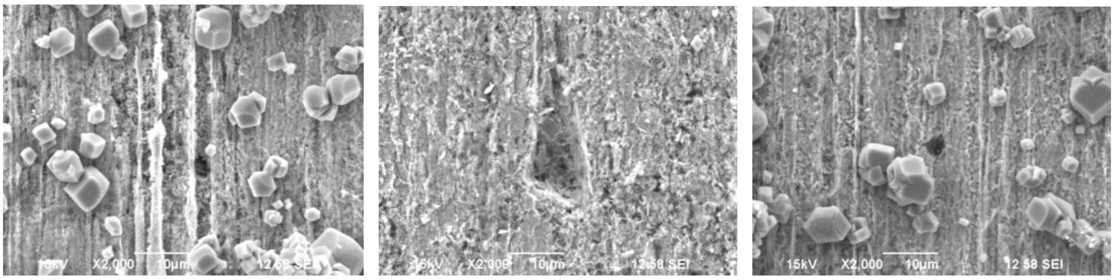

(a) Parent (b) HAZ (c) Weld

Figure 98. Surface morphology (with film) of parent, HAZ, and weld after 9 days.

The corrosion products were then removed by Clarke's solution and scanned by SEM again. The images of the segments are shown in Figure 99. Localized attack was observed on the surfaces of all segments. The diameters of the pitting attacks are all in the same magnitude at around 10 µm. The depth of the pits was quantified afterward.

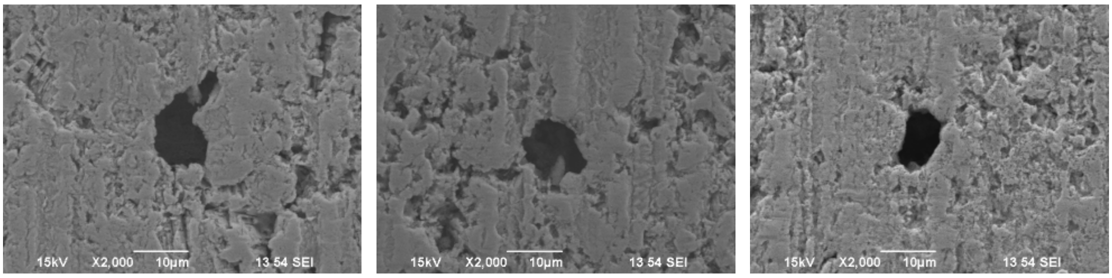

(a) Parent (b) HAZ (c) Weld

Figure 99. Surface morphology (without film) of parent, HAZ, and weld after 9 days.

The infinite focus microscope (IFM) was used to measure the depth of localized attack. The IFM images and corresponding surface profiles of parent metal, HAZ metal, and weld metal are shown in Figure 100, Figure 101, and Figure 102. The pitting corrosion was visually revealed by the IFM images and also quantified by the surface profile analysis. The ratios of the pitting corrosion rate over the general corrosion rate for parent, HAZ, and weld are 7.5, 4 and 3.3, respectively. The pitting rates were significantly higher than the general corrosion rate. The IFM and SEM analysis are in good agreement with the electrochemical noise data.

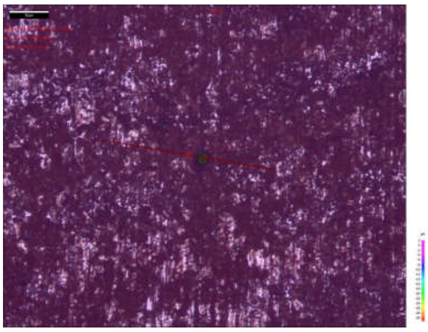

Pit depth=30μm
Localized corrosion rate=1.43mm/y
General corrosion rate=0.19mm/y

$$\frac{Localized \ \ corrosion \ \ rate}{General \ \ corrosion \ \ rate} = \mathbf{7.5}$$

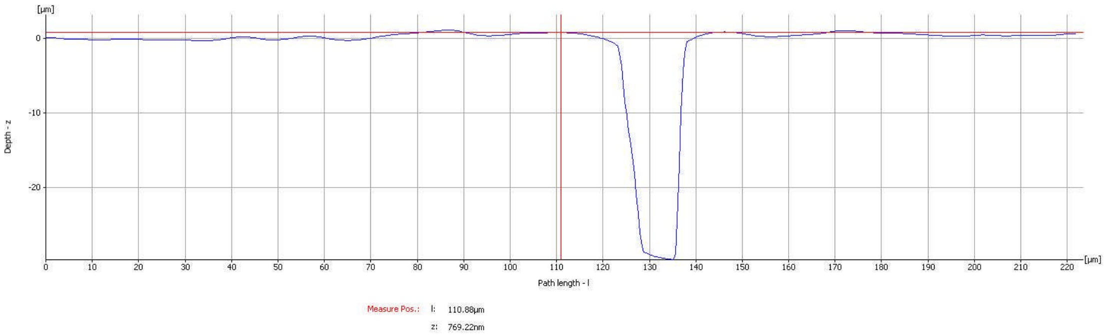

Figure 100. IFM image and profile at the line in the image of parent metal (without film) after 9 days.

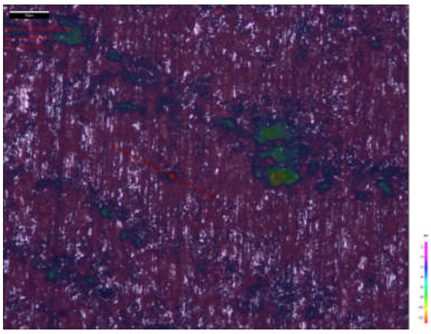

Pit depth=13µm
Localized corrosion rate=0.72mm/y
General corrosion rate=0.18mm/y

$$\frac{Localized \quad corrosion \quad rate}{General \quad corrosion \quad rate} = \mathbf{4}$$

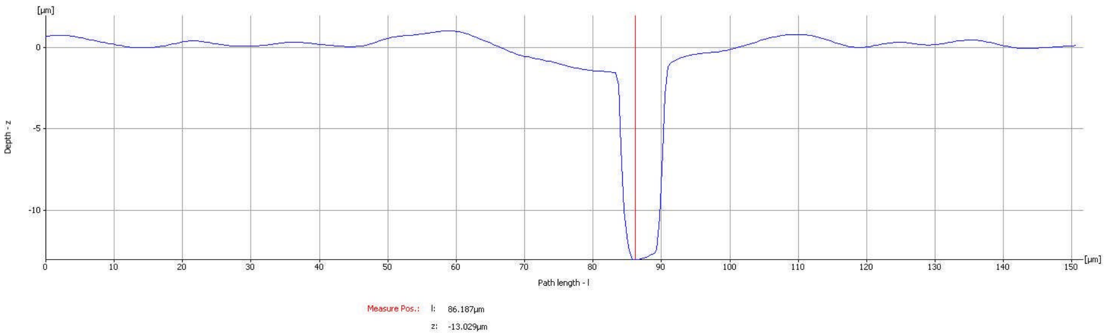

Figure 101. IFM image and profile at the line in the image of HAZ metal (without film) after 9 days.

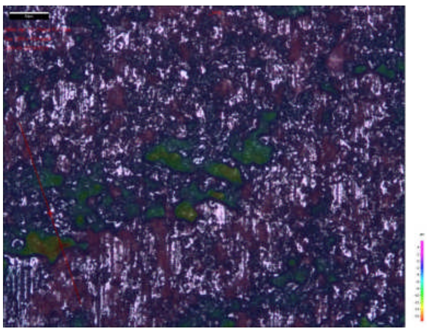

Pit depth=17µm
Localized corrosion rate=1mm/y
General corrosion rate=0.3mm/y

$$\frac{Localized \quad corrosion \quad rate}{General \quad corrosion \quad rate} = \mathbf{3.3}$$

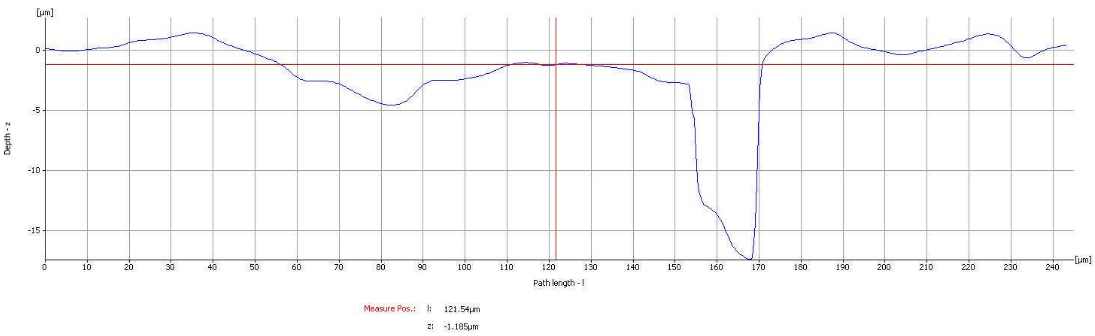

Figure 102. IFM image and profile at the line in the image of Weld metal (without film) after 9 days.

6.1.5.2 Summary

The formation and partial removal of iron carbonate layers were simulated in the weldment corrosion system. From the experimental results, it has been observed that the formation of iron carbonate layer significantly decreased the intrinsic corrosion rate of all segments.

The magnitude of galvanic current was reduced by the formation of iron carbonate as well. However, the metal polarity did not follow the trend which was observed from the previous experiments.

Localized corrosion attack was detected on the surface of all segments. Clear transient was observed from the electrochemical noise data, which corresponds to the localized corrosion event. SEM and IFM analysis further confirms the occurrence of localized corrosion.

6.2 Environmental effects on weldment corrosion in CO_2/H_2S system

Similar experiments were conducted in a slightly sour system (50 ppm H_2S). In this series of experiments, the effects of H_2S, acetic acid and corrosion inhibitor on the weldment in sour systems were studied.

6.2.1 The effects of 50 ppm H_2S

Intrinsic corrosion rate The weldment specimen was exposed to pure CO_2 for one hour before 50 ppm H_2S was added into the system. The intrinsic corrosion rate of each uncoupled segment was measured by LPR for the whole experimental period. The results are shown in Figure 103. From the results, it is clearly seen that the corrosion rate of each segment decreased immediately after the 50 ppm H_2S was introduced into the system. This is due to the fast formation of a thin and protective iron sulfide layer, which limited the surface area available to the corrosive species. The retardation effects of H_2S on the intrinsic corrosion rate are quite similar to the corrosion inhibitor.

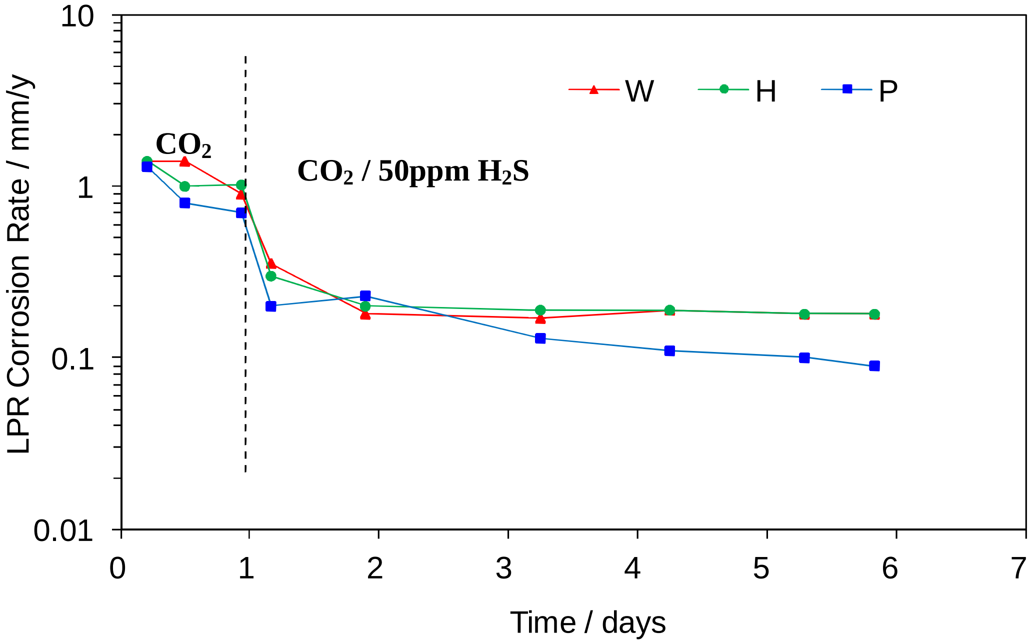

Figure 103. LPR corrosion rate of uncoupled weldment vs. time (60°C, pH 5, 1 wt% NaCl purged with CO_2 and 50 ppm H_2S).

Galvanic current The galvanic current measurement results of coupled segments are shown in Figure 104. According to the test result, it appears that the metal polarity during the whole test period still followed the general trend: the weld is anodic, the HAZ is neutral and the parent is cathodic. The magnitude of galvanic current was reduced by the introduction of 50 ppm H_2S. This suggests that H_2S retarded the galvanic effects. However, the addition of H_2S did not change the metal polarity.

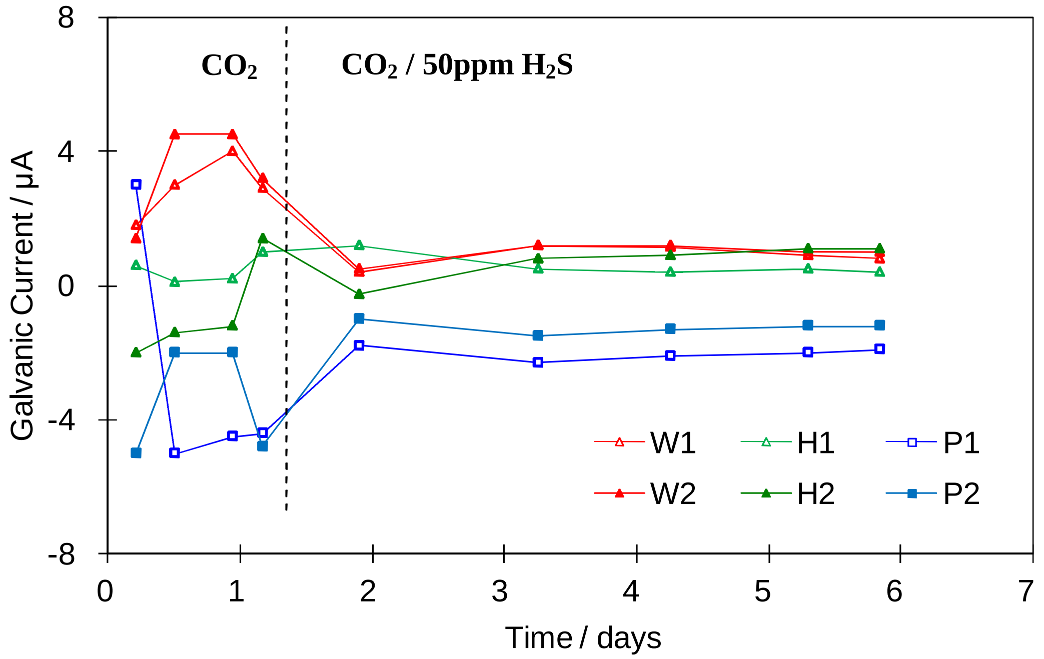

Figure 104. Galvanic current of coupled weldment vs. time (60°C, pH 5, 1 wt% NaCl purged with CO_2 and 50 ppm H_2S).

Electrochemical noise Electrochemical noise measurements were conducted for every segment. The data for each segment are similar so that only the noise data of HAZ metal at 4 day in CO_2/H_2S environment is shown (Figure 105). The signature of localized corrosion, transient, was not observed from either potential or current noise data in time domain. This suggests that the localized corrosion is less likely to occur under these test conditions.

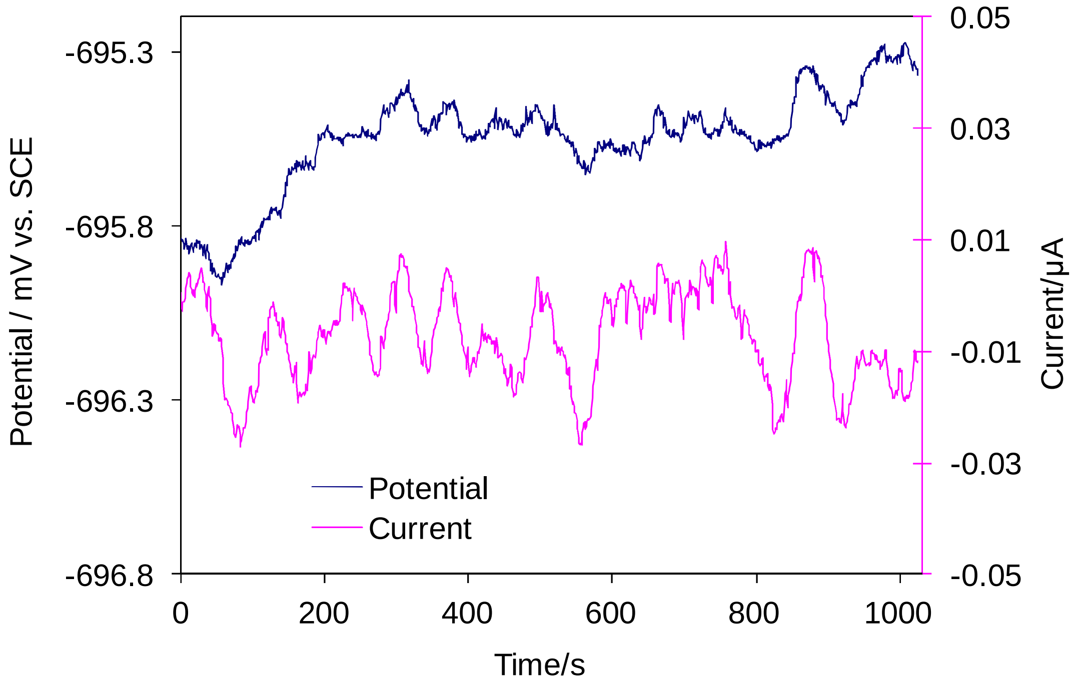

Figure 105. Voltage and current fluctuation on HAZ metal with time (60^{o}C, pH 5, 1 wt% NaCl purged with CO_2 and 50 ppm H_2S, 4day).

Surface analysis The weldment specimen was cleaned by Clarke's solution to remove the corrosion products after the electrochemical noise measurement. The specimen was then scanned by SEM. The SEM images of parent, HAZ, and weld metal are shown in Figure 106. Interestingly, a small hole was detected on the HAZ surface. The diameter of the hole was less than 10 µm. The depth of the hole was quantified by IFW afterward.

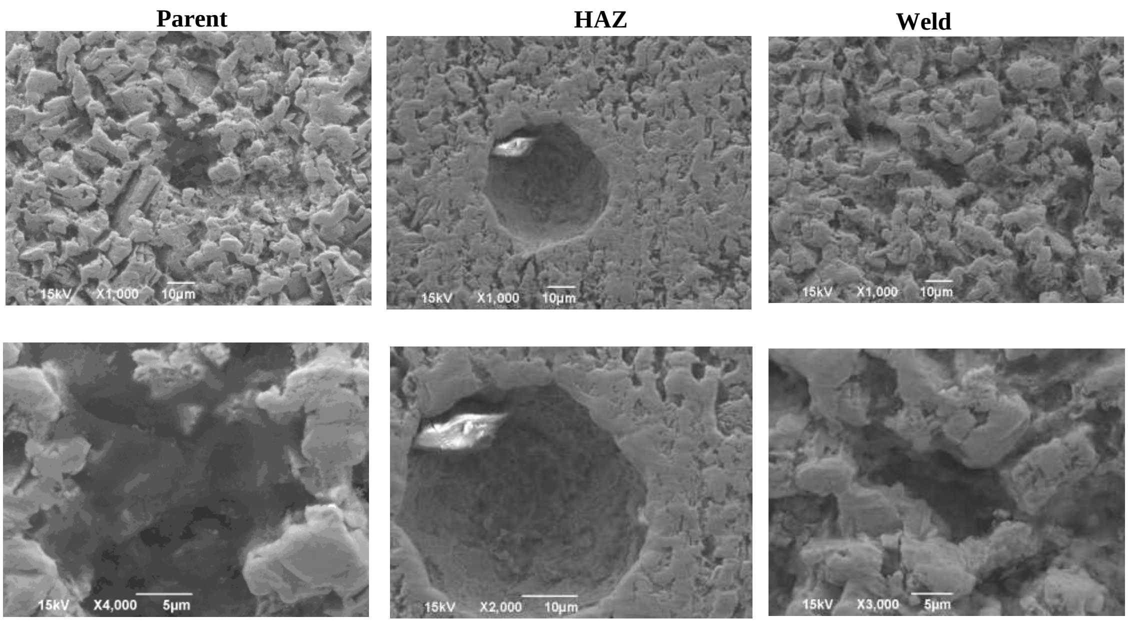

Figure 106. Surface morphology of coupon surfaces (without corrosion products) after corrosion (60^{o}C, pH 5, 1 wt% NaCl purged with CO_2 and 50 ppm H_2S).

The IFM image and surface profiles of one location on the HAZ surface are shown in Figure 107. The depth of the small hole detected by SEM was quantified to be 24 μm corresponding to a pitting rate of 1.8 mm/yr, which is significantly higher than the general corrosion rate of HAZ (0.34 mm/yr). The localized attack was significant. It is worth noting that only one pitting attack was observed on the HAZ surface. Considering the electrochemical noise data which showed no transient, the "pitting" attack observed here may be due to an unusual circumstance. According to the previous work that has been done in ICMT[58], an inclusion or surface imperfection may cause this type of "pitting" attack. When the inclusion on the surface would corrode away, the "pitting" attack would stop. This may explain why the electrochemical noise data did not detect the "pitting" initiation.

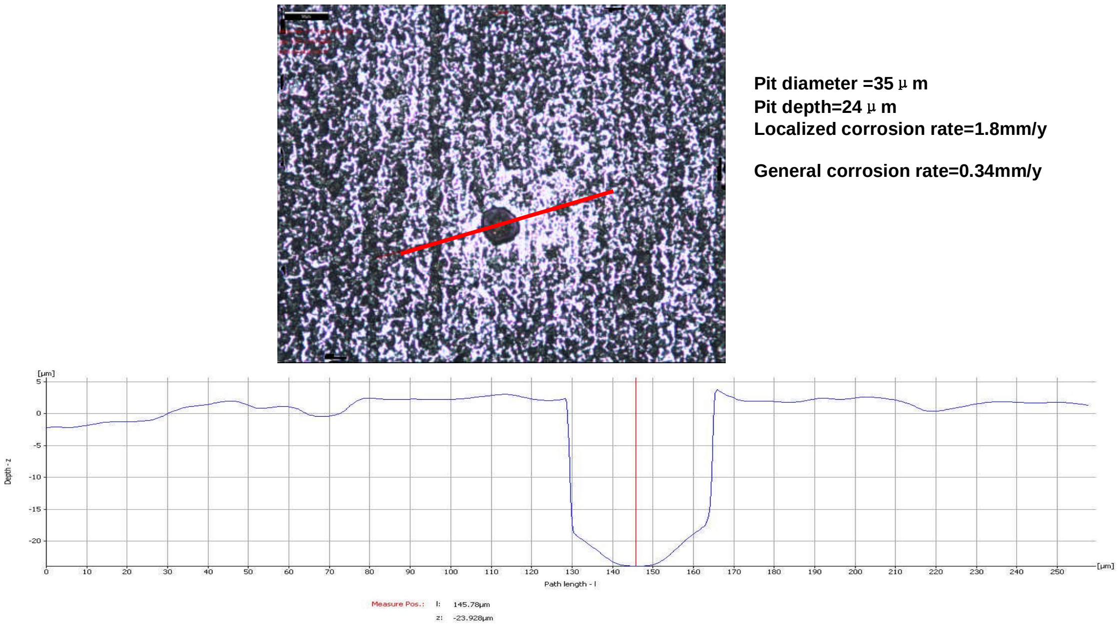

Figure 107. IFM image and profile at the line in the image of HAZ metal after film removal. (60^{o}C, pH 5, 1 wt% NaCl purged with CO_2 and 50 ppm H_2S).

6.2.2 The effects of 100 ppm acetic acid

Intrinsic corrosion rate In this experiment, 100 ppm acetic acid was added into the CO_2/H_2S mixed system. The effects on the intrinsic corrosion rates of unpaired parent, HAZ, and weld metal are shown in Figure 108. As mentioned before, the addition of H_2S reduced the intrinsic corrosion rate by promoting the formation of a protective iron sulfide layer. After the 100 ppm acetic acid was injected into the test solution, the intrinsic corrosion rate of each segment all slightly increased but was still relatively low compared with the affected corrosion rate in the pure CO_2 system.

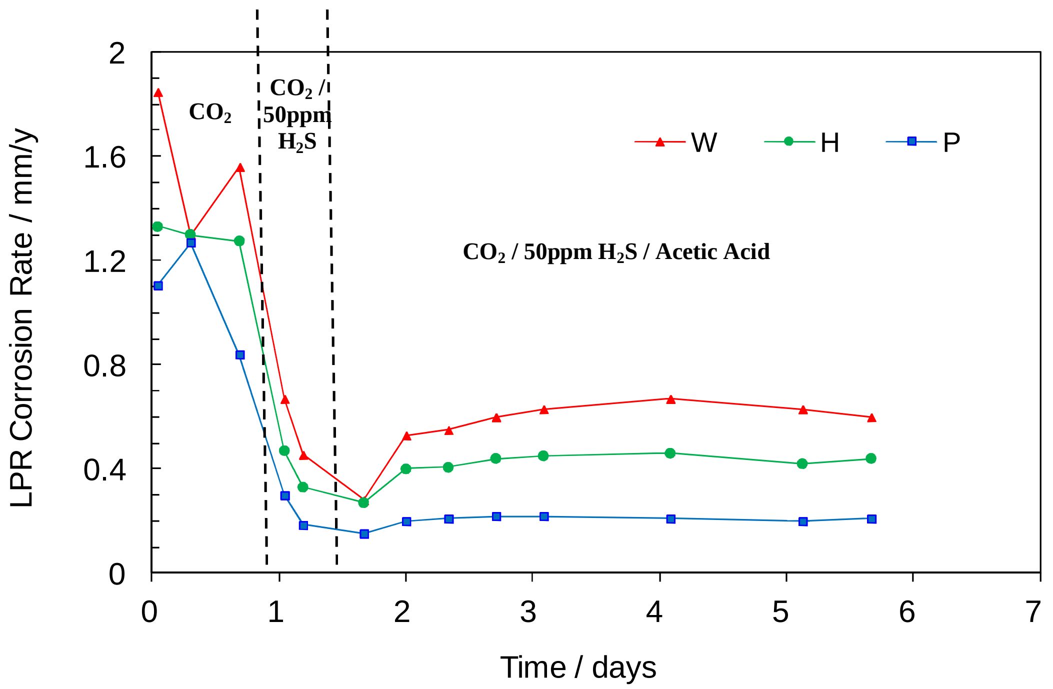

Figure 108. LPR corrosion rate vs. time (60°C, pH 5, 1 wt% NaCl purged with CO_2 and 50 ppm H_2S) with 100 ppm undissociated acetic acid solution.

Galvanic current The galvanic current measurement results of coupled segments are shown in Figure 109. For metal polarity, the weld metal always behaved active and the parent metal appeared to be more noble. One of the HAZ metal samples changed from being neutral to anodic after 100 ppm undissociated acetic acid was added. The results also show that the addition of 100 ppm undissociated acetic acid slightly increased the magnitude of the galvanic current.

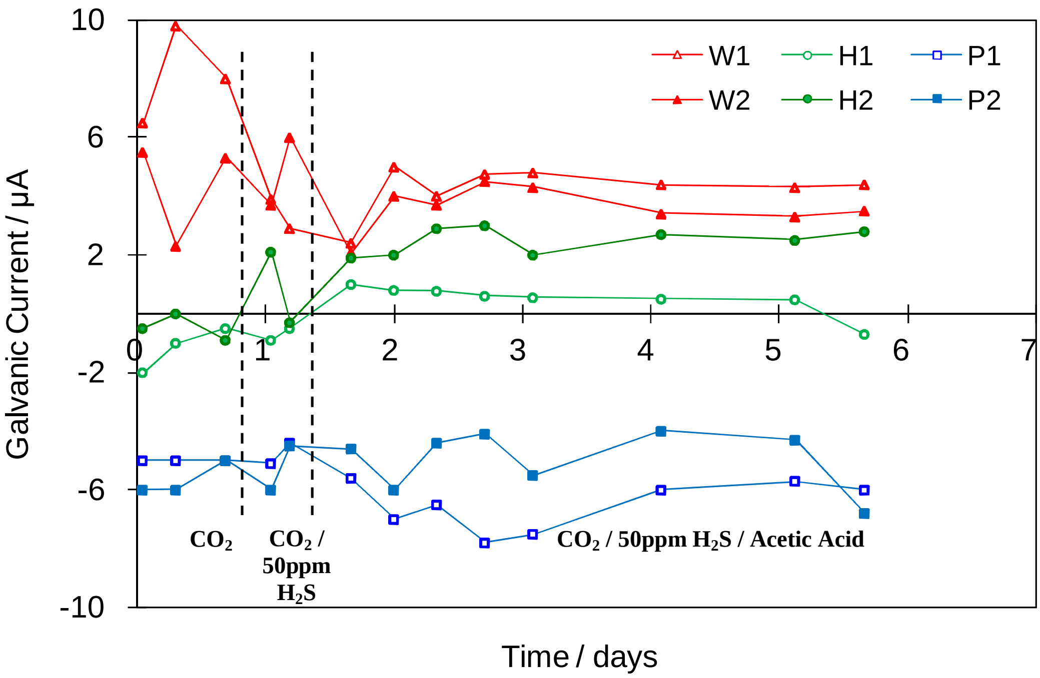

Figure 109. Galvanic current of coupled weldment vs. time (60°C, pH 5, 1 wt% NaCl purged with CO_2 and 50 ppm H_2S) with 100 ppm undissociated acetic acid solution.

The total corrosion rate was calculated from the uncoupled intrinsic corrosion rate and coupled galvanic corrosion rate based on the equations mentioned previously. The results are shown in, Figure 110, Figure 111, and Figure 112. Similar to previous results, the total corrosion rate of parent metal decreased while the total corrosion rate of weld metal increased due to the galvanic current. However, the galvanic effects were not significant.

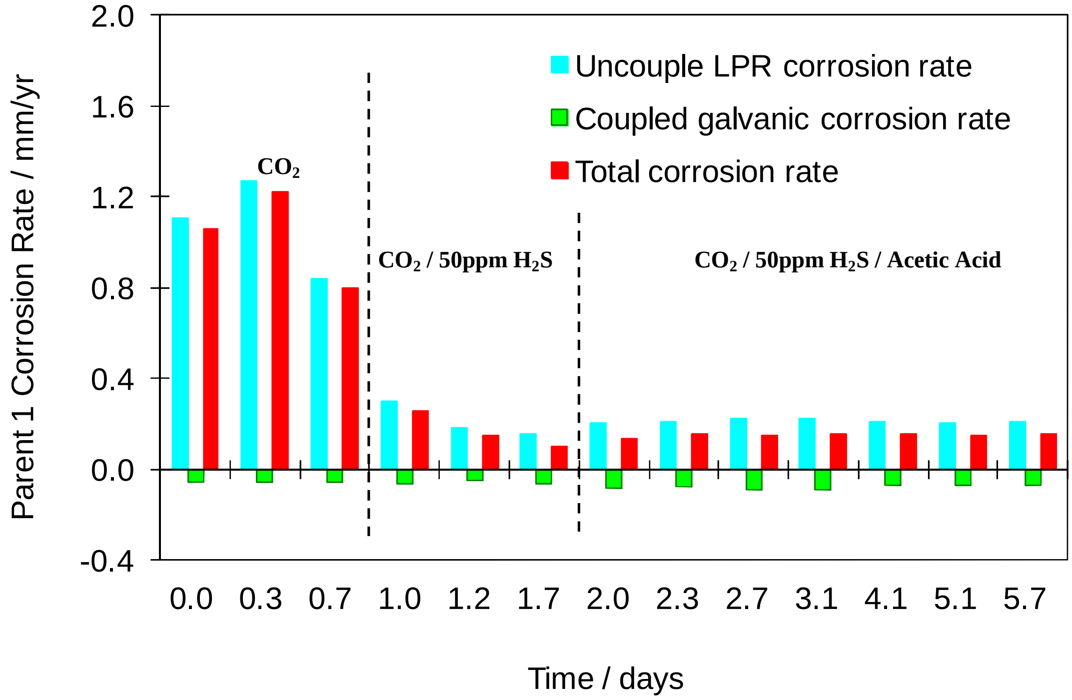

Figure 110. Calculated total corrosion rate of the parent metal compared to the measured uncoupled corrosion rate (60°C, pH 5, 1 wt% NaCl purged with CO_2 and 50 ppm H_2S) with 100 ppm undissociated acetic acid solution.

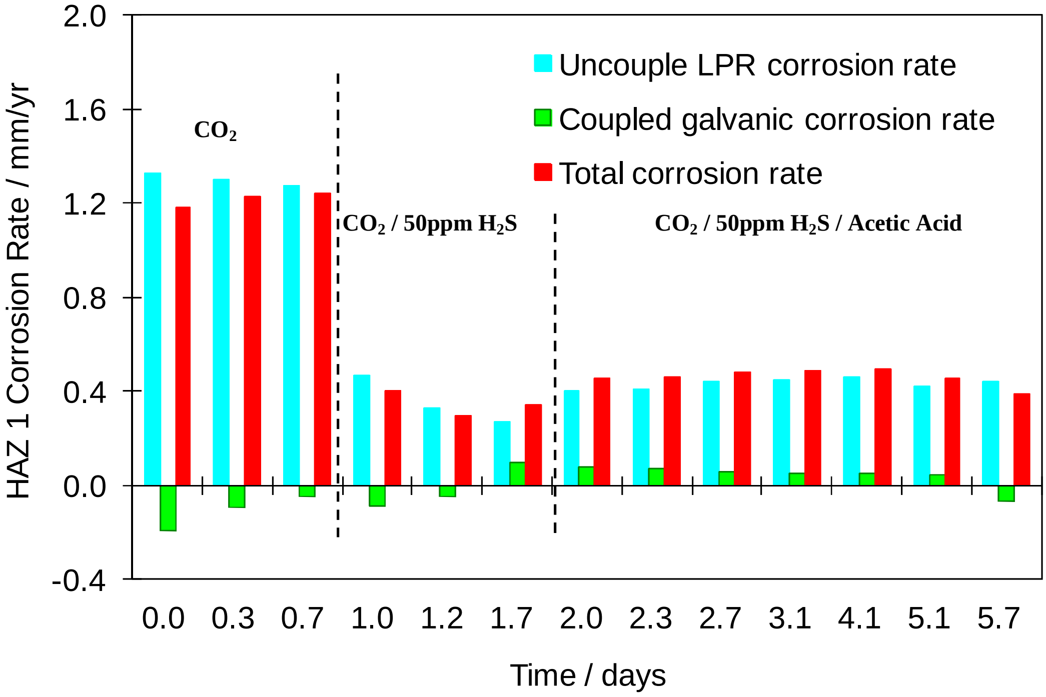

Figure 111. Calculated total corrosion rate of the HAZ metal compared to the measured uncoupled corrosion rate (60°C, pH 5, 1 wt% NaCl purged with CO_2 and 50ppm H_2S) with 100 ppm undissociated acetic acid solution.

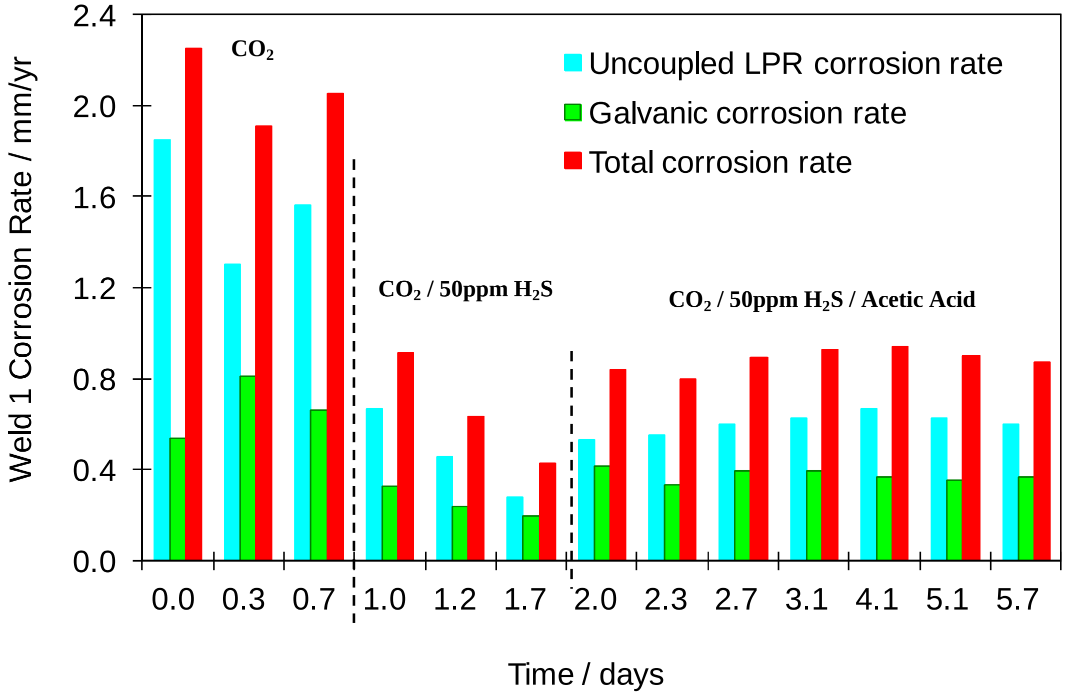

Figure 112. Calculated total corrosion rate of the weld metal compared to the measured uncoupled corrosion rate (60^{o}C, pH 5, 1 wt% NaCl purged with CO_2 and 50 ppm H_2S) with 100 ppm undissociated acetic acid solution.

Electrochemical noise Electrochemical noise measurements were conducted for all segments of weldment specimen. All noise data show similar features; thus, a set of potential and current noise data of HAZ was selected and presented here. The results are shown in Figure 113. The sign of localized corrosion (transient) was not detected from both the potential and current noise data.

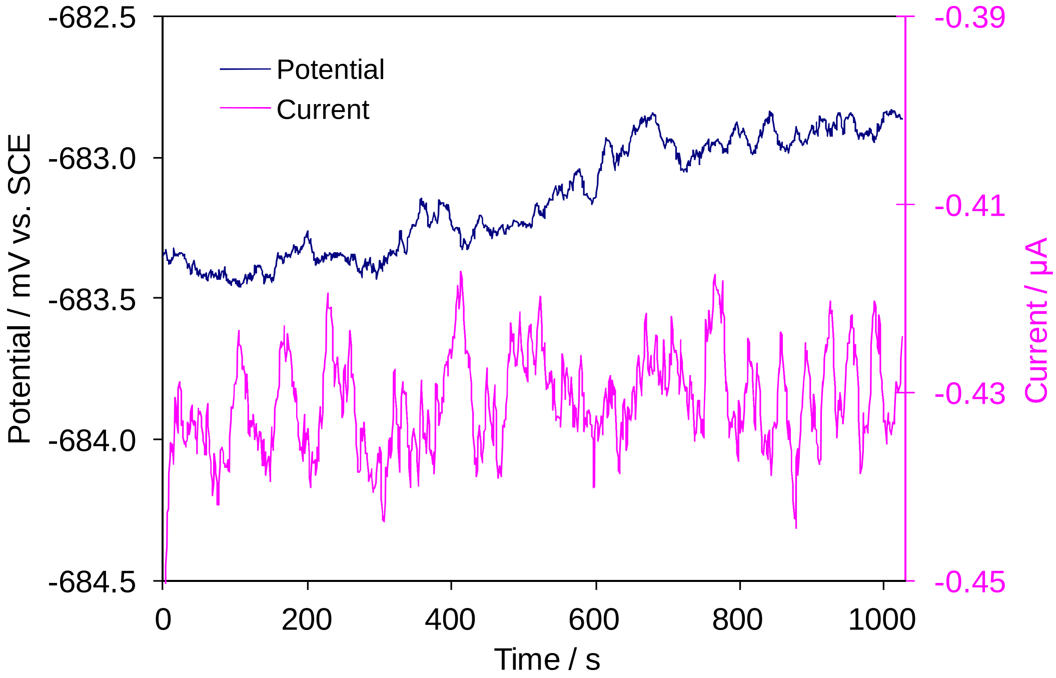

Figure 113. Voltage and current fluctuation with time (60°C, pH 5, 1 wt% NaCl purged with CO_2 and 50 ppm H_2S) with 100 ppm undissociated acetic acid solution.

Surface analysis Corrosion products were removed from the weldment specimen and then scanned by SEM. The images of all segments are shown in Figure 114. Clearly, a localized attack was observed on the HAZ surface. The size of the pit was about 10 µm wide, which is considered to be small. Interestingly, no other type of pit was detected on the HAZ surface. Considering the electrochemical noise data, this pit may also come from inclusions or surface imperfections.

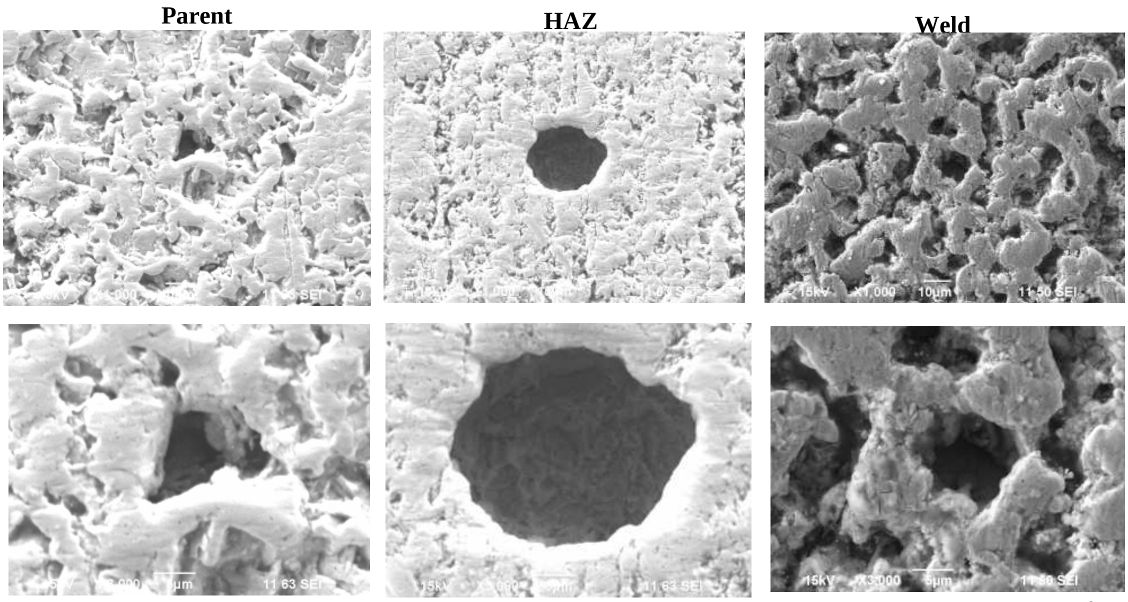

Figure 114. Surface morphology of coupon surfaces (without film) after corrosion (60^oC, pH 5, 1 wt% NaCl purged with CO_2 and 50 ppm H_2S) with 100 ppm undissociated acetic acid solution.

6.2.3 The effects of 20 ppm corrosion inhibitor

Intrinsic corrosion rate The effects of the corrosion inhibitor on the intrinsic corrosion of uncoupled parent, HAZ, and weld metal in the CO_2/H_2S mixed system are shown in Figure 115. From the results, it is clearly seen that the addition of the corrosion inhibitor significantly retarded the intrinsic corrosion rate. This is most likely due to the formation of a protective corrosion inhibitor layer on the steel surface acting as a diffusion barrier. The retardation effects on the intrinsic corrosion rate of the corrosion inhibitor were as expected.

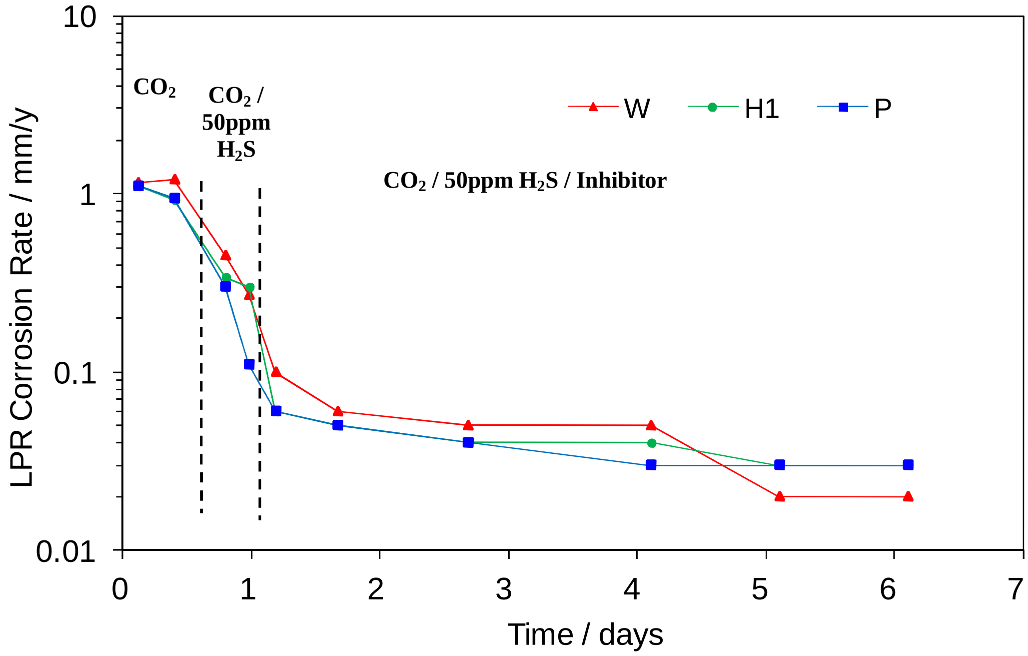

Figure 115. LPR corrosion rate vs. time (60°C, pH 5, 1 wt% NaCl purged with CO_2 and 50 ppm H_2S) with 20 ppm inhibitor.

Galvanic current The galvanic current measurement results of coupled segments are shown in Figure 116. The test result shows that the polarity of parent, HAZ, and weld metal remain unchanged until the 20 ppm corrosion inhibitor was injected. One of the HAZ metals became anodic. This phenomenon was not observed from the previous experiments. The addition of 20 ppm corrosion inhibitor reduced the magnitude of the galvanic corrosion to a significantly low level (about 6 times lower than the one without inhibition).

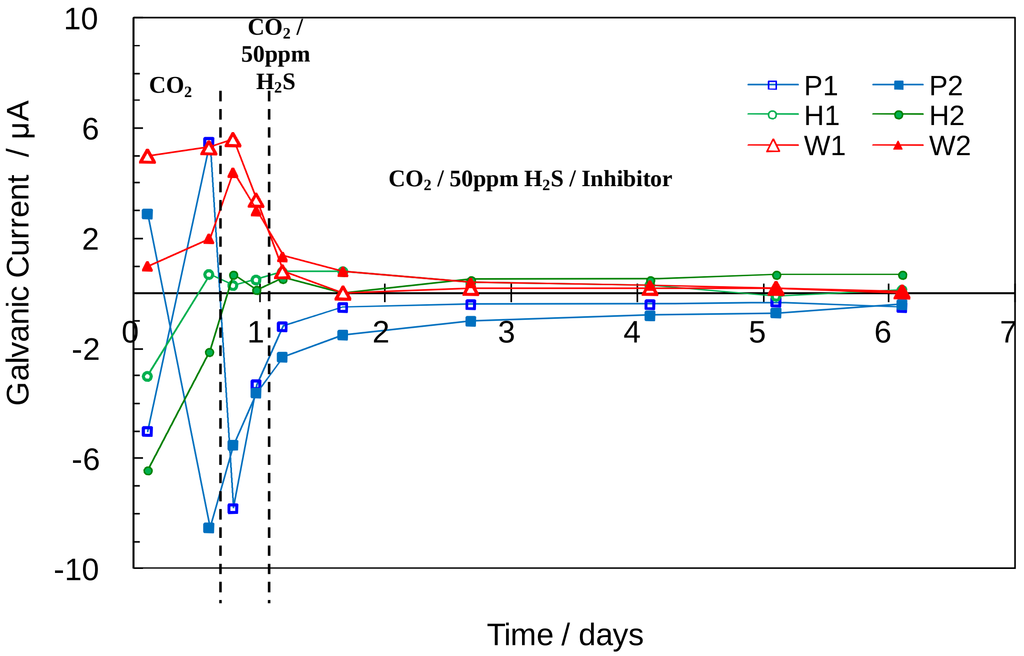

Figure 116. Galvanic current of coupled weldment vs. time (60°C, pH 5, 1 wt% NaCl purged with CO_2 and 50 ppm H_2S) with 20 ppm inhibitor.

The comparisons of the calculated total corrosion rates, measured uncoupled corrosion rates and coupled galvanic currents of three segments: parent, HAZ, and weld metal are shown in Figure 117, Figure 118, and Figure 119 respectively. It appears that the galvanic current did not significantly contribute to the total corrosion rate of each segment (less than 10%) whether it accelerated or retarded the corrosion rate.

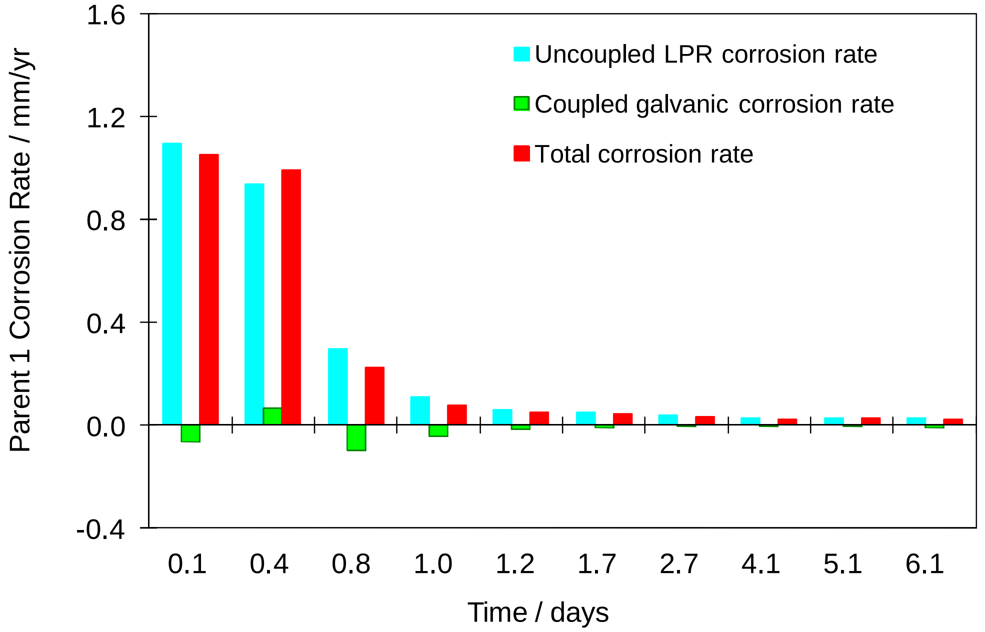

Figure 117. Calculated total corrosion rate of the parent metal compared to the measured uncoupled corrosion rate (60^oC, pH 5, 1 wt% NaCl purged with CO_2 and 50 ppm H_2S) with 20 ppm inhibitor.

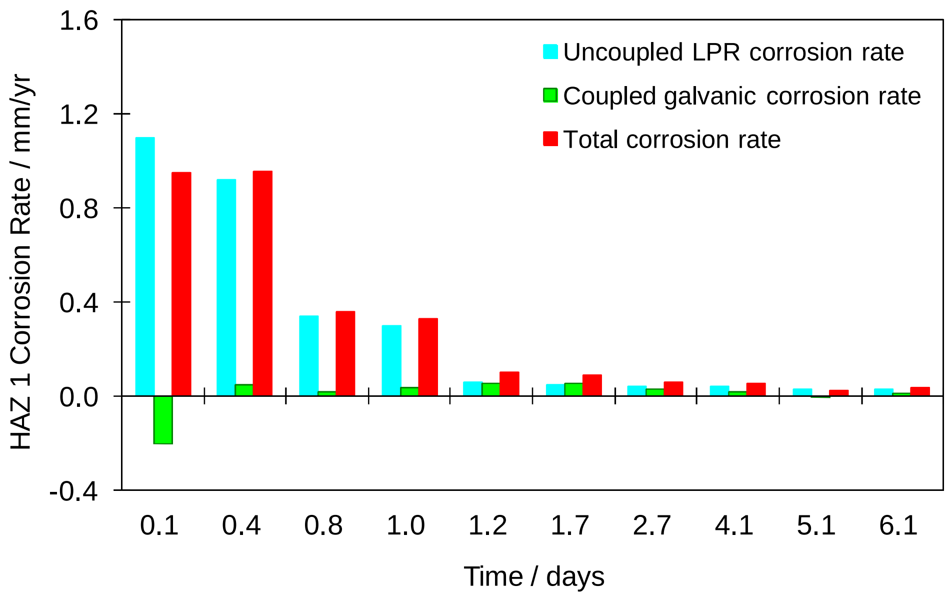

Figure 118. Calculated total corrosion rate of the HAZ metal compared to the measured uncoupled corrosion rate (60^oC, pH 5, 1 wt% NaCl purged with CO_2 and 50 ppm H_2S) with 20 ppm inhibitor.

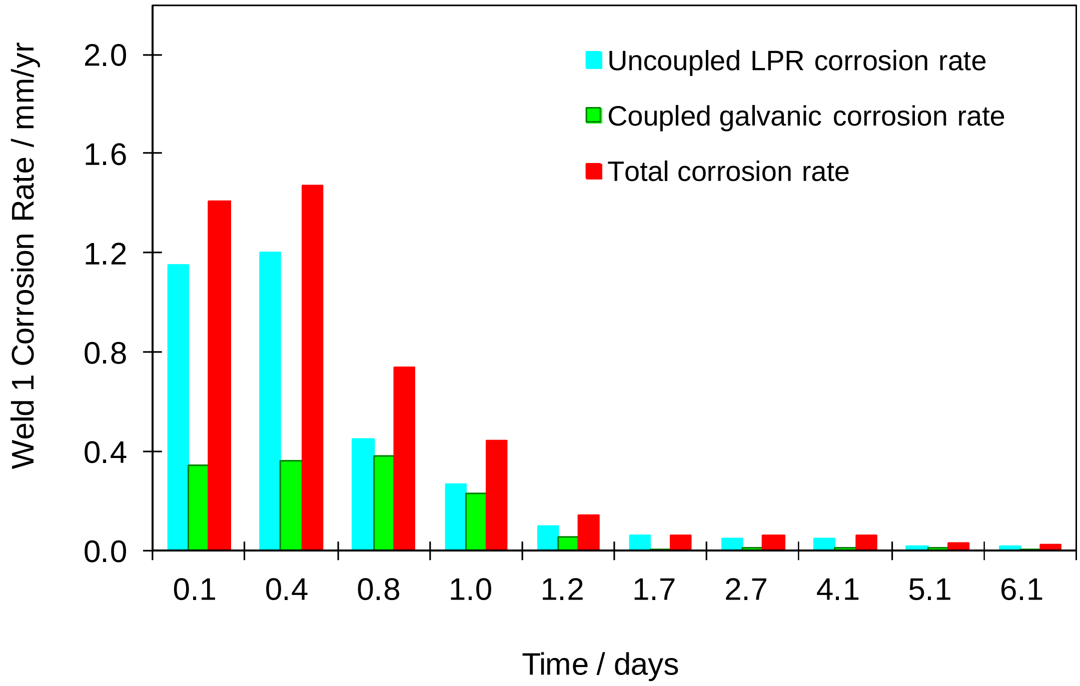

Figure 119. Calculated total corrosion rate of the Weld metal compared to the measured uncoupled corrosion rate (60^{o}C, pH 5, 1 wt% NaCl purged with CO_2 and 50 ppm H_2S) with 20 ppm inhibitor.

Surface analysis After the experiment, the corrosion products were removed from the weldment surface by Clarke's solution. The SEM images of parent, HAZ, and weld metal after film removal are shown in Figure 120. Apparently, no sign of localized corrosion attack was observed.

Parent HAZ Weld

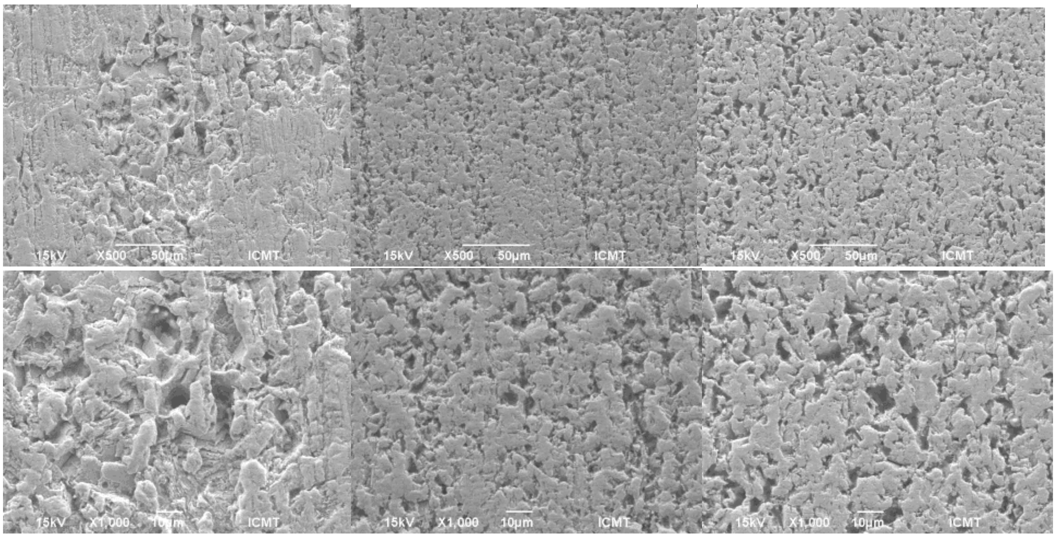

Figure 120. Surface morphology of coupon surfaces (without film) after corrosion (60^oC, pH 5, 1 wt% NaCl purged with CO_2 and 50 ppm H_2S) with 20 ppm corrosion inhibitor.

CHAPTER 7 APPLICATION OF A MICRO ELECTROCHEMICAL CELL IN THE STUDY OF WELDMENT CORROSION

7.1 Background of micro electrochemical cell

The micro electrochemical cell uses a pipette filled with the test solution to conduct the electrochemical measurement. Working with inside reference and counter electrodes, the pipette system becomes a microscopic electrochemical cell, which can be applied to determine the electrochemical characteristics on the individual micro structural region of interest[61].

The welding process produces structural heterogeneities on a small scale. Understanding the corrosion properties of an individual microstructure region in conjunction becomes very important. The micro electrochemical cell allows the local electrochemical measurement to be performed on a specific region which applies a high resolution corrosion measurement in weldment research.

Micro-electrochemical measurement techniques have been widely used in the corrosion study of stainless steel. In 2007, T. Ladwein located Cr-carbides and Cr-depleted zones in welded high grade martensitic stainless steels by using a combined approach of atomic force microscopy and an electrochemical EPR test.[62] Garcia used an electrochemical cell in the pitting corrosion study of weld joints of austenitic stainless steels (AISI 304 and 316L) and found the HAZ was the most critical zone for pitting corrosion for both materials[63]. However, no similar studies have been done on carbon steel corrosion. The purpose of this study is to determine if the micro-electrochemical measurement techniques can be used in investigating the corrosion of carbon steel in a CO_2 system, especially the corrosion of weldments.

7.2 Experimental set up for micro electrochemical cell

The micro electrochemical cell setup shown in Figure 121 consists of a Teflon shelter and an attached disposable pipette tip. An Ag/ AgCl electrode was used as the reference electrode. The counter electrode was a platinum wire. Both reference and counter electrode were put inside the Teflon shelter. A syringe filled with test electrolyte attached on the shelter applies the solution from a lateral outlet.

The electrochemical cell was attached to a steel stand which fixes the specimen in a horizontal level and applies a vertical force of 10 N on the specimen through the pipette tip to prevent the crevice corrosion between the specimen and the tip.

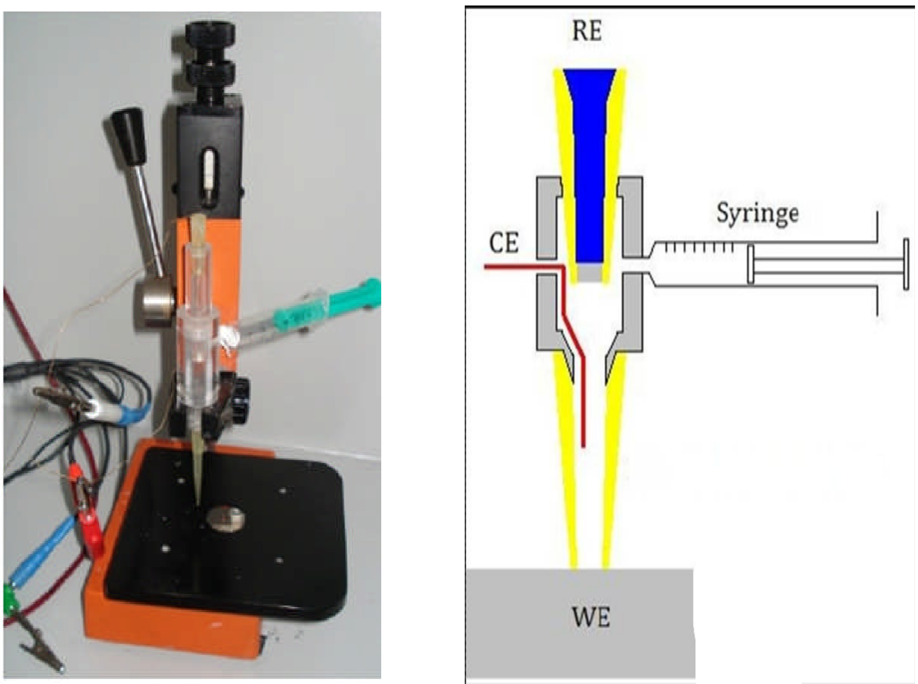

Figure 121. Micro electrochemical cell setup[7].

All the tests were performed in a glove box (shown in Figure 122) which was deoxygenated by purging with CO_2 gas during the test period. The first test was conducted in the dry/ wet system (shown in Figure 123). In the dry/wet system, the specimen surface was exposed in gas phase except for a local spot which was covered by the pipette tip. The second test was performed in the wet/wet system (Figure 124). In the wet/wet system, the whole specimen surface was exposed in the electrolyte which consisted of the same component as the one in the pipette tip. The purpose of the wet/ wet test design was to investigate the local corrosion behavior under the effect of galvanic current in the further work.

Figure 122. Micro electrochemical cell setup in a glove box.

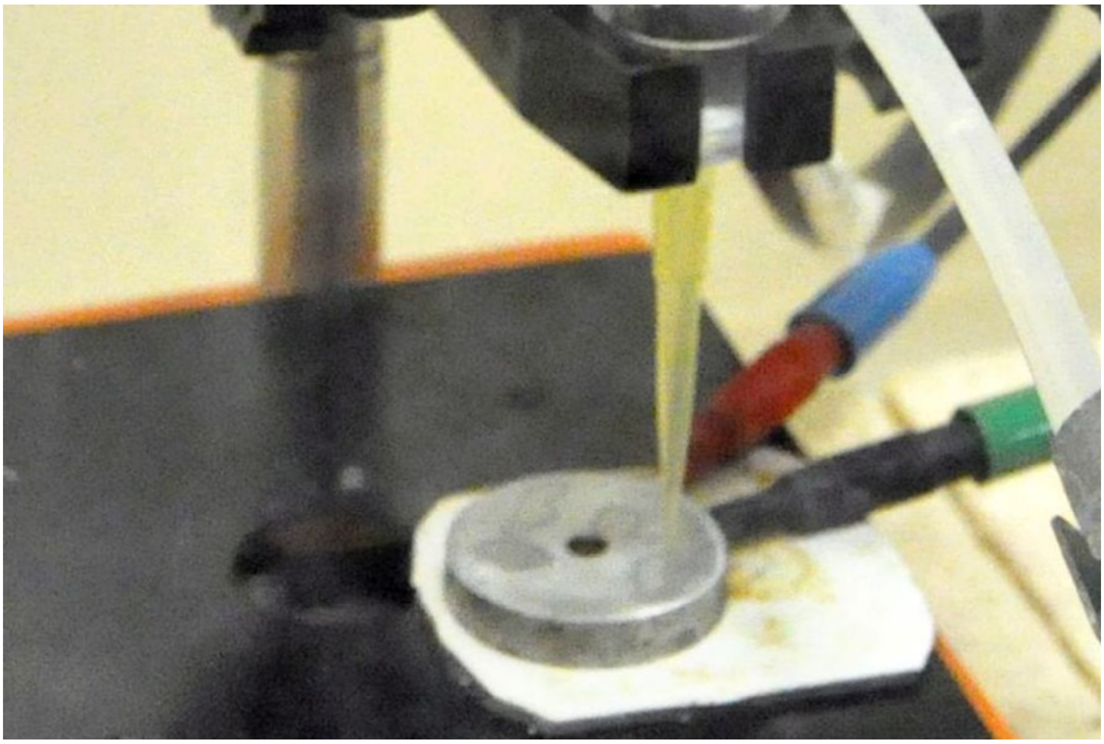
Figure 123. Micro electrochemical cell setup in dry/ wet system

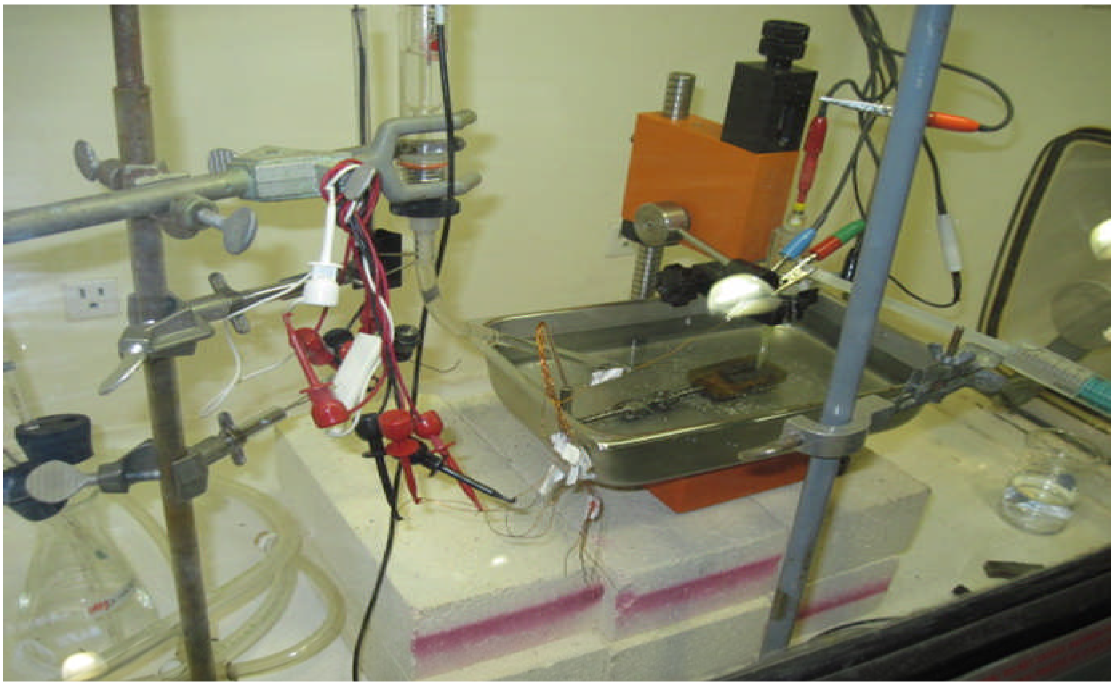
Figure 124. Micro electrochemical cell setup in wet/ wet system

7.3 Results and discussion

7.3.1 The corrosion behavior of X65 measured by conventional electrochemical measurement and micro electrochemical cell measurement

The LPR curves from a conventional three-electrode system (conducted in a standard glass cell) and micro cell are shown in Figure 125. It appears that the linear polarization curve from micro cell is as straight and smooth as the polarization curve from a standard glass cell. The slopes of the two curves that represent the polarization resistance are also similar. The corrosion rate measured in the micro cell was 0.96 mm/yr which is consistent with the corrosion rate result of 0.93 mm/yr from the experiment conducted in the glass cell. This suggests that the micro electrochemical cell is capable of making a good and accurate LPR measurement in a dry/wet CO_2 corrosion system.

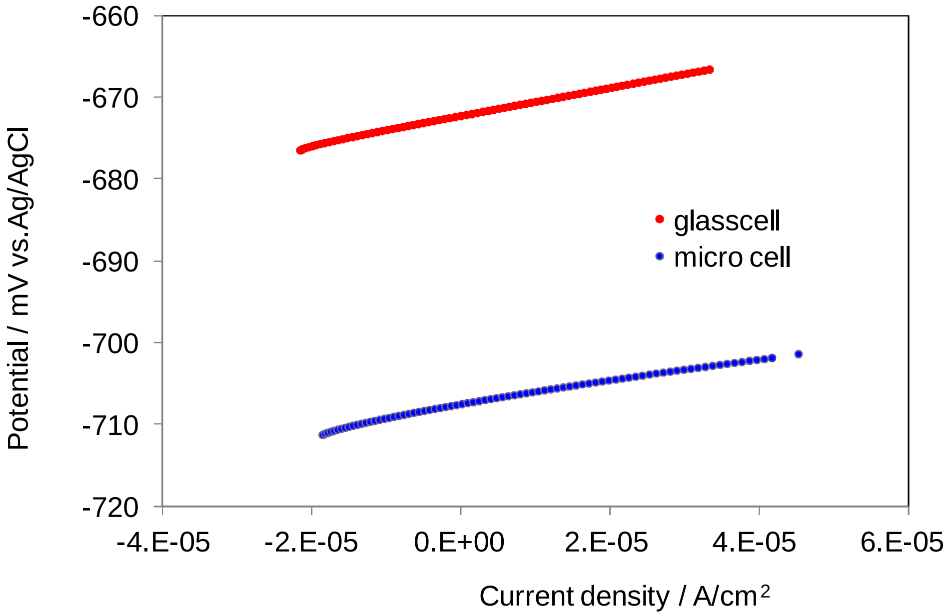

Figure 125. LPR curves of X65 from glass cell and micro cell at 1 wt% NaCl, 25ºC and pH 3.9.

The EIS curves from glass cell and micro cell are compared in Figure 126. The two curves have no significant differences. This suggests that micro cell works well in EIS measurement as well as LPR measurement in a dry/wet CO_2 corrosion system.

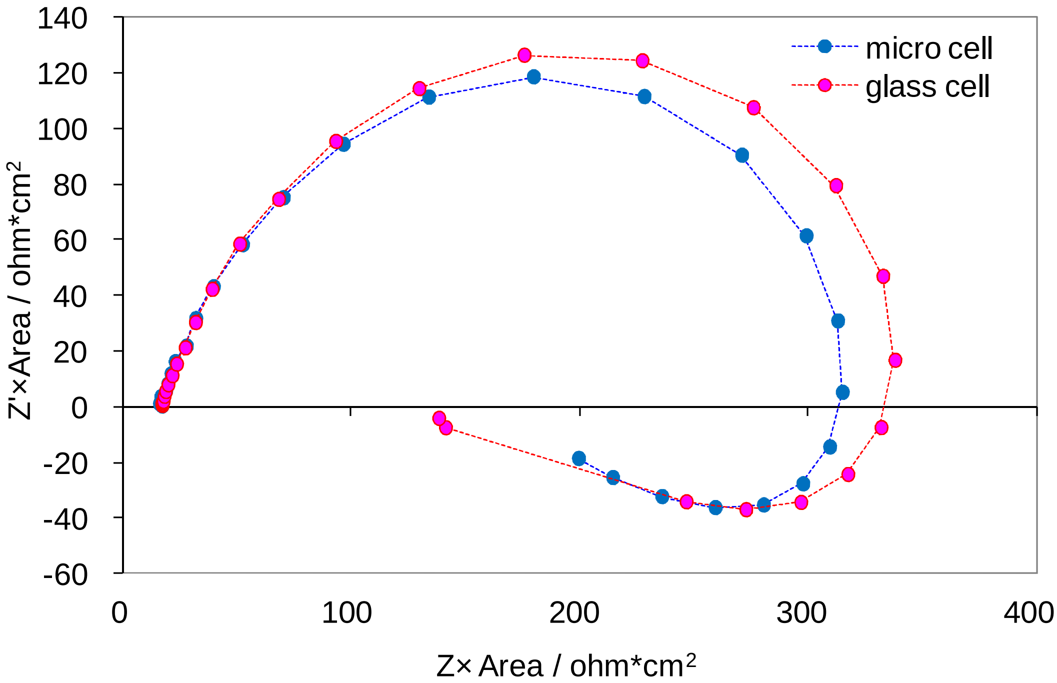

Figure 126. EIS loops of X65 from glass cell and micro cell at 1 wt% NaCl, 25ºC and pH 3.9.

The potentiodynamic sweeps measurement was also conducted in glass cell and micro cell. The comparison of two curves is shown in Figure 127. The shapes of the sweeps are almost identical except for a slight difference in the corrosion potential which was caused by using different reference electrodes in different cells.

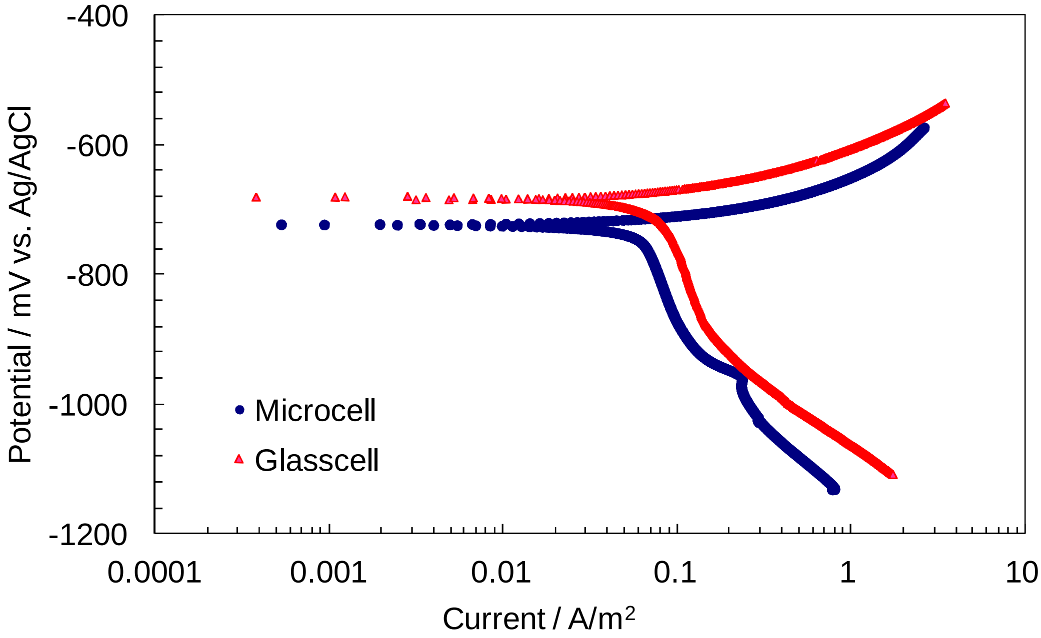

Figure 127. Sweep curves of X65 from micro cell and glass cell at 1 wt% NaCl, 25°C and pH 3.9.

Based on the comparable experimental results, it can be concluded that the typical electrochemical techniques such as LPR, EIS and potentiodynamic sweeps can be applied in micro electrochemical cell and provide similar results as in glass cell.

7.3.2 The corrosion behavior of weldment measured by conventional electrochemical measurement and micro electrochemical cell measurement

The purpose of applying a micro electrochemical cell in this study is to study the galvanic effects in a local region of the weldment. Therefore, it is necessary to see if the micro electrochemical cell works in the wet/wet system the same way as it works in the dry/wet system.

The LPR curves from micro electrochemical cell in dry/wet and wet/wet systems are shown in Figure 128. Both curves appear to be smooth, which means the measurement is applicable in both systems. The LPR corrosion rate obtained from a wet/wet system was around 0.73 mm/yr while the corrosion rate from a dry/wet system was about 0.85 mm/yr. The two corrosion rate values are in good agreement.

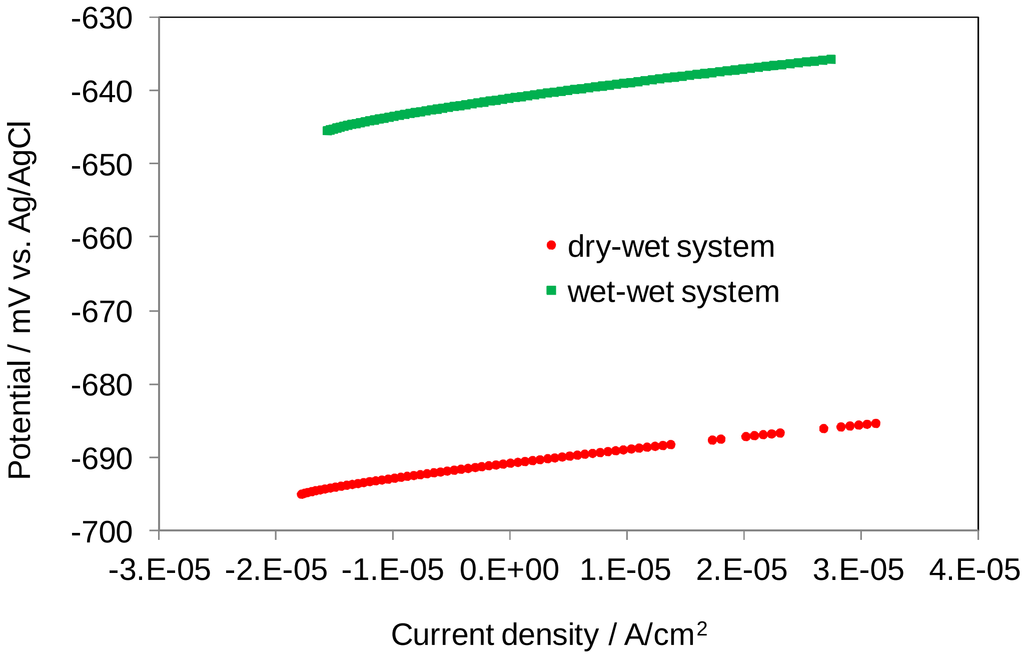

Figure 128. LPR curves of parent metal from dry/ wet and wet/ wet system in micro cell at 1 wt% NaCl, 25ºC and pH 3.9.

EIS was conducted in both dry/wet and wet/wet systems. The comparison is shown in Figure 129. Basically, there is no difference between the two EIS curves. This indicates that EIS can also be conducted in a wet/wet system.

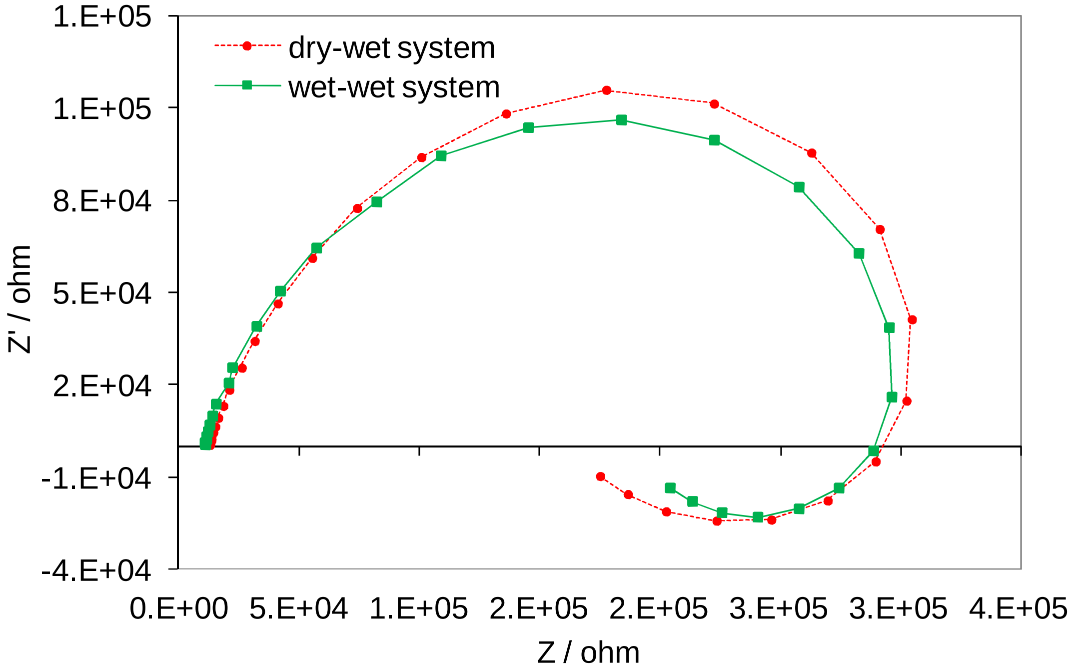

Figure 129. EIS curves of parent metal from dry/ wet and wet/ wet system in micro cell at 1 wt% NaCl, 25ºC and pH 3.9.

The corrosion rates of parent metal, weld metal, and HAZ measured by micro electrochemical cell in dry/wet and wet/wet systems as well as the corrosion rates measured by conventional three-electrode systems in a glass cell are compared in Figure 130, Figure 131, and Figure 132, respectively. Test results show the corrosion rates from different systems are slightly different but of the same magnitude. The corrosion rate measured in a glass cell was an average corrosion rate based on the whole specimen surface area. However, what the micro electrochemical cell measured is the corrosion rate in a much smaller location. This might be the reason why there is a slight difference between the results from the two different systems.

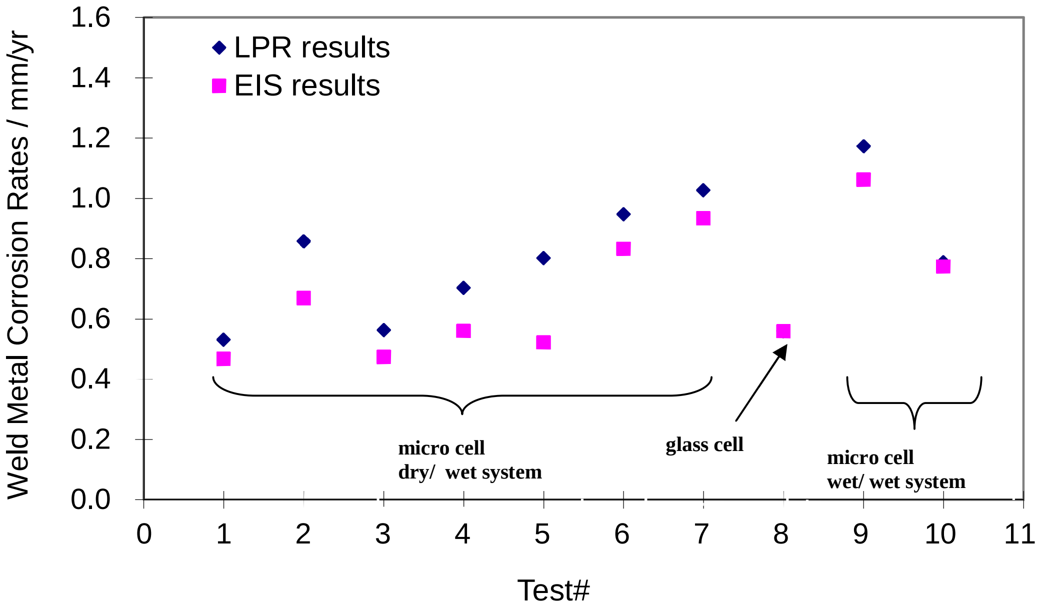

Figure 130. Comparison corrosion rates of weld metal from dry/ wet, wet/ wet system in micro cell and glass cell.

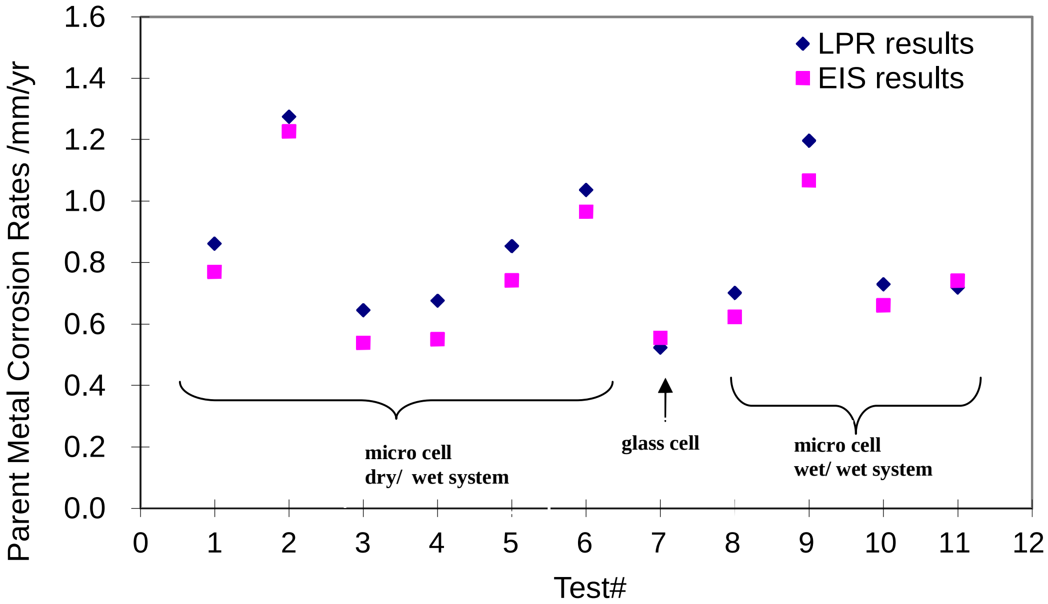

Figure 131. Comparison corrosion rates of parent metal from dry/ wet, wet/ wet system in micro cell and glass cell.

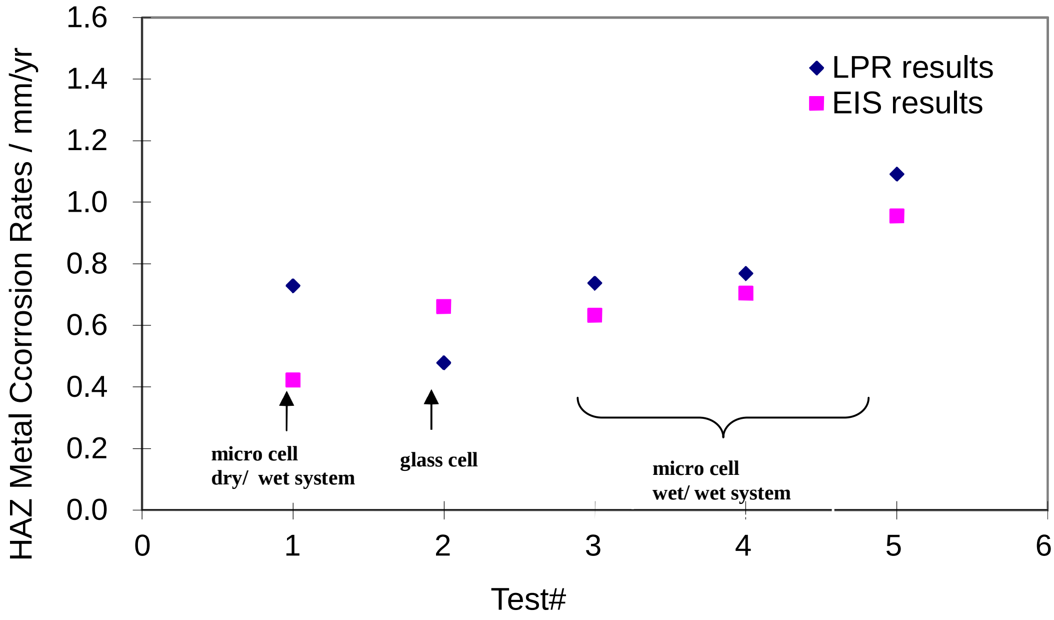

Figure 132. Comparison corrosion rates of HAZ from dry/ wet, wet/ wet system in micro cell and glass cell.

CHAPTER 8 CONCLUSIONS AND FUTURE WORK

8.1 Conclusions

Experiments have been performed to study the environmental effects on weldment corrosion. The research work has been separated into two parts: weldment corrosion in a CO_2 system and weldment corrosion in a CO_2/H_2S mixed system. In a pure CO_2 system, the effects of temperature, chloride concentration, acetic acid, corrosion inhibitor and the formation of iron carbonate on the intrinsic and the galvanic corrosion of weldment were investigated. Meanwhile, the effects of the addition of acetic acid and corrosion inhibitor on the weldment corrosion were also studied in the CO_2/H_2S mixed system. According to the experimental results, the following conclusions can be drawn.

1. For the standard carbon steel weldment tested, there is no significant difference between the intrinsic corrosion rates of the parent metal, the HAZ, and the weld metal under the same conditions.
2. For the standard carbon steel weldment tested, the metal polarity mostly follows the same trend under all test conditions: the weld metal appears to be more active, the HAZ is neutral and the parent metal is more noble with respect to the other two metals. However, under the condition of iron carbonate formation, where the localized corrosion was detected, the metal polarity of each segment changed.
3. An increase of temperature from 25^oC to 60^oC significantly increases the intrinsic corrosion rate of each segment of the weldment as well as the magnitude of galvanic current flowing between the segments.

4. At $20^{o}C$, an increase of chloride ion concentration from 5 wt% to 10 wt% decreased the intrinsic corrosion rate of each segment due to the absorption of chloride ions. However, when the temperature increased to $60^{o}C$, an increase of chloride ion concentration increased the intrinsic corrosion rate. This suggests that the interaction between chloride ions and steel surface may be different at high temperatures. The chloride ion concentration appears to have no significant effects on the galvanic current.
5. The addition of 100 ppm acetic acid significantly increased the intrinsic corrosion rate of each segment of the weldment and the galvanic current was increased as well in both sweet and sour systems.
6. The addition of 20 ppm corrosion inhibitor significantly decreased the intrinsic corrosion rates of all segments of weldment and the galvanic current flowing between the segments in both sweet and sour systems.
7. The formation of protective iron carbonate film reduced the corrosion rate of all materials and led to lower galvanic currents between the weld segments. A partially dissolved protective film initiated localized corrosion, with higher general corrosion rates and galvanic currents, as compared to the protective film covered surface. The localized corrosion event was detected by the electrochemical noise technique where the data include typical potential and current noise transients.
8. The addition of 50 ppm H_2S rapidly decreased the intrinsic corrosion rate of the weldment specimen due to the fast formation of the iron sulfide layer.

9. A Micro-electrochemical cell has been successfully applied in the study of the corrosion of standard carbon steel weldment in sweet systems.

8.2 Future work

The initial effort on studying the environmental effects on weldment corrosion has been made in this project. The results were consistent and promising. The effects of several parameters have been revealed. However, more areas related to this topic need to be investigated. The following suggestions can be taken into consideration for future work.

1. Study the environmental effects on the alloyed weldment in both sweet and sour systems.
2. Study the effect of microstructure on the weldment corrosion.

REFERENCES

1. J. Davis, Corrosion of Weldments, ASM International, 2006.

2. G. A. Nelson, "Prevention of Localized Corrosion in Sulfuric Acid Handling Equipment", Corrosion, Vol. 14, No. 3, 1958, pp. 45-50.

3. S. Turgoose, J. Palmer, and G. Dicken, "Preferential Weld Corrosion of 1% Ni Welds: Effect of Solution Conductivity and Corrosion Inhibitors", Corrosion/05, Paper No. 05275, NACE International, Houston, Texas, 2005.

4. E. Gulbrandsen and A. Dugstad, "Corrosion Loop Studies of Preferential Weld Corrosion and Its Inhibition in CO_2 Environments", Corrosion/05, Paper No. 05276, NACE International, Houston, Texas, 2005.

5. D. Queen, C. Lee, and J. Palmer, "Guidelines for the Prevention, Control and Monitoring of Preferential Weld Corrosion of Ferritic Steel in Wet Hydrocarbon Production Systems Containing CO_2", SPE, Paper No. 87552, 2004.

6. S. Olsen, B. Sundfer, and J. Enerhaug, "Weld Corrosion in C-steel Pipelines in CO_2 Environments- Comparison between Field and Laboratory Data". Corrosion/97, Paper No. 43, NACE International, Houston, Texas, 1997.

7. C. Lee, S. Bond, and P. Woollin, "Preferential Weld Corrosion: Effects of Weldment Microstructure and Composition", Corrosion/05, Paper No. 05276, NACE International, Houston, Texas, 2005.

8. P. I. Nice and ǿ Strandmyr, "Materials and Corrosion Control Experience within the Statfjord Field Seawater Injection Systems", Corrosion/93, Paper No. 64, NACE International, Houston, Texas, 1993.

9. J. W. Palmer, J. L. Dawson, T. Ulrich, and A.N. Rothwell, "Inhibition of Weld Corrosion under Flowing Conditions – the Development of Test Procedures", Corrosion/93, Paper No. 119, NACE International, Houston, Texas, 1993.

10. R. J. Pargeter and T.G. Gooch, "Welding C-Mn Steels for Sour Service", Corrosion/95, Paper No. 63, NACE International, Houston, Texas, 1995.

11. T. Hodgkiess, N. Eid and W.T. Hanbury, "Corrosion of Welds in Seawater", Desalination, Vol. 27, No. 2, 1978, pp. 129–136.

12. A. N. Rothwell, "Weld Corrosion: Causes and Solutions", Corrosion Prevention and Control, Vol. 39, 1992, pp. 113.

13. M. W. Joosten and G. Payne, "Preferential Corrosion of Steel in CO_2 Containing Environments", Corrosion/88, Paper No. 211, NACE International, Houston, Texas, 1988.

14. V. S. Voruganti, H. B. Luft, D. DeGreer, and S. A. Bradford, “Scanning Reference Electrode Technique for the Investigation of Preferential Corrosion of Weldments in Offshore Applications”, Corrosion, Vol. 47, No. 5, 1991, pp. 343.

15. M. Eashwar and S. C. Dexter, “Relation of Bacterial Settlement Patterns to Anodic Activity on Stainless Steel Weldments”, Corrosion/99, Paper No. 174, NACE International, Houston, Texas, 1999.

16. H. Ogawa, Y. Tomoe, T. Hara, and A. Sakamoto, “A Case Study of the Uneven Corrosion of A Choke Valve at A Gas-well Head”, Corrosion/2000, Paper No. 4, NACE International, Houston, Texas, 2000.

17. I. G. Winning, D. McNaughtan, N. Bretherton, and A. J. McMahon “Evaluation of Weld Corrosion Behavior and the Application of Corrosion Inhibitors and Combined Scale/Corrosion Inhibitors”, Corrosion/04, Paper No. 04538, NACE International, Houston, Texas, 2004.

18. F. Gui, D. Hill, C. Kang, and C. Joia, “Inhibition of Galvanic Corrosion of Carbon Steel and Nickel Alloy in Oil and Gas Production Applications”, Corrosion/2010, Paper No. 10333, NACE International, Houston, Texas, 2010.

19. M. Sephton and P. C. Pistorius, “Localized Corrosion of Carbon Steel Weldments”, Corrosion, Vol. 56, No. 12, 2000.

20. D. McNaughtan and I. G. Winning, “Comparison of segmented weld corrosion tests with short and long pre-corrosion and the influence of synergist in corrosion inhibitors”, SPE/04, Paper No. 87553, Society of Petroleum Engineers, 2004.

21. C. de Waard and D. E. Milliams, “Carbonic Acid Corrosion of Steel”, Corrosion, Vol. 31, Paper No. 5, 1975, pp. 177.

22. C. de Waard and D. E Milliams, “Predictive Model for CO_2 Corrosion Engineering in Wet Natural Gas Pipelines”, Corrosion/91, Paper No. 577, NACE International, Houston, Texas, 1991.

23. C. de Waard and U. Lotz, “Prediction of CO_2 Corrosion of Carbon Steel,” Corrosion/93 Paper No. 69, NACE International, Houston, Texas, 1993.

24. C. de Waard, U. Lotz, and A.Dugstad “Influence of Liquid Flow Velocity on CO_{2_2} Corrosion: A Semi-empirical Model”. Corrosion/95, Paper No. 128, NACE International, Houston, Texas, 1995.

25. L. D. S. Gray, B. G. Anderson, M. J. Danysh, and P. R. Tremaine, “Effect of pH and Temperature on the Mechanisms of Carbon Steel Corrosion by Aqueous Carbon Dioxide”, Corrosion/90, Paper No. 40, NACE International, Houston, Texas, 1990.

26. L. D. S. Gray, B. G. Anderson, M. J. Danysh, and P. R. Tremaine, “Mechanisms of Carbon Steel Corrosion in Brines Containing Dissolved Carbon Dioxide at pH 4”, Corrosion/89, Paper No. 464, NACE International, Houston, Texas, 1989.

27. S. Nesic, J. Postlethwaite, and S. Olsen “An Electrochemical Model for Prediction of Corrosion of Mild Steel in Aqueous Carbon Dioxide Solutions”, Corrosion, Vol. 52, 2003, pp.280.

28. S. Olsen, “CO_2 Corrosion Prediction Model – Basic Principles”, Corrosion/2005, Paper No. 05551, NACE International, Houston, Texas, 2005.

29. M. R. Bonis and J. L. Crolet, “Basics of the Prediction of the Risks of CO_2 Corrosion in Oil and Gas Wells”, Corrosion/89, Paper No. 466, NACE International, Houston, Texas, 1995.

30. Y. M. Gunaltun. “Combining Research and Field Data for Corrosion Rate Prediction” Corrosion/96, paper No. 27. NACE International, Houston Texas, 1996.

31. W. P. Jepson, C. Kang, M. Gopal, and S. Stitzel, “Model for Sweet Corrosion in Horizontal Multiphase Slug Flow”, Corrosion/97, Paper No. 11, NACE International, Houston Texas, 1997.

32. R. Zhang, M. Gopal, and W. P. Jepson, “Development of a Mechanistic Model for Predicting Corrosion Rate in Multiphase Oil/water/gas Flows”, Corrosion/97, Paper No. 601, NACE International, Houston Texas, 1997.

33. R. C. John, K. G. Jordan, S. D. Kapusta, A. L. Young, and W. T. Thompson, “SweetCor: An Information System for the Analysis of Corrosion of Steels by Water and Carbon Dioxide”, Corrosion/98, Paper No. 20, NACE International, Houston Texas, 1998.

34. C. D. Adams, J. D. Garber, and R. K. Singh, “Computer Modeling to Predict Corrosion Rates in Gas Condensate Wells Containing CO_2", Corrosion/96, Paper No. 31, NACE International, Houston Texas, 1996.

35. B. F. M. Pots, “Mechanistic Models for the Prediction of CO_2 Corrosion Rates under Multi-phase Flow Conditions”, Corrosion/95, Paper No. 137, NACE International, Houston Texas, 1995.

36. S. Nesic and K. J. Lee, "The Mechanistic Model of Iron Carbonate Film Growth and the Effect on CO_2 Corrosion of Mild Steel", Corrosion/02, Paper No.237, NACE International, Houston Texas, 2002.

37. E. Dayalan, F. D. deMoraes, J. R. Shadley, S. A. Shirazi, and E. F. Ribicki, "CO_2 Corrosion Prediction in Pipe Flow under $FeCO_3$ Scale-forming Conditions", Corrosion/98, Paper No. 51, NACE International, Houston Texas, 1998.

38. A. Dugstad, "The Importance of $FeCO_3$ Supersaturation on the CO_2 Corrosion of Carbon Steel", Corrosion/92, Paper No. 14, NACE International, Houston Texas, 1992.

39. S. Nesic and L. Lunde, "CO_2 Corrosion of Carbon Steel in Two-Phase Flow", Corrosion, Vol. 50, pp. 717, 1994.

40. S. N. Smith and M. Jooston, "Corrosion of Carbon Steel by H_2S in CO_2 Containing Oilfield Environments", Corrosion/2006, Paper No. 06115, NACE International, Houston Texas, 2006.

41. R. D. Kane and M. S. Cayard, "Review of Published Literature on Wet H_2S Cracking", Corrosion/99, Paper No. 99420, NACE International, Houston Texas, 1999.

42. A. Miyasaka, K. Denpo, and H. Ogawa, "Corrosion And Cracking Of Steel In Production Of Gas With Liquid HS And Brine", Offshore Technology Conference, Paper No. 5154, 1986

43. E. L. Piccolo, L. Scoppio, C. S. Materiali, P. I. Nice, and S. Nodland, "Corrosion and Environmental Cracking Evaluation of High Density Brines for Use in HPHT Fields", Corrosion/05, Paper No. 97593, NACE International, Houston Texas, 2005.

44. P. R. Rhodes, "Environment-Assisted Cracking of Corrosion-Resistant Alloys in Oil and Gas Production Environments: A Review", Corrosion, Vol. 57, No. 11, 2001.

45. J. Gomez, S. Barquera, C. Fisicas, and R. Perez, "Effect of Wet Hydrogen Sulfide Environments on the Cracking Susceptibility of Medium Strength Microalloyed Pipeline Steels for Oil and Gas Transport", Corrosion/2003, Paper No. 03530, NACE International, Houston Texas, 2003.

46. J. G. Maldonado and J. W. Skogsberg, "Cracking Susceptibility Of Duplex Stainless Steel At An Intermediate Temperature In The Presence Of H_2S

Containing Environments", Corrosion/2004, Paper No. 04134, NACE International, Houston Texas, 2004.

47. D. W. Shoesmith, P. Taylor, M. G. Bailey, and D. G. Owen, "The Formation of Ferrous Monosulfide Polymorphs during the Corrosion of Iron by Aqueous Hydrogen Sulfide at 21^{o}C", Journal of the Electrochemical Society, Vol. 125, 1980, pp. 1007-1015.

48. D. W. Shoesmith, "Formation, Transformation and Dissolution of Phases Formed on Surfaces", Lash Miller Award Address, Electrochemical Society Meeting, Ottawa, Nov. 27, 1981.

49. W. Sun and S. Nesic, "A Mechanistic Model of H_2S Corrosion of Mild Steel", Corrosion/2007, Paper No. 07665. NACE International, Houston, Texas, 2007.

50. H. P. Hack, Galvanic corrosion test methods, NACE international, 1993.

51. R. Cottis and S. Turgoose, Electrochemical Impedance and Noise, NACE International, 1999.

52. P. Marcus and F. Mansfeld, Analytical Methods in Corrosion Science and Engineering, CRC, 2005.

53. T. Ladwein and M. Sorg, "Micro-electrochemical Techniques for Characterization of the Behavior of Corrosion Resistant Alloys (CRA)", Corrosion/08, Paper No. 08389, NACE International, Houston, Texas, 2008.

54. J. Maier, B. Kinsella, S. Bailey, and T. Becker, "Local Electrochemistry and Scanning Probe Microscopy Techniques to Clarify Intergranular Cracking Phenomena in Weldable Martensitic Stainless Steels", Corrosion/09, Paper No. 09088, NACE International, Houston, Texas, 2009.

55. M. Stern and A. L. Geary, "Electrochemical Polarization", Journal of the Electrochemical Society, Vol. 104, No.1, 1957, pp.56.

56. J. R. Kearns and J. R. Scully, Electrochemical Noise Measurement for Corrosion Applications, ASTM, 1996.

57. J. Hickling, J. Goellner, A. Burkert and A. Heyn: "Evaluation of a Round Robin Experiment on Electrochemical Noise", Corrosion/98, Paper No. 385, NACE International, Houston, 1998.

58. H. Fang, “Investigation of Localized Corrosion of Carbon Steel in H_2S Environments”, Ph. D Dissertation, Ohio University, 2012.

59. H. Sun, H. Fang, J. Davis and R. Hudgins, “Elemental Sulfur Corrosion and Inhibition in the Presence of Sulfur Solvent”, Corrosion/2011, Paper No. 11125, NACE International, Houston, 2011.

60. H. Fang, “Low Temperature and High Salt Concentration Effects on General CO_2 Corrosion for Carbon Steel”, Master Thesis, Ohio University, 2006.

61. R. Ambat, “Localized corrosion information using high resolution measurement devices”, Eurocorr 2005.

62. T.L. Landwein, J. Maier, B. Kinsella, H. Yanliang, S Huizinga, M. Wilms, “Identification of Sensitized Area in Austenitic and Aupermartensitic 13% Cr Stainless Steels by Micro-electrochemical EPR Tests (ME-EPR) and Atomic Force Microscopy (AFM)”, Eurocorr 2007.

63. C.Garcia, F. Martin, P.de Tiedra, Y. Blanco and M. Lopez, “Pitting Corrosion of Welded Joints of Austenitic Stainless Steels Studied by Using an Electrochemical Minicell”, Corrosion Science, Vol.50, 2008, pp.1184-1194.

APPENDIX:GALVANIC CURRENT CALCULATION

When two types of metal with different corrosion potential are coupled together, a galvanic current will be generated and flow through the two metals. One metal will corrode more and the corrosion of the other metal will be suppressed. The total galvanic current partially contributes to the anodic side as well as the cathodic side. Appendix Figure 133 shows a schematic of a galvanic coupling. $Icorr_1$ represents the uncoupled corrosion current (intrinsic corrosion current) and $I_{corr1,coupled}$ represents the coupled corrosion current which is affected by the galvanic current. The yellow line represents the measured galvanic current as show in the Figure. Apparently, part 1 which is part of measured galvanic current contributed to the anodic side (accelerating).

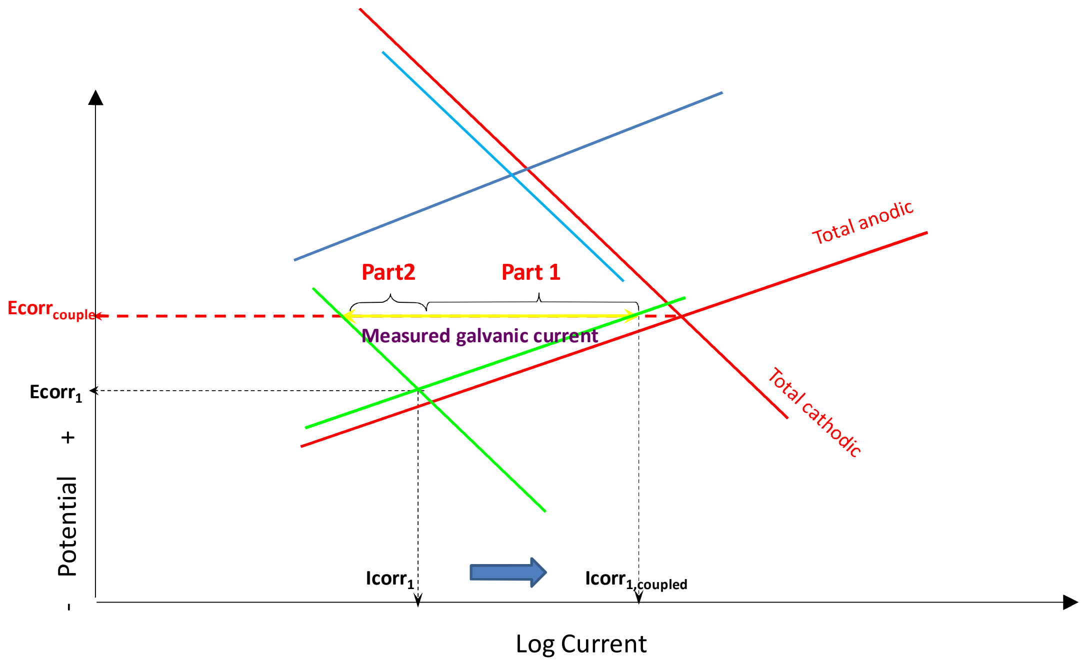

Figure 133. A schematic of galvanic coupling.

To calculate the ratio of part 1 to part 2, the triangle underneath the yellow line is zoomed in and shown in Figure 134. Yellow line represents the measured galvanic current and the two green lines represent the cathodic reacion (proton reduction) and anodic reaction (iron dissolution). According to the Talfel slop calculation, the absolute value of cathodic Tafel slop, β_c is three times higher than the anodic Tafel slop, β_a at the same temperature. Therefore, the ratio of part 1 to part 2 equals 3. This suggests that 3/4 of the galvanic current relates to changes in the anodic rate.

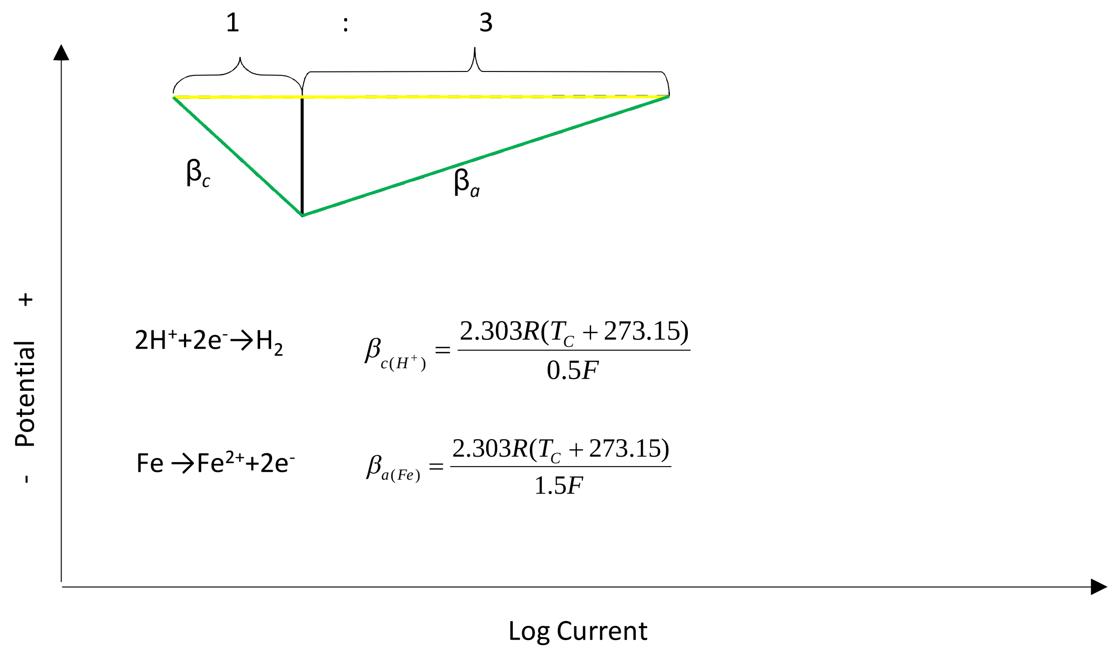

Figure 134. Calculation for the contribution of galvanic current on the anodic side.

The galvanic current effect on the cathodic side can be calculated by the same method. As shown in Figure 135, 3/4 galvanic current relates to the change in anodic reaction (suppressing cathode).

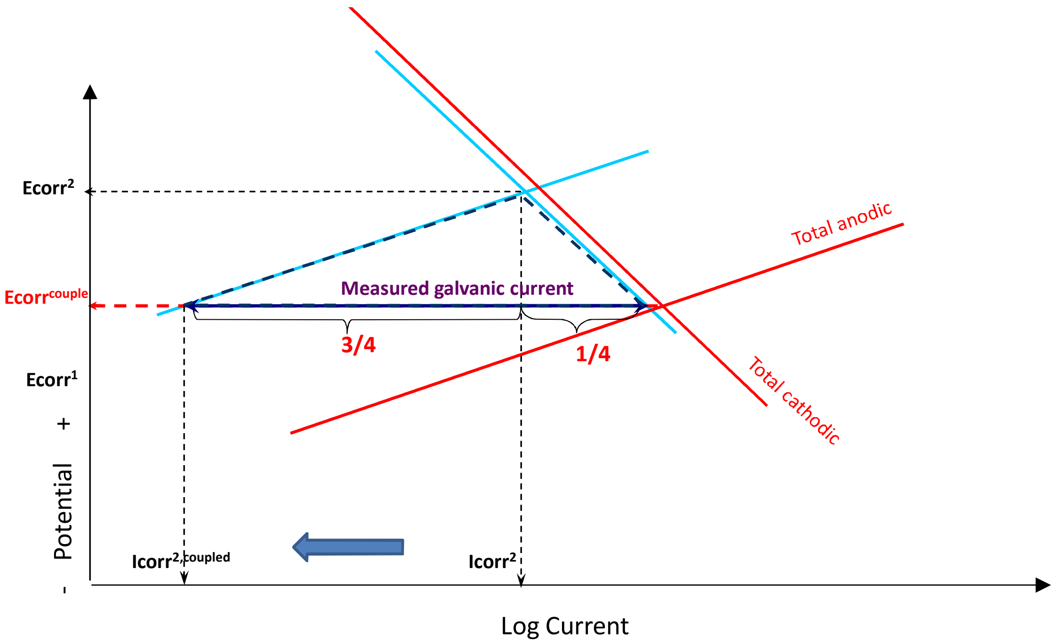

Figure 135. Calculation for the contribution of galvanic current on the cathodic.

Consequently, the equations can be written as below.

$$Coupled \quad corrosion \quad rate_{\ anode} = Uncoupled \quad corrosion \quad rate_{anode} + \frac{3}{4} Galvanic \quad corrosion \quad rate$$

$$Coupled \quad corrosion \quad rate_{\ cathode} = Uncoupled \quad corrosion \quad rate_{cathode} - \frac{3}{4} Galvanic \quad corrosion \quad rate$$